# Satellite monitoring of post-mining rehabilitation and the quantification of backfill dynamics using differential SAR interferometry

by
Shelley Adelaide Haupt

*Thesis presented in fulfilment of the requirements for the degree of Master of Science in the Faculty of Science at Stellenbosch University*

Supervisor: Dr J Engelbrecht

Co-supervisor: Dr JN Kemp

Department of Geography and Environmental Studies

March 2018

# DECLARATION

By submitting this thesis electronically, I declare that the entirety of the work contained therein is my own, original work, that I am the sole author thereof (save to the extent explicitly otherwise stated), that reproduction and publication thereof by Stellenbosch University will not infringe any third party rights and that I have not previously in its entirety or in part submitted it for obtaining any qualification.

SA HAUPT

Date: March 2018

# ACKNOWLEDGEMENTS

I would like to acknowledge the following people and institutions for their contribution towards this research:

- My supervisor, Dr Jeanine Engelbrecht for her guidance and support throughout this project.
- My co-supervisor Dr Jaco Kemp who introduced me to SAR, for his guidance and valuable input.
- The CSIR Meraka Institute for their generous funding.
- Data provided by European Space Agency (ESA).
- The Centre for Geographic Analysis (CGA) for provided data and willingness to help whenever I needed.
- The South African Weather Services (SAWS) for rainfall data.
- My colleague and friend, Andre Theron for all his help with just about everything.
- My family, Mom (Diane), T'nielle and Evan for their love and support throughout my university career.
- The Jones family for their love and support.
- My fellow masters students and friends for always encouraging me.
- Finally, my dad who taught me that nothing is impossible.

# ABSTRACT

Mining has severe environmental and social consequences and post-mining rehabilitation needs to take place before land re-zonation can occur. Post-mining rehabilitation is the process in which previously mined areas are returned to some degree of their natural state or to a condition that can sustain an intended post-mining land-use. Common rehabilitation practices, specifically in open-pit mines include backfilling and subsequent re-vegetation. Due to the risks involved with open-pit post-mining rehabilitation and to comply with the legislation governing mine closure, long-term monitoring of backfill settlement dynamics and the success of revegetation strategies are required. To overcome the limitations of field-based approaches, differential Synthetic Aperture Radar interferometry (dInSAR) has been used to detect measure and monitor surface deformation with millimetre accuracy.

In the first objective of this study conventional dInSAR techniques were used to detect surface deformation in a rehabilitated backfilled open-pit mine, using multi-sensor Synthetic Aperture Radar (SAR) data. The results indicated that although deformation measurements could be extracted, some anomalous patterns were observed across X-, C-, and L- wavelengths. In particular, heave features were observed as opposed to subsidence. Potential reasons for anomalous features were investigated and could be attributed to uncompensated topography and signal noise due to the presence of vegetation. Based on the results, recommendations included an updated Digital Elevation Model (DEM) for the successful removal of topographic phase contributions and the use of more advanced dInSAR techniques.

The second aspect of mine rehabilitation involves the revegetation of backfilled areas. Vegetation indices derived from multispectral data, such as the Enhanced Vegetation Index (EVI), have been widely used to monitor the productivity of vegetation. However, their use is limited in areas with persistent cloud cover and inclement weather. Due to the all-weather observations provided by SAR sensors, revegetation practices can be monitored using SAR data. This second objective evaluated the use of C-band SAR parameters to model EVI (simEVI) derived from Landsat 8 data using Random Forest (RF) algorithms. The results indicated that using a combination of all the SAR parameters yielded the highest adjusted $R^2$ (=0.715). Overall, the results indicated that there was an overestimation of simEVI in the dry season and underestimation in the peak of the growing season. Limitations of this investigation included the known saturation effects of C-band as well as the statistical phenomenon known as regression dilution bias. In general, modelled SAR EVI results mimicked the EVI trends and can therefore be considered as an alternative in areas where persistent cloud cover prevents the use of

conventional multispectral EVI. However, with no or limited optical data, the modelled SAR EVI may not be suitable to monitor vegetation productivity in this investigation.

Future research into the use of remote sensing to monitor post-mining rehabilitation is recommended and could provide valuable information to assist various stakeholders in improving post-mining rehabilitation strategies. The findings could contribute toward the operational monitoring of post-mining rehabilitation.

**Keywords**

Post-mining rehabilitation, remote sensing, differential SAR interferometry, backfill settlement dynamics, Enhanced Vegetation Index

# OPSOMMING

Mynbou het ernstige omgewings en sosiale gevolge en die area moet rehabilitasie ondergaan voordat hersonerring kan plaasvind. Mynbou-rehabilitasie is die proses waarby voorheen ontginde gebiede aan ‘n voorheen natuurlike toestand of na 'n toestand wat 'n beoogde grondgebruik kan onderhou, terugbesorg word. Algemene rehabilitasiepraktyke, spesifiek vir oopgroefmyne, sluit opvulling van die put en die daaropvolgende hervestiging van plantegroei in. As gevolg van die risiko's wat verband hou met die rehabilitasie van oopgroefmye, asook om te voldoen aan mynsluitings wetgewing, word vereis dat die opvulling-dinamika en plantegroei hervestigings sukses oor ‘n lang termyn gemonitor word. Om beperkings op veldgebaseerde benaderings te oorkom, was differensiële Sintetiese Apertuur Radar (SAR) -interferometrie gebruik om oppervlak deformasie teen millimeter akkuraatheid op te spoor, te meet en te monitor.

In die eerste afdeling van hierdie studie is konvensionele dInSAR tegnieke gebruik om oppervlak deformasie in 'n gerehabiliteerde teruggevulde oopgroefmyn wat, met behulp van SAR-data, bekom vanaf verskeie sensors te identifiseer. Die resultate het aangedui dat hoewel deformasiemetings gemaak kon word, sommige afwykende patrone tussen die X-, C- en L-golflengtes waargeneem was. In besonder was opheffing in teenstelling met insakking waargeneem. Potensiële redes vir afwykende eienskappe was ondersoek en kon aan ongekompenseerde topografie en seingeruis as gevolg van die teenwoordigheid van plantegroei toegeskryf word. Aanbevelings uit die resultate sluit in die gebruik van 'n opgedateerde DEM, vir die suksesvolle verwydering van topografiese fase bydraes, en die toets van gevorderde dInSAR tegnieke.

Die tweede aspek van myn rehabilitasie behels die hervestiging van plantegroei oor opgegevulde gebiede. Plantegroei indekse wat van multispektrale data, soos die Verbeterde Plantegroei Indeks (EVI) afgelei is, word wyd gebruik om die gesondheid en produktiwiteit van plantegroei te monitor. Die gebruik daarvan in gebiede met volgehoue wolkbedekking en onweer, is egter beperk. As gevolg van die weer-onhafhanklike waarnemings wat deur SAR sensors gemaak word, kan plantengroei hervestigings praktyke met behulp van SAR-data gemonitor word. Die tweede doel van die studie was om die gebruik van C-band SAR parameters, om die simulasie van EVI (simEVI) afegelei van Landsat 8 data deur die gebruik van Random Forest (RF) algoritmes, te evalueer.

Die resultate het aangedui dat die gebruik van 'n kombinasie van al die SAR parameters die hoogste aangepaste $R^2$ opgelewer het (= 0.715). Oor die algeheel het die resultate aangedui dat daar 'n oorskatting van simEVI in die droë seisoen en ‘n onderskatting gedurende die piek van die groeiseisoen is. Beperkings van hierdie ondersoek sluit die bekende versadigings-effekte van C-band asook die statistiese verskynsel wat bekend staan as regressie verdunnings vooroordeel in.

Oor die algemeen het gesimuleerde SAR EVI-resultate egter die EVI-tendense gevolg en kan daarom as 'n alternatief beskou word. Veral in gebiede waar aanhoudende wolkbedekking die gebruik van konvensionele multispektrale EVI verhoed. In die algemeen het SAR EVI resultate die EVI tendense gevolg en kan dus beskou word as ‘n alternatief in areas waar aanhoudende wolkbedekking die gebruik van konvensionele multispektrale EVI verhoed. Hierdie ondersoek toon egter dat gemodelleerde SAR EVI nie geskik is om plantegroei produktiwiteit te monitor in die afwesigheid van genoeg optiese data nie.

Toekomstige navorsing oor die gebruik van afstandswaarneming om mynbou rehabilitasie te moniteer, word aanbeveel. Dit kan waardevolle inligting verskaf om verskeie belanghebbendes in die verbetering van die mynbou-rehabilitasie strategieë by te staan. Verder kan die bevindings tot die operasionele monitering van mynbou rehabilitasie bydra.

**Trefwoorde**

mynbou-rehabilitasie, afstandswaarneming, differensiële SAR-interferometrie,

opvullings-dinamika, verbeterde plantegroei indeks

# CONTENTS

# TABLES



# FIGURES

# ACRONYMS AND ABBREVIATIONS

| | |
|---|---|
| cm | centimetre |
| DEM | Digital Elevation Model |
| DInSAR | Differential SAR Interferometry |
| DLR | German Aerospace Centre |
| EFA | Ecological Function Analysis |
| ESA | European Space Agency |
| EVI | Enhanced Vegetation Index |
| FBD | Fine Beam Dual |
| FBS | Fine Beam Single |
| GPS | Global positioning systems |
| HH/HV/VV/VH | Horizontal and Vertical combinations of polarisation |
| HoA | Height of ambiguity |
| InSAR | SAR Interferometry |
| LAI | Leaf Area Index |
| LiDAR | Light Detection and Ranging |
| LOS | Line of Sight |
| MCF | Minimum Cost Flow |
| mm | millimetre |
| MPRDA | Mineral and Petroleum Resources Development Act |
| NDMI | Normalized Difference Moisture Index |
| NDVI | Normalized Difference Vegetation Index |
| OBSett | Opencast Backfill Settlement Prediction Package |
| POLInSAR | Polarimetric SAR Interferometry |
| PSI | Persistent Scatterers Interferometry |

| | |
|---|---|
| RF | Random Forest |
| SAR | Synthetic Aperture Radar |
| SBAS | Small Baseline Subset |
| simEVI | Simulated EVI |
| SLC | Single Look Complex |
| SRTM | Shuttle Radar Topography Mission |

# 1 INTRODUCTION

## 1.1 Background to the study

The mining industry is, and has been for many years, a vital component of the development of South Africa as it contributes to economic development, infrastructure, and employment (Swart 2003; Tanner & Möhr-Swart 2007). However, mining activities have significant social and environmental impacts that are not fully recognised or dealt with (Tanner & Möhr-Swart 2007). These include acid mine drainage, pollution caused by dust and damage to the biodiversity of the vegetation in the area (Nazare 2005). This has left South Africa with a legacy of negative social and environmental impacts as it relates to mining activities (Swart 2003). The search for innovative, multidisciplinary solutions to address mining-related challenges have been identified as the key to ensuring the economic and developmental contributions to the mining industry while enhancing safety and reducing environmental impacts (Hermanus 2014).

The Mineral and Petroleum Resources Development Act (MPRDA) of 2002 necessitates the integration of social, economic and environmental factors into all phases of mining operations to ensure more sustainable practices (Swart 2003). This includes mine planning, mineral extraction, mine closure and the post-closure phases of mining operations. The MPRDA specifically aims to protect the environment for the benefit of present and future generations while increasing the economic and social benefits from mining (Swart 2003). There has been a growing awareness of the social and environmental impacts of abandoned mines due to inadequate closures practices. Therefore, strict regulations on mine-closure, especially pertaining to surface stabilisation and re-vegetation, are enforced to minimise long-term impacts on human health, biodiversity and ecosystem services.

Post-mining rehabilitation is the process in which previously mined areas are returned either to some degree of their natural state or to a condition that can sustain an intended post-mining land-use (Limpitlaw et al. 2005). In South Africa, guidelines for the rehabilitation of land disturbed by mining was first published by the Chamber of Mines in 1981 and the legal guideline, rehabilitation objectives and procedures have continued to evolve (Tanner & Möhr-Swart 2007). Internationally, there have been several rehabilitation guidelines including the Australian mine rehabilitation, mine closure, and completion guidelines. These guidelines have also been adapted and incorporated into South Africa's guidelines for rehabilitation of coal mines.

Generally, rehabilitation practices have a number of advantages which include stabilising the surface and preparing it for alternative land-use developments like agriculture, forestry, recreation or wildlife habitat (Erener 2011). In most cases, effective rehabilitation requires significant innovation to identify appropriate land-use opportunities not only to mitigate environmental, health and safety risks but also to stimulate economic development after mining. The process of rehabilitation is particularly challenging in open-pit mines (Limpitlaw et al. 2005). Open-pit (also called opencast) mining is a commonly used technique to extract coal ore in South Africa. The coal ore (known as overburden material) is excavated by drilling, blasting, and subsequent removal leaving a void. Consequently, there is a complete disruption of the surface which affects the soil, fauna, flora and surface hydrology (GDACE 2008). In the case of open-pit mining, this implies that the process of rehabilitation may involve the movement of large volumes of material in a process called backfilling.

Backfilling is the process of filling large voids with a combination of tailings, water and small amounts of cement to promote regional stability (Brown 2011). As there is no formal requirement from mining companies to uniformly compact the soil or accurately monitor inter-backfill displacement, backfilled areas are prone to differential compaction and consolidation settlement (Fenn, du Kanda & Dukhan 2015). These backfill materials are prone to settling over extended periods and the settlement rates vary over space and time (Fenn, du Kanda & Dukhan 2015; Mhlongo & Ampo 2016). This results in surface displacement caused by the readjustment of the overburden above the voids that mining activities have created, and which vary significantly in space and over time (Singh & Dhar 1997). The impact of mining subsidence can occasionally be catastrophic, destroying property and even leading to the loss of life (Bell, Stacey & Genske 2000). Therefore, the surface instabilities inherent to backfill settlement pose restrictions on the identification of post-mining land-use options. For example, infrastructure development on potentially unstable surfaces would require additional measures to ensure that human health and safety is not compromised. Furthermore, ongoing monitoring would be required to identify areas that may be affected by damage to infrastructure and the environment.

Following backfilling, open-pit rehabilitation plans may involve covering the backfill material with topsoil and planting vegetation to help consolidate the material. This process, known as revegetation, is regarded as the most widely accepted and useful way to improve the condition of degraded mined soils (Mensah 2015). A goal of revegetation strategies is to design a suitable plant succession that will provide adequate surface cover and increase the fertility of the soil (Mensah 2015). However, revegetation of previously mined areas is often difficult because mine

soils are frequently acidic, have low fertility rates and low nutrient contents (Carvalho et al. 2013). To counteract this, the addition of organic matter and liming can improve the revegetation potential and have a beneficial effect on surface stability (Carvalho et al. 2013). This implies that the success of revegetation strategies depends on a number of factors including soil preparation, fertilisation, and irrigation (GDACE 2008).

Risks involved with mine rehabilitation, requires systems to monitor settlement dynamics and the success of revegetation strategies for the long-term. The continuous monitoring and analysis of rehabilitated revegetated areas will help determine the rate at which areas are progressing towards the desired post-mine land-use and could also highlight deficiencies that are evident (Vickers, Gillespie & Gravina 2012). The early identification of deficiencies would assist with the formulation of mitigation strategies. To monitor the success of rehabilitation practices, mining companies use a combination of in situ observations and remote sensing technologies (Felinks, Pilarski & Wiegleb 1998). However, the disadvantages of in situ observations are well described and include the fact that observations take place at discrete points. Additionally, frequent observations would be required to monitor vegetation productivity and surface stability over time. The process of in situ monitoring therefore poses significant time- and cost constraints if intended for long-term, operational monitoring (Herrera et al. 2007). Remote sensing technology has improved the capability of acquiring information about the earth and its resources for global, regional and local assessments (Tote et al. 2010). The use of satellite imagery makes it possible to monitor changes brought about by rehabilitation in previously mined areas (Petja 2009).

Furthermore, regulatory and legislative pressure to ensure suitable and sustainable post-mining landscapes, the use of innovative, multidisciplinary solutions to monitor post-mining rehabilitation options needs to be explored. Scientific evidence and case studies need to inform various options (Swart 2003). Remote sensing techniques are rapidly evolving and information obtained can lead to significant improvements in monitoring post-mining rehabilitation. This research, therefore aims to assess the potential contribution of remote sensing techniques to monitor the success of rehabilitation with an emphasis on monitoring backfill settlement dynamics and the productivity of revegetated areas.

## 1.2 **Problem formulation**

Open-cast mining disturbs large areas of land and can lead to social- and environmental challenges (Erener 2011). These include South African legislation dictates that the owner of a mine remains responsible for all liabilities relating to it until a closure certificate has been issued. The current South African legislative framework governing mine closure requires that mine areas are returned into a viable and sustainable post-mining land-use (Limpitlaw et al. 2005. In particular, the Mineral and Petroleum Resources Development Act (Act 28 of 2008), requires the rigorous mitigation of both biophysical and socio-economic impacts (Limiptlaw et al. 2005).

Rehabilitation of open-pit mines involves backfill placement at various levels directly in the pit (Hills 1994). Once completed, the backfilled material contains varying degrees of compactness. Consequently, backfill settling rates are dynamic over time and space (Hills 1994). The amount and rate of settling associated with backfill are difficult to predict (Goodwin, O'Neill & Anderson 2003). Factors that influence the settling of backfill material include the method of placement, backfill material properties, the hydrological system and the time taken for the backfill to settle (Hills 1994). Until recently, there has been little pressure to monitor backfill settlement as there was often no infrastructure built on these areas (Fenn, Kanda & Dukhan 2015). However, with the regulatory pressures on ensuring both environmentally and socio-economically favourable post-mining land-use, the pressure of mitigating the risks of subsidence and backfill settlement is increasing. In fact, the Mine and Health Safety Act (Act No. 29 of 1996) stipulates that, where there is a risk of ground movement due to mining operations, mining companies must take reasonable measures to ensure that deformation is effectively monitored (South Africa 1996).

To comply with these requirements, researchers have investigated and attempted to predict backfill settlement using ground-based and laboratory techniques with varying levels of success (Fenn, du Kanda & Dukhan 2015; Zhao et al. 2014). Furthermore, conventional in situ monitoring approaches have been used to detect, measure and monitor surface deformation associated with backfill settlement (Fenn, du Kanda & Dukhan 2015; Hills 1994; Reed, Hughes & Singh 1987). These include Global Positioning Systems (GPS) surveys and geodetic leveling approaches (Raucoules, Colesanti & Carnec 2007). Generally, these methods offer precise measurements and are frequently used by risk management departments (Raucoules, Colesanti & Carnec 2007). However, they do have several limitations.

These include the high costs (both monetary and manpower) of monitoring large areas at frequent time intervals and the difficulty of accessing remote or isolated monitoring sites (Dong et al. 2015). To overcome the limitations of in situ monitoring approaches, remote sensing techniques for operational monitoring of surface deformation have also been considered.

Among these methods, differential SAR interferometry (dInSAR) has proven to be particularly useful in monitoring surface subsidence in mining environments and is known to be sensitive to centimetre (cm) to millimetre (mm) scale movements of the surface (Massonnet & Feigl 1998). DInSAR offers several important advantages when compared to the conventional methods used to monitor and measure surface deformation. DInSAR techniques provide a synoptic view which is an effective tool for the initial assessment of surface deformation that overcomes the limitation of a point-based monitoring system that ground-based techniques provide (Engelbrecht, Inggs & Makusha 2011). Furthermore, since deformation measurements are made remotely, observations of remote or isolated field areas are possible. Therefore, significant scope exists to test the contribution of dInSAR approaches for long-term operational monitoring of settlement dynamics on rehabilitated open-pit mines. DInSAR techniques provide an opportunity to 1) evaluate the rate at which backfilled material is settling by assessing the deformation at specific points over time, 2) determine the spatial extent of settling areas and 3) identify the triggers (for example rainfall) involved in backfill settlement. The information gathered from the dInSAR results could aid developers and engineers to predict backfill dynamics and to understand settlement rates and consequently, to comply with mine closure legislation.

The second aspect of mine rehabilitation involves the revegetation of backfilled areas. Monitoring backfill settling dynamics using remote sensing techniques is relatively untested. A considerable amount of research has been devoted, however, to the development of algorithms to monitor the productivity of vegetation using a variety of remote sensors (Brom et al. 2012; Erener 2011; Felinks, Pilarski & Wiegleb 1998). In fact, the maturity of remote sensing algorithms for the monitoring of vegetation trends has evolved to a stage where it is an internationally accepted alternative to in situ observations (Xie et al. 2008). Therefore, an opportunity exists for the integration of remote sensing techniques in monitoring of the success of revegetation strategies.

Remote sensing data can contribute to monitoring systems by providing timely, synoptic, cost-effective and repetitive information (Atzberger 2013). Remote sensing technologies for the monitoring of long-term vegetation trends are mature, while additionally dInSAR possesses the

potential to monitor settlement dynamics. For this reason, the recommendation is that these approaches be applied to assess their potential contribution to operational post-mining rehabilitation monitoring systems. The results of this study can aid in the development of a long-term operational monitoring system for post-mining rehabilitation using remote sensing techniques.

## 1.3 **Research aim and objectives**

The overall aim of this study is to test a set of remote sensing techniques and their contribution to the monitoring of post-mining rehabilitation using satellite data. Its focus will be on monitoring backfill dynamics using dInSAR techniques and monitoring of the vegetation productivity using a combination of Synthetic Aperture Radar (SAR) and optical data. Following the broader aim of the project, the research seeks to address the following research questions:

- Can surface deformation associated with backfill settlement be measured using differential radar interferometry techniques?

- Can a combination of SAR and optical data be used for monitoring the vegetation productivity on rehabilitated open-pit mines?

The ultimate objective of the research is to determine to what extent remote systems can address the known challenges of monitoring the success of rehabilitation strategies. The research is divided into two components. The first component will focus on implementing conventional dInSAR methods to detect and monitor surface deformation caused by the settling of backfill material in rehabilitated open-pit mines. Particular emphasis will be placed on monitoring the dynamics of backfill settling, including the settling rates, and how they change over time and the time frame until stability is reached. Since the use of dInSAR to monitor backfill settlement dynamics is relatively untested, the research will attempt to test the operational limitations of using dInSAR to measure settling dynamics. It will use a real-world rehabilitated open-pit mine as a test case. The second component will focus on using a combination of SAR and optical data to assess the productivity of vegetation on rehabilitated mines compared to the surrounding vegetation.

Figure 1.1 illustrates the overall research design. Chapter 1 introduced the background of post-mining rehabilitation. Thereafter, it outlined the problem formulation and the aim and objectives. Section 1.4 presents a description of the study area.

Chapter 2 will review the literature of backfill settlement and revegetation and current monitoring approaches and Chapter 3 will present the methods used in the study. Finally, Chapters 4 and 5 will present the results and discussion and, thereafter, the concluding chapter, Chapter 6 will synthesise all the findings and make recommendations for future research.

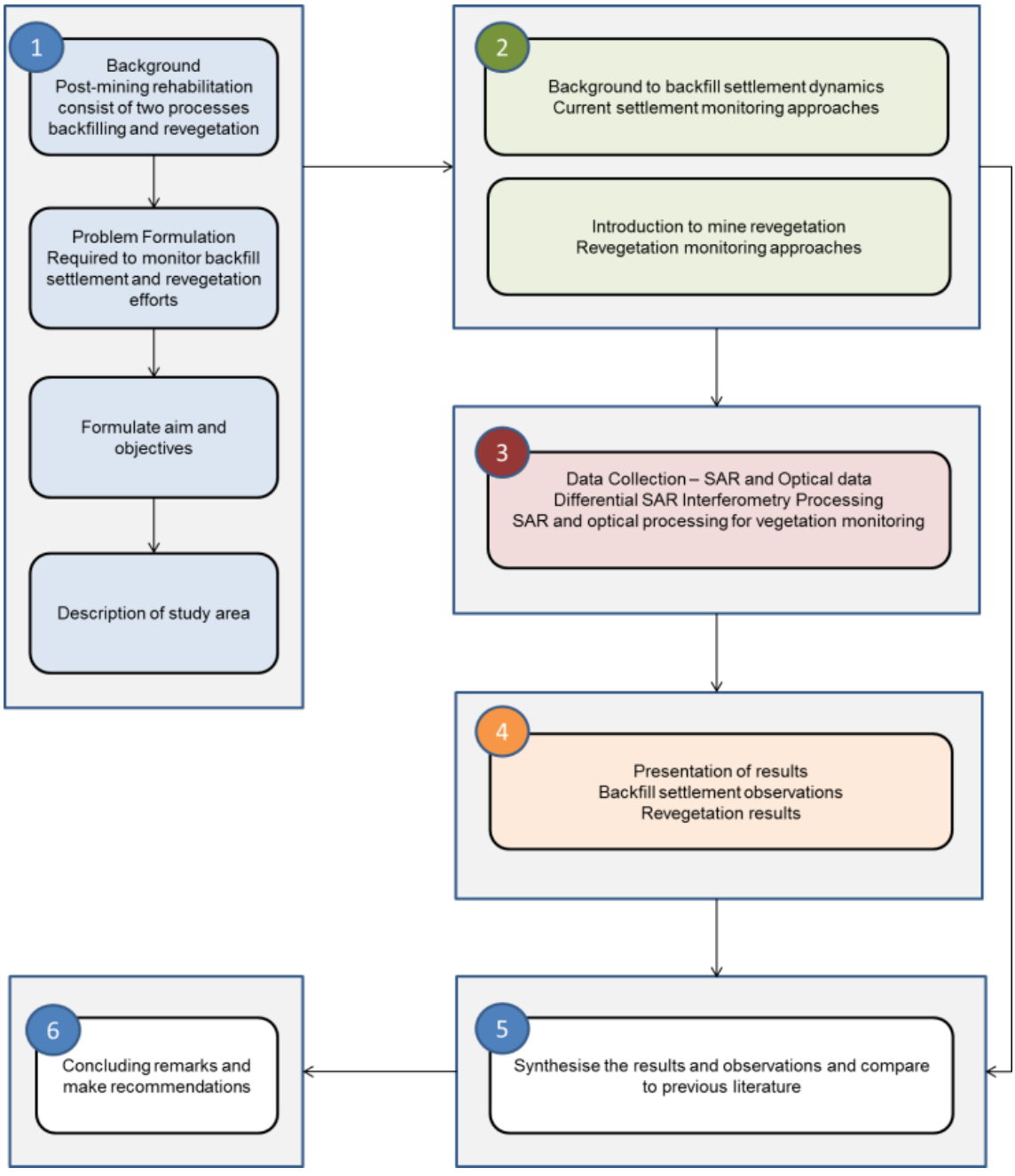


Figure 1.1 Research design, which contains contents and chapter structure of this study.

## 1.4 Description of study area

The study area is situated in the coal mining region of the Mpumalanga province of South Africa (Figure 1.2). South Africa is the seventh largest coal producer in the world and coal is the primary energy source for electricity generation. The area of interest is one of several rehabilitated open-pit mines in this region (Figure 1.3A and Figure 1.3B). Open-pit mining has ceased and the area has been backfilled and revegetated and is associated with the Grassland Biome of South Africa. The natural vegetation (which will be referred to as undisturbed vegetation) consists of short dense grass with small scattered rocky outcrops and some woody vegetation species (Figure 1.3C and Figure 1.3D) (Carbutt et al. 2011). The main vegetation type is classified as the Eastern Highveld Grassland (Mucina & Rutherford 2006). Figure 1.3D shows the natural vegetation and surrounding mining areas. Rainfall in this region is seasonal and occurs primarily in the summer months (December to February) and the growing season lasts approximately half the year from November to March (Carbutt et al. 2011). The winter season is generally cold and dry (Carbutt et al. 2011). Large parts of the grassland have been transformed into agriculture, grazing and mining activities.

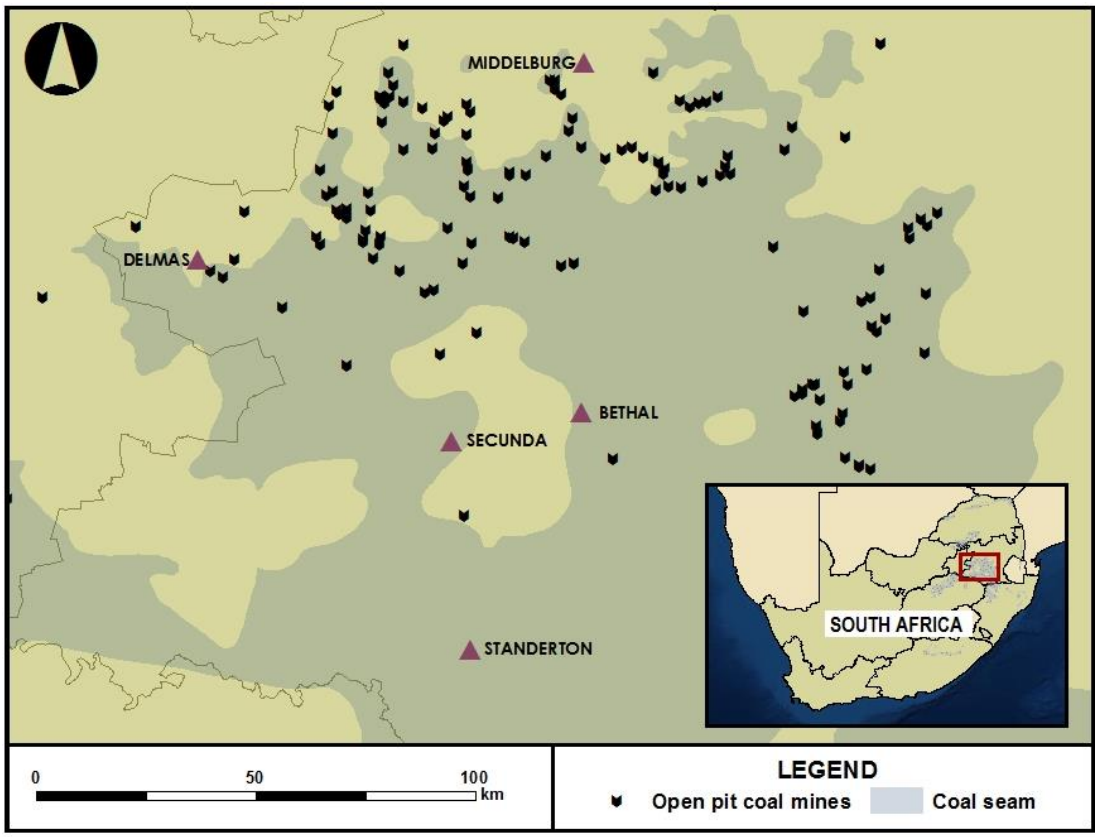


Figure 1.2 Study Area of open-pit mine in the Mpumalanga Province of South Africa

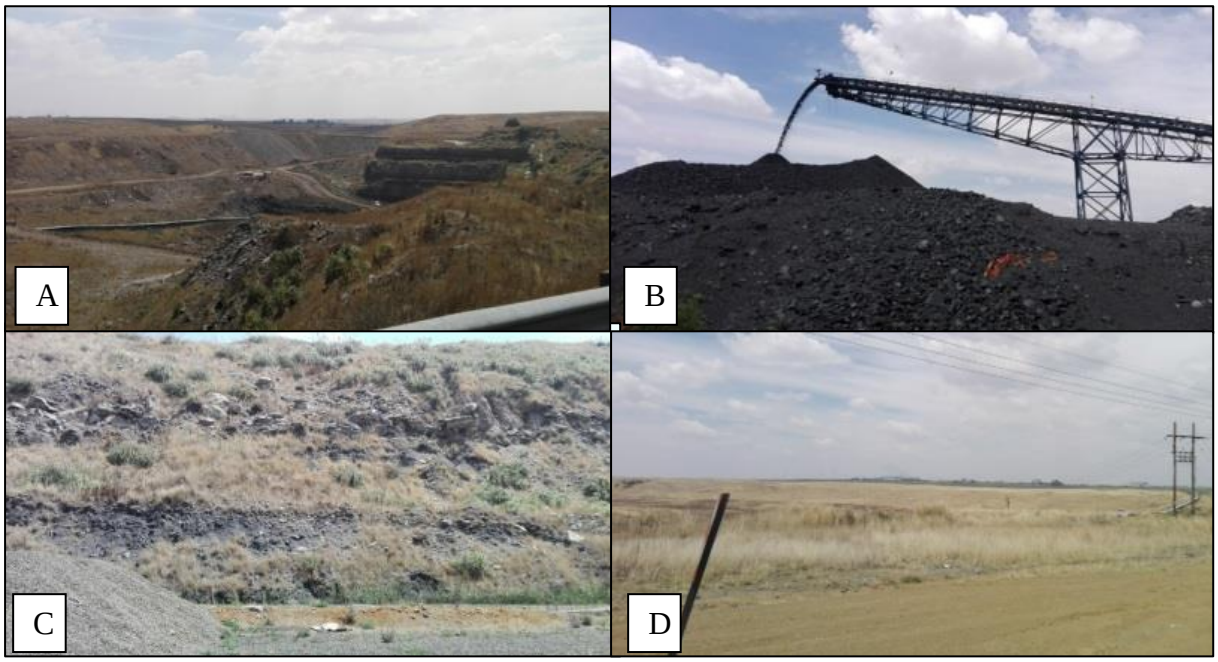


Figure 1.3 A) The natural topography of the area of interest B) Coal deposits C) Vegetation and rocky outcrops D) Natural vegetation containing mostly grassland

# 2 LITERATURE REVIEW

As detailed in Section 1.1, post-mining rehabilitation promotes economic and environmental sustainability. This is commonly done by backfilling the void and then revegetating the backfilled area. To assess the success of these rehabilitation efforts, continuous monitoring is needed to manage and to promote sustainability. This includes monitoring backfill settlement rates to determine when the surface is stable as well as monitoring the productivity of revegetation.

Section 2.1 provides an overview of backfill settlement dynamics and a brief description of backfill settlement rates as determined by international case studies. Section 2.2 then outlines current techniques to monitor settlement rates with a specific focus on the concept of radar interferometry for surface deformation monitoring. The second component of this chapter (Section 2.3) provides a description of revegetation in post-mining environments and current methods to monitor the health and productivity of revegetation practices. This chapter emphasises the role of satellite data for long-term operational monitoring.

## 2.1 Backfill settlement dynamics

Mine backfilling has become an integral part of open-cast mining operations (Hassani, Mortazavi & Shabani 2008). Research has been devoted to further the understanding of the mechanisms and controls involved in backfill settlement behaviour (Hassani, Mortazavi & Shabani 2008). However, very few studies have been conducted on ground subsidence in backfilled areas (Zhao et al. 2014). Researchers have observed that large-scale ground subsidence can be induced by backfill placement, potentially resulting in severe damage to the building, roads, shafts and other facilities (Zhao et al. 2014). Therefore, the prediction and modelling of backfill settlement properties depending on the backfill material used, the method of placement and the local conditions; can assist with the design of an optimal backfill strategy (Gourc, Arif & Olivier 2007).

Backfill settlement rates have two distinct stages: 1) short-term settlement which occurs at a high rate immediately after backfilling and, 2) long-term settlement which is less rapid and often varies significantly in time and space over an area (Goodwin, O'Neill & Anderson 2003).

The different settlement rates as a function of time, is summarised graphically in Figure 2.1 (Fenn, du Kanda & Dukhan 2015). Immediately after backfilling, the bulk of compaction and consolidation occurs assisted, to some degree, by the weight of the machinery used (Fenn, du Kanda & Dukhan 2015; Reed, Hughes & Singh 1987). Following the initial compaction, additional volume changes occur and consolidation settlement rapidly takes place due to the dissipating air and water pressures. Thereafter, creep settlement occurs at a slower rate until the water table recovers. Interim periods of collapse settlement also occur and can accelerate the creep process (Fenn, du Kanda & Dukhan 2015). Creep settlement refers to the secondary consolidation, which is caused by the gradual rearrangement of the material fragments into a more stable configuration (Fenn, du Kanda & Dukhan 2015). This usually occurs after immediate settlement that takes place within a time period of about seven days. Collapse settlement is the sudden increase in settlement and loss of strength as a result of wetting (Li, Vanapalli & Li 2016). The collapse settlement of open-cast mine backfill settlement are a consequence of physical weathering from groundwater contact (Reed & Singh 1986). This sudden ground movement can destroy property and in extreme cases threaten safety (Chandarana, Momayez & Taylor 2016). Movements in open-pits that have been backfilled most commonly occur as a result of creep settlement, collapse settlement and heave (Hills 1994). These can often occur in combinations depending on the circumstances. Heave (or uplift) has also been observed in a number of opencast mine backfills. It can be associated with the removal of overburden mounds and in some cases with the saturation, due to the surface water ingress, of the few metres of the fill (Hills 1994).

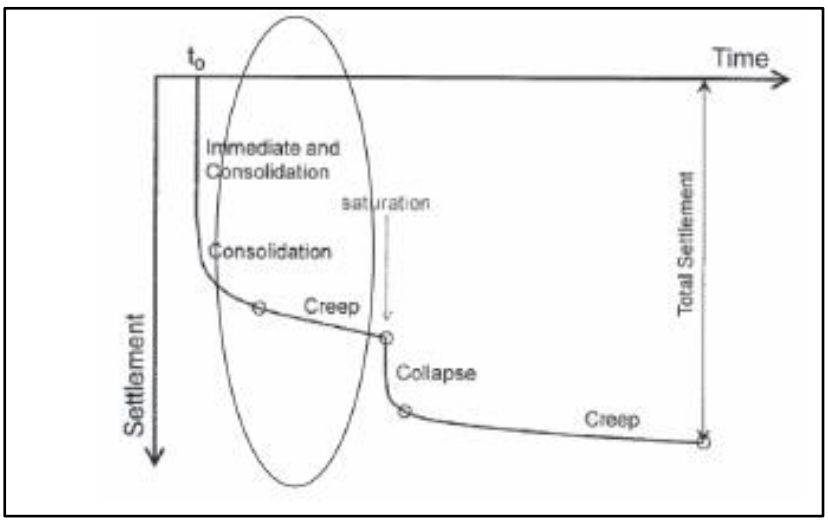


Figure 2.1 Terminolgy of settlement stages and rates as a function of time Source: (Fenn, du Kanda & Dukhan 2015)

The exact rate of backfill settlement and the timeframe until stability is reached depends on a number of factors. These include the timing of backfilling operations, the compactive state of the backfill, the inundation of backfill and the influence of the surrounding material (Hills 1994). The variability of backfill dynamics in space and time is a concern since the stability of the surface dictates the suitable post-rehabilitation land-use options. Creep and collapse settlement, for example, are irreversible and would affect and potentially damage any structures built on the area (Fenn, du Kanda & Dukhan 2015). Therefore, the development of roads, houses or other infrastructure on opencast backfill would pose several challenges (Hills 1994). For rehabilitation initiatives, an understanding of the behaviour of backfill settlement is required. Furthermore, an approach is necessary to determine when surface stability is reached.

Investigations into the prediction of backfill settlement have been widely reported. The predictions, based on analytical and numerical models at various scales, have provided varying levels of accuracy (Fenn, du Kanda & Dukhan 2015; Goodwin, O'Neill & Anderson 2003; Hassani, Mortazavi & Shabani 2008). One of the first known studies investigated the suitability of restored surface coal mines for the purpose of structural development in the North-East of England (Kilkenny (1968) cited in Reed, Hughes & Singh 1987). In the study, shallow backfilled areas were observed and indicated that the settlement rates followed a semi-logarithmic decay with respect to time (Kilkenny (1968) cited in Reed, Hughes & Singh 1987). The same methodology was adopted to derive backfill settlement observations for three different rehabilitated mines (Reed, Hughes & Singh 1987). The results showed that, between 15 mm and 451 mm of total settlement was measured across the three different sites. Settlement rates were 10 mm per annum. The overall conclusions were that settlement rates were faster in newer fill material and slower on the older fill. This confirms the observation by Fenn, du Kanda and Dakar (2015) presented in Figure 2.1.

A technique to examine and predict backfill settlement using an empirical model called Opencast Backfill Settlement Prediction Package (OBSett) was proposed by Hills (1994). The technique was used to compare predicted settlement rates versus known settlement rates at a site that was monitored in England using a numerical model approach. In the study, 2480 in situ measurements were taken over a 19-month period and the results were averaged monthly. The predicted settlement rates were compared to the actual rates, and the results shows settlement rates between 2 mm and 370 mm. The investigation resulted in a determination of the factors that influence backfill settlement rates. These include: 1) timing of the backfill operation (the time it took for backfilling process to occur), 2) composition and rock types comprising the backfilled

material, 3) control and compaction processes during backfill placement and 4) the effect of groundwater, climate and the overall hydrological regime (Hills 1994). A recommendation emanating from research suggests that ongoing monitoring of backfill settlement could aid future predictions of settlement dynamics prior to backfilling or upon completion of backfilling (Hills 1994).

In addition to in situ monitoring of backfill settlement rates, several researchers have employed numerical simulation models to predict backfill behaviour (Fenn, du Kanda & Dukhan 2015; Goodwin, O'Neill & Anderson 2003). One such model, known as the SEEP/W model, was used to predict backfill settlement based on groundwater recovery (Hills 1994; Mhlongo & Ampo 2016; Reed, Hughes & Singh 1987). The results of the research confirmed that high backfill settling rates were associated with high levels of groundwater recovery. The results illustrate how the local hydrological regime can influence settlement dynamics. In particular, since dewatering practices are implemented while mining operations are on-going, the inflow of water into mines is prevented (Mhlongo & Ampo 2016). Once mining operations cease, the natural groundwater regime is re-established and this, affects backfill settlement rates (Mhlongo & Ampo 2016). Other numerical models include the Sowers method which is currently the most widely used method for estimating settlement (Fenn, du Kanda & Dukhan 2015). This technique has been applied to determine settlement rates and surface stability using the in situ density of backfill material as a proxy for displacement (Fenn, du Kanda & Dukhan 2015).

One proposed method used X-ray computer tomography to evaluate the fundamental mechanisms at work with various fill material during the process of creep settlement in opencast coal mines over a certain period of time (Goodwin, O'Neill & Anderson 2003). A significant recommendation made by this study is that opencast backfills can weather, erode and experience different moisture changes with time and this may have a significant impact on settlement processes (Goodwin, O'Neill & Anderson 2003). A broad-scale monitoring system is necessary if vital information about backfill settlement dynamics is needed to guide post-rehabilitation practices.

## 2.2 **Subsidence monitoring techniques**

Several studies have implemented a variety of techniques to detect and monitor ground subsidence due to mining. These approaches generally rely on collecting in situ measurements, extracting measurements based on remote sensing datasets or a combination of the two.

Conventionally, ground subsidence is measured using surveying techniques such as, tilting, spirit levelling, and GPS surveys (Herrera et al. 2007).

Although, these techniques offer precise measurements, there are limitations such as high costs for wide-area coverage measurements are on a point-by-point basis (Ng et al. 2010). Furthermore, in the case of sudden deformation incidents ground–based networks are implemented only after an event has occurred (Raucoules, Colesanti & Carnec 2007). Therefore, there is a need for rapid, cost-effective, and synoptic monitoring programs that can aid in both pre- and post- subsidence evaluation. To overcome the limitations of ground-based techniques remote sensing datasets have been used to detect and monitor mining-induced ground subsidence (Hu et al. 2016; Joyce et al. 2014).

Remote sensing approaches for deformation monitoring include airborne Light Detection and Ranging (LiDAR) surveys, which involve the process of extracting the distance from an aircraft to the earth's surface by measuring the travel time of the emitted pulse (McClusky & Tregoing 2013). To examine the effect of ground surface subsidence using LiDAR, point-clouds collected at different dates are used to create Digital Elevation Models (DEM) which indicate the topography (Mcclusky & Tregoning 2013). These can form elevation-difference maps which indicate the absolute vertical motion of the ground surface in the time interval between the surveys (Mcclusky & Tregoning 2013). Therefore, LiDAR has shown the potential to measure ground deformation associated with mining abstraction (Joyce et al. 2014). The advantages of using LiDAR for ground deformation is that high-density deformation maps can be produced and measurements can be obtained in all terrain and vegetation conditions (Mcclusky & Tregoning 2013). However, the vertical positioning precision of LiDAR systems (between 5 mm and 10 mm) is inadequate for the detection of small local deformations (Hu et al. 2016; Joyce et al. 2014). Therefore, backfill settlement monitoring using LiDAR would be challenging since typical rates of between 10 and 350 mm are lower than the vertical accuracies reported for LiDAR collections. LiDAR data acquisitions are also weather dependent and data acquisitions in adverse weather conditions would not be possible (McClusky & Tregoing 2013). Finally, the costs of obtaining a long time series of LiDAR datasets are high (Joyce et al. 2014).

To overcome the challenges of deformation measurements using in situ and LiDAR surveys, a considerable amount of research has been devoted to algorithms to extract surface deformation measurements from space-borne SAR) data. SAR interferometry approaches provide broad coverage, high sensitivity to ground motions and high spatial and temporal resolution under all

weather conditions (Dong et al. 2015). Section 2.2.2 presents studies that have used SAR to detect deformation in mining environments. Following this introduction to SAR, Section 2.2.1 provides SAR interferometry techniques for detecting and monitoring deformation.

### 2.2.1 **Introduction to SAR and Differential Interferometry SAR (dInSAR)**

SAR is a branch of remote sensing that exploits microwave radiation to form images of the Earth's surface. SAR sensors are also active sensors (i.e., they emit their own radiation) implying that data collections are possible any time during the day or night (Moreira et al. 2013). It operates at various wavelengths of the electromagnetic spectrum and includes L-band (~ 23 cm), C-band (~5 cm) or X-band (~3 cm). At these wavelengths, the microwave signal penetrates the cloud cover and can, therefore, acquire data regardless of weather conditions (Raucoules, Colesanti & Carnec 2007). This provides advantages over optical techniques as it is useful for monitoring areas that are prone to persistent cloud cover and inclement weather (Massonnet & Feigl 1998).

SAR sensors record the amplitude and phase of signals reflected (also called scattered) from the surface (Zhou, Chang & Li 2009). SAR interferometry (InSAR) is the measurement of the change of the phase of the signal over time. The phase of the signal is related to the distance of the sensor from the illuminated targets on the ground (Barla , Tamburini , Del Conte & Giannico 2016). If two images differ in time or position, the phase between the two images can be compared (Massonnet & Feigl 1998). The resulting difference of the phase shows an interference pattern known as an interferogram (Massonnet & Feigl 1998). The interferogram contains information of different phase contributions including 1) flat-earth and topography, 2) ground surface displacement, 3) variations due to atmosphere, 4) orbital contributions and 5) phase noise (Colesanti & Wasowski 2006; Ferretti et al. 2007; Massonnet & Feigl 1998). With the aim of detecting surface displacement, the various contributions of the interferometric phase need to be removed or compensated for to isolate the phase term due to displacement. If surface deformation took place between the two image acquisitions, a change in phase would be recorded in the interferogram. The change in phase due to deformation can be isolated and measured resulting in a differential interferogram. This technique is known as dInSAR.

Differential interferometric techniques are able to detect deformation ranging between centimetres or millimetres (Bamler & Hartl 1998). Previous investigations on SAR interferometry in mining environments have contributed to a selection of optimal sensor parameters required for long-term monitoring (Engelbrecht 2013). In general, the limitations are

informed by two factors 1) the sensor parameters, such as wavelength, polarisation, incidence angle and effective resolution, and 2) the deformation feature characteristics including the size and the rate of deformation (Massonnet & Feigl 1998) .

Line-of-sight deformation between two image acquisitions is measured at a fraction of the wavelength (Hanssen 2005). Shorter wavelengths such as X-band and C-band are more likely to detect small-scale or gradual deformation features. However, shorter wavelengths are scattered by small objects such as tree leaves and vegetation cover. This causes a decorrelation of the phase signal (known as volume decorrelation) that introduces signal noise, thereby affecting the detection of deformation (Hanssen 2001). C- and X-band SAR data can detect small-scale deformation in the absence of vegetation (Massonnet & Feigl 1998). In contrast, longer wavelengths like L-band are able to penetrate through vegetation minimising volume decorrelation effects and are more likely to interact with the ground surface. However, L-band data is less sensitive to small-scale deformation features.

DInSAR measurements are also influenced by the polarisation of the signal (Engelbrecht & Inggs 2013). SAR sensors can collect data at different polarisations and either transmit or receive these horizontally (HH) or vertically (VV). VV polarisation has been found to interact more strongly with vegetation (Zalite et al. 2016). For that reason, HH polarisation is preferred, since the signal has improved penetration capabilities that can penetrate through vertically orientated vegetation and have a strong return from the ground (Engelbrecht et al. 2014). HV and VH polarisation experience the most significant decorrelation in the presence of vegetation and should be avoided for detecting subsidence.

In addition to the presence of vegetation, any landcover change causes signal decorrelation. This effect is increased by the increasing time frame between image acquisitions (known as the temporal baseline) (Engelbrecht et al. 2014). The temporal baseline between two acquisitions should be long enough to detect the deformation phenomenon of interest (Hanssen 2005). However, temporal baselines that are too long can be associated with significant changes at the surface. Therefore, to avoid temporal decorrelation, temporal baselines should be as short as possible (Hanssen 2005).

The spatial baseline between two image acquisitions is another important sensor limitation. Spatial baseline decorrelation is related to the orbital separation or interferometric baseline between two satellite orbits (Osmanoğlu et al. 2015). If the orbital separation between two image

acquisitions is larger than the critical baseline, then there will be total decorrelation (Osmanoğlu et al. 2015). The critical baseline is the theoretical maximum value for an interferometric pair of images for which the phase contributions of surface targets would no longer be correlated (Engelbrecht, Inggs & Makusha 2011). Another important parameter is the height of ambiguity, which is an indicator of the topographic sensitivity of the interferogram (Colesanti & Wasowski 2006). The height of ambiguity is the change in elevation that would result in a phase change of one fringe and is dependent on the perpendicular baseline of the sensor. There is low sensitivity to the topography if the ambiguity height is large and high sensitivity if the ambiguity height is small. Therefore, for the accurate retrieval of deformation, a larger ambiguity height (low sensitivity to topography) is preferred. An external source of elevation data such as a DEM could remove the topographic phase contribution. However, if there are errors present in the DEM, these are likely to propagate to the differential interferograms, and residual topographic phase contributions will still be present.

The pixel resolution of the scenes dictates the minimum size of deformation features detectable using conventional repeat-pass interferometry. For conventional dInSAR techniques interferometric measurement is meaningless on a single pixel because it can include noise in an unpredictable way. The successful interpretation of features depends on the structure of the image as well as the agreement of several neighbouring pixels (Massonnet & Feigl 1998). Furthermore, a geophysical phenomenon is difficult or impossible to recognise unless it is at least 10 pixels wide. For large deformation features, low spatial resolution SAR sensors such as Sentinel-1A (~15 m resolution) are suitable for monitoring deformation over time. However, for small-scale deformation features, which happen more gradually, higher resolution data is needed.

Advanced approaches have been developed to address the limitations of conventional dInSAR techniques. One such techniques known as Persistent Scatterer Interferometry (PSI), allows the detection of submillimetre movements of the ground at locations characterised by stable natural or man-made reflectors (Engelbrecht & Inggs 2013; Prati, Ferretti & Perissin 2010). When using PSI, one scatterer may dominate the reflected signal and greatly reduce decorrelation of the signal. However, in vegetated non-urban areas, the density of these persistent scatterers is generally low. This limits the ability to extract deformation measurements in vegetated areas of interest (Section 1.4).

### 2.2.2 **Deformation monitoring using SAR**

Several studies have shown the ability to successfully detect deformation due to mining activities using conventional differential SAR interferometry (dInSAR) techniques. The effectiveness of using multi-sensor SAR data was used to monitor mining induced subsidence. Ge, Chang & Rizos (2007) used ERS-1/2, JERS-1, RADARSAT-1 and ENVISAT satellites to monitor mine subsidence in a region with seven active mine collieries. Results of the study showed that for monitoring using longer wavelengths (in this case JERS-1) for mine subsidence is more robust in the presence of vegetated or agricultural cover. It is also more suitable for areas that are experience a high rate of ground deformation (Ge, Chang & Rizos 2007). This was in accordance with Wegmüller et al. (2004) where mining induced subsidence was monitored using L-band SAR images to resolve the limitations of C-band data. Three deformation features were easily identified in areas where mining was ongoing, including two forested areas that C-band interferogram could not identify. This suggests that at longer wavelengths the decorrelation is reduced and fewer image acquisitions may be needed to map the surface displacement that C-band acquisitions may not detect (Wegmüller et al. 2004).

The conventional dInSAR approach was used to monitor very fast mining-induced subsidence in the Upper Silesian Coal Basin in Poland using TerraSAR-X data (Przylucka et al. 2015). A total of 28 differential interferograms were generated, identifying 31 subsidence troughs in a 900 $km^2$ area for an 11 month period. The high spatial resolution and short revisit time of TerraSAR-X allowed for the detection of up to 245 mm of displacement in 54 days and up to 660 mm of cumulated displacements for certain subsidence troughs (Przylucka et al. 2015). In the study, it was assumed that a subsidence trough triggered by underground mining suffers the greatest deformation in its central part. Taking this into account most of the deformation signals present decorrelation in the central area and this could be attributed to the magnitude of the displacement. A possible reason is that this magnitude was beyond the detection threshold of the TerraSAR-X sensor, which is half of the wavelength of X-band sensors (1.5 cm). This study recommends the use of longer wavelengths such as C-or L-band sensors. The same phenomenon was observed in Engelbrecht et al (2013), where dInSAR techniques were used to detect deformation in mining areas that were vegetated using L-band ALOS PALSAR data. The results showed that L-band data could successfully detect deformation, however due to the availability of L-band data, it was recommended that for routine monitoring C-band data should be considered. It was noted that C-band data are used for the measurement of deformation; the maximum detectable deformation will only be 2.8 cm per pixel. This means that deformation

measurements at the centres of subsidence basins may be inaccurate where the actual deformation exceeds this rate (Engelbrecht et al. 2013). These studies showed the advantages of using longer wavelengths to detect mining-induced subsidence. They found that shorter wavelength data is more sensitive to small-scale deformation typically associated with backfill settlement in open-pit mines. Therefore, longer wavelengths may not be suitable for the quantification of backfill settlement rates (Section 2.1).

There have been limited studies that have used dInSAR to monitor subsidence in open-pit mines. In open-pit mining, large slope failures are preceded by measurable displacement (Szwedzicki 2001). Herrera et al. (2010) used an advanced dInSAR technique known as the coherent pixel technique to map slope instabilities in an open-pit mining area in Spain, using historical ERS-1/2 and ENVISAT data. This technique isolated the contributions of the different terms that contribute to the interferometric phase. The open-pit mine was monitored for two periods 1998-2000 and 2003-2009. Deformation rates varied between -2.4 mm and -8.2 mm per year. This was validated in the field and the radar deformation showed agreement with the computed instabilities.

A study used RADARSAT-1 data to detect slope instabilities in a block cave of an open-pit mine in Phalaborwa, South Africa (Woo et al. 2012). This was used with ground-based geodetic data to calibrate a model that modelled the cave breakthrough of the pit wall. The comparisons of the displacements modelled and those observed by dInSAR were in agreement and the results indicated that dInSAR techniques provide an additional degree of confidence for the model that was used (Woo et al. 2012). In fact, displacement magnitudes predicted by numerical models were approximately 20% lower than those seen in from the dInSAR measurements (Woo et al. 2012). This finding was significant because the study then used RADARSAT-2 for the period 2009-2010 to detect surface displacement. The subsidence predicted by the model closely fitted the dInSAR measurements during the same period. Geodetic data showed more variability than the dInSAR measurements. This could be due to the point-by-point approach that geodetic methods undertake. This variability has the potential to trigger false alarms or give misleading trends (Woo et al. 2012). Following this study, later work included polarimetric interferometry (POLInSAR) techniques to overcome decorrelation when in the presence of vegetated areas. Dong et al. (2015) conducted a spatio-temporal analysis of ground subsidence due to underground coal mining in Huainan China. ALOS PALSAR images were acquired from 2007 to 2010 and interferometry revealed a ground subsidence rate of 15 cm per year.

The ability of dInSAR to map ground deformation with centimetre to millimetre precision over large areas at a fraction of ground truth costs has stimulated the adoption of dInSAR techniques for ground deformation monitoring (Samsonov, d'Oreye & Smets. 2013). However, these techniques have not been applied to quantify backfill settlement. Therefore, the results could aid in understanding backfill settlement rates in open-pit mining, as well as the process of post-mining rehabilitation efforts.

## 2.3 **Mine revegetation and monitoring**

Mining activities have severe environmental consequences such as vegetation deterioration, soil erosion, geological hazards and environmental pollution, which restricts the sustainable development of mining areas (Chen et al. 2017). Furthermore in the process of surface mining, vegetation cover, and drainage patterns are disturbed over large areas (Brom et al. 2012). Practices that remove the vegetative material prevent the addition of organic matter into the soil and this leads to the reduction of soil fertility and the deterioration of soil structure, water holding capacity and biological activities (Mensah 2015) After backfilling is completed, revegetation commences. For open-pit mining the revegetation process commonly involves the removing of the topsoil and the storing it for when rehabilitation commences. Once the area has been backfilled with the backfilled material (which is known as the overburden and is made up of the rock strata above the coal seam), the material is shaped to something similar to the original landscape profile (Nazare 2005). This area is then reseeded with a mixture of grass species (Nazare 2005). To rebuild the resilience of a disturbed ecosystem, it is critical to restore as many aspects of natural vegetation as possible (Makineci, Gungor & Kumbasli 2011). Therefore, the revegetation of the undisturbed vegetation in the site and how it this process succeeds needs to be known.

Until recently, mines have not been very successful in returning land to its pre-mining agricultural productivity, especially large, rehabilitated open-pit mines (Limpitlaw et al. 2005). This is partially due to a lack of understanding about the replacement of topsoil and vegetation sustainability (Limpitlaw et al. 2005). Preservation of land capability can only be achieved by managing and monitoring resources (Limpitlaw et al. 2005). It is important to re-evaluate the health and productivity of planted species and monitor the progress of rehabilitated land until the vegetation is sustainable (Erener 2011). Revegetation of the area is considered sustainable when the vegetation in the area is self-supporting. Irrespective of mining regulations, the ability to interpret early signs of rehabilitation success or failure is desirable for management. Long-term monitoring of rehabilitated sites can facilitate an assessment of the ecological development of the

rehabilitation over time and also provide data to help determine the success and sustainability of rehabilitated communities (Vickers, Gillespie & Gravina 2012). Section 2.3.1 provides several revegetation monitoring approaches. Sections 2.3.2 and 2.3.3 introduce the use of remote sensing to monitor revegetation.

### 2.3.1 **Revegetation monitoring approaches**

Conventional field and laboratory measurements have been used to monitor the progress of rehabilitation until the vegetation is self-supporting. These include sampling sites for analysis of landscape integrity, examining soil surface indices (soil stability index, soil infiltration index and nutrient index) and assessing revegetation dynamics (Erener 2011). Research conducted in Australia assessed the development of rehabilitated grasslands on a mined open-pit by means of in situ ecological monitoring for a period of three years (Vickers, Gillespie & Gravina 2012).

Rehabilitated areas were compared to reference sites that had not been adversely impacted by mining. Results indicated that the total cover of rehabilitation sites was similar to those of the reference sites, but that the herbaceous biomass did not increase with increasing rehabilitation age (Vickers, Gillespie & Gravina 2012). The study emphasised that continued monitoring and analysis of rehabilitated sites will, in time, help determine the rate at which these sites are progressing towards their intended post-mining land-use. Similarly, forest tree species on rehabilitated sand mine in Australia were ecologically monitored (Audet et al. 2013). The sites were monitored on an annual basis from 2005 to 2010. The general rehabilitation outlook appeared promising, but older sites appeared to deviate to natural vegetation species in the area. Future studies would benefit from an in depth spatio-temporal analysis to verify ecological mechanisms on a finer scale (Audet et al. 2013). Another method that has been used to monitor the performance of rehabilitated land-cover is Ecological Function Analysis (EFA) which was developed by the Commonwealth Scientific and Industrial Research Organisation (CSIRO) (Randall 2004). This field-monitoring approach uses simple indicators to assess how well a landscape is working based on three core parts. These include: 1) landscape function analysis, 2) vegetation and structure composition and 3) habitat complexity (Randall 2004). This method was used to compare post-mining rehabilitation samples to samples representing both pre-mining native forests and reference sites representing potential landscape analogues (Gould 2012). The results indicated that the vegetation established in post-mining rehabilitation does not resemble the pre-mining native forest in composition and structure, nor does it resemble the potential landscape analogue land units. Disadvantages of EFA are that it relies on physical monitoring

and may lead to human error if there is no consistent training. Additionally, the scale and location of transects may be an issue as they may include a very small section of an entire rehabilitated landform. Data may only show that a site is progressing to a self-supporting state yet, on a large landform, there may be areas that are underdeveloped (Randall 2004)

Methods such as in situ ecological monitoring and EFA may be suitable for small-scale monitoring, but they are inefficient at a regional scale (Karan, Samadder & Maiti 2016). Additionally, although rehabilitation is a long-term process, mining regulations require short time frames for assessing rehabilitation success (Gould 2012). With ground-based techniques, this will be inefficient and costly over large areas. Therefore, to overcome these difficulties remote sensing systems such as the use of satellite imagery have been used more frequently to assess and monitor various types of vegetation changes (Felinks, Pilarski & Wiegleb 1998).

### 2.3.2 **Optical remote sensing for vegetation monitoring**

There has been an increasing availability of remotely sensed images due to the rapid development of remote sensing technology in the last decades (Xie, Sha & Yu 2008). Remote sensing techniques offer an opportunity to monitor vegetation in a practical and economical means particularly over large areas (Xie, Sha & Yu 2008). This is important in surface mining and rehabilitation monitoring as repeated measurements at frequent intervals are required (Petropoulos, Partsinevelos & Mitraka 2013). Well-established methods have been derived to obtain information about vegetation in post-mining landscapes from both optical and SAR remote sensing techniques (Brom et al. 2012; Karan, Samadder & Maiti 2016). The main advantages of remote sensing are its ability to cover large areas, high temporal frequency and its lower cost compared to ground-based techniques and monitoring. Furthermore, spatial and temporal change can be monitored at various scales (Felinks, Pilarski & Wiegleb 1998).

Investigating vegetation properties has been widely reported in remote sensing applications. It has been established that monitoring the evolution of the physical characteristics of crops is of interest for both correct resource utilisation planning and timely availability of information about environmental changes (Ferrazzoli et al. 1997). Several studies have confirmed the ability of remote sensing for monitoring post-mining landscapes. For example, it has been used for land cover classification of post-mining landscapes (Felinks, Pilarski & Wiegleb 1998), change detection of vegetation in coal waste dumps (Brom et al. 2012), and assessing the condition of revegetation on rehabilitated mines with the use of vegetation indices (Erener 2011; Huete et al. 1997; Jiang et al. 2008). However, the assessment of the vegetation health of reclaimed or

rehabilitated areas is often limited. This is due to the difficulties in discriminating between the types of vegetation species and separating the naturally vegetated and the revegetated areas using multi-temporal data sets. A study conducted by Felinks, Pilarski & Wiegleb (1998) assessed the vegetation of a coal mining area with a combination of satellite optical data (Landsat TM), airborne optical data (CASI-data) and ground-based techniques. The study highlighted the fact that remote sensing techniques can provide exhaustive information since the whole area was investigated. However, this may not show what is truly on the ground and therefore ground-truth data is needed to quantify the vegetation on the ground. The environmental effects and decrease of natural vegetation caused by open-pit mining activities were identified from NOAA-AVHRR and Landsat satellite imagery (Latifovic et al. 2005). Similarly, Koruyan et al (2012), using Landsat and ASTER satellite imagery, demonstrated the effect of areal expansion of marble quarries and the subsequent changes in vegetation. Results showed a reduction in natural vegetation as the open-pits expanded and that natural revegetation would take several years to restore without human-induced restoration.

Another well-established method to assess the changes in vegetation is the use of multispectral data. Multispectral optical sensors can easily distinguish the basic distribution of green vegetation, which can be related to the photosynthesis of plants (Shao & Zhang 2016). Furthermore, multispectral vegetation indices have been widely used to perform vegetation classifications and the estimate of biophysical parameters (Shao & Zhang 2016). The definition of vegetation indices is dimensionless, ratio- based measurements computed from a combination of spectral characteristics (Asner et al. 2003). Vegetation indices define transformation of data to maximise sensitivity to the parameter of interest whilst minimising sensitivity to other terms. Vegetation indices can be computed directly without any bias or assumptions regarding land cover class, soil type or climatic conditions (Huete et al. 2002).Vegetation indices can be related to characteristics such as vegetation canopy, a composite property of leaf chlorophyll, leaf area, canopy cover and structure (Jiang et al. 2008).

Vegetation indices were first introduced by Tucker & Sellers (1986). They found that the arithmetic combinations of vegetation reflectance in the red and near infrared regions of the electromagnetic spectrum are useful to distinguish vegetation (Atzberger 2013). Today the Normalized Difference Vegetation Index (NDVI) is one of the most well-known and more frequently used indicators of vegetation cover, particularly the presence and condition of green vegetation (Limpitlaw 2006). Research conducted in Turkey used Landsat TM images to monitor and evaluate the vegetation condition of a rehabilitated mine (Erener 2011). Several vegetation

indices were calculated and indicated that there was an increase in vegetation from 1987 to 2006. NDVI was used to assess the progress in rehabilitation in old, closed collieries in KwaZulu-Natal, South Africa (Limpitlaw 2006). The study indicated that there was a significant increase in the spectral response associated with vegetation present on the old coal dumps and that this could be directly correlated with rehabilitation success (Limpitlaw 2006). A change detection study undertaken by Brom et al. (2012) used satellite data to assess vegetation cover, moisture properties and the surface temperature of a brown coal dump from 1984 to 2009. These were evaluated using NDVI for vegetation cover and the Normalized Difference Moisture Index (NDMI) derived from Landsat 5 and 7 imagery. Results indicated that there was an increase in surface temperature and a decrease in NDVI and NDMI after the removal of vegetation cover pre-mining. The study showed the importance of the effective planning of rehabilitation for mining areas (Brom et al. 2012).

Although NDVI provides researchers with a way to monitor vegetation, it has a tendency to saturate in high leaf areas and is sensitive to background reflectance (Rocha & Shaver 2009). This is a limiting factor when applied to areas where vegetation is dense and there are a variety of crops (Huete et al. 1997). The Enhanced Vegetation Index (EVI), which is considered to be a modified NDVI, was developed to improve the sensitivity of the vegetation index in areas of high biomass and to reduce atmospheric influences (Matsushita et al. 2007; Morse-Mcnabb, Sheffield & Clark 2013). EVI measurements incorporate the blue band into the calculation of the band ratio. However, this does not provide additional biophysical information on vegetation properties, but is aimed at reducing noise and uncertainties associated with atmospheric effects (Jiang et al. 2008). The Moderate Resolution Imaging Spectroradiometer (MODIS) Land Discipline Group adopted the improvement of the EVI as the second global-based vegetation index for monitoring the Earth's terrestrial photosynthetic vegetation activity. It has gained the attention of many researchers (Matsushita et al. 2007). A comparative study was shown by Karan, Samadder & Maiti (2016), where NDVI and EVI were used to monitor reclamation success in coal mine degraded areas for land cover classification. Results showed that NDVI and EVI achieved similar results and are complementary vegetation indices. Huete et al. (2002) suggested that although NDVI is sensitive to chlorophyll, EVI is more responsive to the canopy structural variations, including the leaf area index (LAI), canopy type and architecture.

Even though, optical methods have been extensively used to monitor vegetation changes over large areas, limitations such as cloud cover or inclement weather can be problematic for long-term observations, particularly in tropical regions (Engelbrecht, Kemp & Inggs 2013). This is

significant for this study because the area of interest falls within the Mpumalanga Region of South Africa that is prone to summer rainfall during the peak of the growing season (Section 1.4). The all-weather condition, day/night capability of SAR sensors provide an opportunity to overcome the limitations associated with cloud-cover in optical data (Engelbrecht, Kemp & Inggs 2013).

### 2.3.3 **Vegetation monitoring using SAR**

Space-borne SAR data provides an opportunity to monitor vegetation because unlike optical remote sensing techniques, SAR systems are active (microwave) sensors that operate at low frequencies and result in microwaves penetrating vegetation. These microwaves interact with the structural and dielectric properties (related to the water content) of the vegetation as a function of the wavelength of the sensor (Moreira et al. 2013). SAR sensors have the ability to capture data despite the presence of cloud cover, fog, smoke, or dust (Massonnet & Feigl 1998). This has an operational advantage over optical sensors especially for time-critical applications (Lopez-Sanchez & Ballester-Berman 2009). The challenge of using SAR to monitor vegetation is to establish robust relationships between the physical characteristics of the crops and the recorded SAR signal (Lopez-Sanchez & Ballester-Berman 2009).

Various studies have demonstrated the potential of evaluating SAR backscatter for vegetation monitoring particularly in agricultural landscapes (Formaggio, Epiphanio & dos Santos Simoes 2001; McNairn et al. 2014; Shang et al. 2009). Crop parameters can be estimated from radar backscattering measurements when optimum sensor configurations are used (frequency, incidence, and polarisation). The recorded backscatter is a function of several physical properties such as soil surface moisture, surface roughness, vegetation biomass and moisture and the orientation of the vegetation with respect to the SAR look direction, which refers to the direction in which the radar antenna is transmitting a pulse or receiving the return signal (Karjalainen, Kaartinen & Hyyppä 2008).

Research has been conducted to study the correlation of different crop parameters with radar observables such as radar backscatter and interferometric coherence, as well as to analyse the temporal evolution of such observables. (Lopez-Sanchez & Ballester-Berman 2009). Previous studies have shown that shorter wavelength SAR (e.g., X-band and C-band) is capable of producing useful relationships with vegetation parameters when using interferometric or physical-based SAR methods (Main et al. 2016). In the early 2000s, McNairn et al. (2002) assessed the use of RADARSAT-1, SPOT and IRS-1C imagery to map different crop types and

provide information about their condition. The results were used to assess the implications of the crop growth stage for monitoring with the use of SAR imagery. The results suggested that multi-date RADARSAT-1 imagery used with or without optical imagery provided accurate information about crop growth. However, the recorded backscatter was shown to be sensitive to crops with similar canopy structure and could potentially induce confusion when differentiating between similar types of crops such as grain crops (McNairn et al. 2002). More recently, Navarro et al. (2016) assessed the complementary nature of using optical and SAR data for crop parameter retrieval (in particular basal crop coefficient and the length of the crops development stages) and crop type classification. NDVI, derived from SPOT-5 and dual (VV, VH) polarisation backscatter from Sentinel-1A, was used to compute the parameters. There was a significant correlation between NDVI and backscatter and the authors suggested that in areas where there is persistent cloud cover, SAR data could replace optical data. Despite this recommendation, the results showed that it is difficult to properly identify the crop growth stage due to an incomplete data set and emphasised the importance of a high temporal resolution for vegetation monitoring.

The sensitivity of SAR backscatter signatures for crop biophysical parameters has also been investigated. Multi-temporal TerraSAR-X, ENVISAT and PALSAR data acquired at various incidence angles and polarisations was used for sugarcane crops monitoring (Baghdadi et al. 2009). In this study, backscatter was compared to NDVI derived from SPOT 5 imagery. Results suggested that co-polarised (HH, VV) were more highly correlated to the detection of sugarcane harvest than cross-polarised data (HV, VH). Furthermore, the study revealed that there was a strong correlation between backscatter and NDVI as a function of sugarcane parameters. In another study, backscatter from multi-frequency (X-, C- and L-band) SAR data at multi-polarisations for corn and soybean fields was investigated. The relationship between SAR backscatter, LAI and soil moisture was modelled (Jiao et al. 2010). The study revealed that LAI measurements showed a correlation with longer wavelengths, such as L-and C-band, and correlated poorly with the shorter wavelength X-band. This was expected because shorter wavelengths such as X-band provides little penetration with the canopy of the crops (Jiao et al. 2010). Furthermore, the study also highlighted that the highest correlations were reported for HH and HV data for L- and C-band data. Similarly, Ferrazzoli et al. (1997) found that biomass exhibits high correlations with the HV channel at C-band at shallower incidence angles for crops such as colza, alfalfa and wheat. These findings suggest that polarimetric SAR could provide more information for vegetation studies. However, the presence of signal saturation effects disables the biomass estimation of other crops such as corn, sunflower and sorghum (Ferrazzoli

et al. 1997). This phenomenon is reported in McNairn et al. (2002) where HH data at C-band saturates when crops are 1 m high.

Unlike single polarisation, data polarimetric SAR obtains scattering echoes from several polarimetric channels and thus provides richer information (Ji & Wu 2015). Polarimetric decomposition algorithms are used to separate the backscatter signals into elementary scattering contributions. The most common elementary scattering mechanisms are surface, volume and double bounce (Moreira et al. 2013). For vegetation canopies, scattering behaviour can be expected to be related to overall biomass, as well as crop structure (McNairn et al. 2009). Cloude and Pottier (1996) proposed a method to extract average scattering mechanisms from experimental data using a smoothing algorithm based on second-order statistics known as the entropy (H), anisotropy (A) and alpha (α). The Cloude-Pottier decomposition (H-A-α) is based on the assumption that there is always a dominant "average" scattering mechanism in each cell of the image (Lee & Pottier 2009). This method has attracted a considerable amount of attention and has been widely analysed, improved and applied in segmentation, classification and detection applications (Ji & Wu 2015).

Fully polarimetric SAR data and the H-A-α decomposition was used to investigate the relationship between various phenological stages of crops and the change in their scattering behaviour over time (Engelbrecht, Kemp & Inggs 2013). The results showed that scattering mechanisms observed on fully polarimetric RADARSAT-2 data could provide information regarding the peak of the growing season. They also indicated that although information can be derived from multispectral data, the H-A-α decomposition can provide information about the characteristics of the surface of the vegetation (Engelbrecht, Kemp & Inggs 2013).

Although SAR polarimetry has demonstrated that it can provide more information about the scattering mechanisms of vegetation, some decomposition algorithms rely on the use of fully polarimetric SAR data. Full and dual polarisations are two typical operational modes of polarimetric SAR. The fully polarimetric mode measures, a scattering matrix containing the full scattering information of a target (Ji & Wu 2015). For many SAR sensors, such as Sentinel-1A, dual polarisation is frequently used as the operational mode. However, H-A-α decomposition has previously been used to analyse fully polarimetric data. The H-α decomposition was investigated using 21 SAR dual-polarised datasets acquired by six different SAR sensors (Ji & Wu 2015). Results from this study indicated that due to the lack of co-polarisation in dual-polarisation SAR, there is no separation in surface, dipole and multiple scattering and this does not adequately

extract scattering mechanisms. Therefore, co-polarisation is vital for extracting scattering mechanisms. Since Sentinel-1A data is freely available, this could be a limitation when using polarimetric decompositions for vegetation monitoring.

While backscatter and polarimetric SAR parameters have been extensively applied, particularly using C-band radar data, the use of interferometric coherence for vegetation monitoring is limited. Coherence is an estimate of the phase stability of imaged targets in the time between two SAR acquisitions (Weydahl 2001). This means that if the ground surface is undergoing changes caused by moisture changes such as irrigation, thawing, or vegetation being harvested or ploughed there will be a decrease in coherence (Weydahl 2001). Furthermore, coherence will decorrelate if there is a significant change in the volume or biomass of vegetation such as dense shrubs and forested areas (Weydahl 2001). This suggests that an inverse correlation between vegetation biomass and interferometric coherence may be exploited to monitor the health and productivity of vegetation. Coherence provides a unique way to qualify and quantify agricultural change due to its ability to measure phase-level correlations between image pairs (Kemp & Burns 2016).

The potential use of one-day interval coherence derived from pairs of ERS-1/2 SAR tandem acquisitions for crop monitoring was assessed by Blaes & Defourny (2003). This 1-day offset increased the probability of having a high coherence between the two image acquisitions due to temporal decorrelation effects. The study mentioned above assessed three objectives, namely, 1) the correlation between plant height, canopy cover, and coherence, 2) the prediction of wheat crop height, and 3) the influence of soil moisture and backscatter on coherence. The results indicated that there was a strong correlation between the plant height, canopy cover and coherence, but that these were dependent on the geometric crop factors. Another study evaluated the use of polarimetric and interferometric coherence derived from bistatic TerraSAR-X for monitoring phenological changes of various crop types in Iran (Mirzaee et al. 2015). The results indicated that coherence derived from co-polarised HH and VV data could successfully distinguish different crop types. However, interferometric coherence had a relatively constant behaviour with fluctuations mainly related to baseline variations. Sentinel-1A interferometric coherence was related to mowing events on grasslands by Tamm et al. (2016). The results indicated that after mowing events, coherence in VH and VV polarisation was higher than before mowing the grasslands.

Even though interferometric coherence can be used to assess changes in vegetation, various parameters can affect coherence measurements. Both changes in land surface conditions and in soil moisture or surface roughness decreases in interferometric coherence. This needs to be considered when using interferometric coherence as a predictor of vegetation conditions. Soil moisture was found to strongly decrease coherence in a study that used coherence to retrieve crop parameters (Blaes et al. 2003). Furthermore, a decrease in coherence tends to increase with an increase in the time between acquisitions (Engelbrecht & Inggs 2016). Additionally, decorrelation effects are pronounced over short time periods where there are random changes in both the bio- and geophysical properties of the vegetation (Engelbrecht & Inggs 2016).

Studies have also used empirical modelling approaches such as machine learning to predict biophysical parameters using SAR data. An advantage of machine learning is that it can be used for numerous types of data and has been proven to produce reasonable relationships for small and large datasets (Tahsin et al. 2017). Random Forest (RF) is one of these modelling approaches used to investigate the relationship between SAR parameters and biophysical parameters. RF is an ensemble machine-learning algorithm that has proved to be a robust model capable of capturing the complexity of non-linear relationships, and it is seldom affected by problems of overfitting (Breiman 2001). RF is a decision tree based method that can be used for classification and regression. It consists of an ensemble of multiple decision trees, or a set of conditions that produce individual predictions which are aggregates into a single prediction combining the average of all the predicted values (Tahsin et al. 2017). RF produces a variable importance which gives an indication of which parameters contribute little information to the analysis and therefore it is possible to identify which variables provide the highest predictive capability (Horning 2010). An advantage of using RF for regression is that is not very sensitive to the parameters used in the models and using variable importance makes it efficient where a large number of predictors are used. One limitation of using RF for regression is that it is not possible to predict beyond the range of the response values in the training data. Therefore it is recommended that the training data includes samples that cover the entire range of response variables (Horning 2010).

The relationship between savannah woody vegetation cover and volume and Envisat ASAR C-band SAR backscatter was explored using multiple linear regression and RF (Main et al. 2016). Airborne LiDAR data was used to validate the predictive SAR models for total cover and total canopy volume. The results of the study showed that the RF model produced a higher accuracy than the multiple linear regression method. The results of the RF model also indicated that there

was an underestimation in high cover areas and an overestimation in low cover areas (Main et al. 2016). One possible reason for the underestimation is that C-band signals have limited ability to penetrate dense vegetation (Main et al. 2016). This was also noted by Shao & Zhang (2016) when the predictive ability of RADARSAT-2 backscatter and vegetation indices derived from Landsat 8 (OLI) to estimate above-ground biomass forest vegetation was tested. Various machine-learning algorithms were used and although the objective of the study was not to compare algorithms, the study showed that RF outperformed the other tested approaches. Concluding remarks were that C-band SAR data have a weaker penetration through vegetation than longer wavelength radar, such as L-band. This could lead to a negative effect on capturing vertical vegetation structure information, especially in dense vegetation coverage areas (Shao & Zhang 2016).

# 3 METHODS AND MATERIALS

To explore the contribution of remote sensing technology to the success of monitoring open-pit rehabilitation strategies, several sources of remote sensing data were obtained for further processing and analysis. The analysis focused on two distinct components 1) monitoring backfill settlement dynamics and 2) monitoring the success of revegetation strategies. Section 3.1 and Section 3.3, respectively, discuss each of these two data and analysis approaches adopted for the investigation.

## 3.1 Backfill settlement dynamics

Although in situ measurements of backfilled areas provide high precision measurements, it is often practically impossible to implement the monitoring of expansive areas over long periods of time (Section 2.2). For this reason, dInSAR techniques were adopted for this investigation. This section outlines the methods and materials used to detect and measure surface deformation associated with backfill settlement using dInSAR techniques. Section 3.1.1 provides a brief description of all the SAR imagery and ancillary data. Thereafter Section 3.2 outlines the conventional dInSAR processing sequence and this forms the first component of the research design as illustrated in Section 1.3.

### 3.1.1 Data collection

A vast number of satellites hosting sensors capable of capturing SAR data have been collecting data since 1992. The space-borne sensors available for research purposes capture data on one of three wavelengths namely X-band (~ 3 cm), C-band (~ 5 cm) or L-band (~ 23 cm). Mining and backfilling have been taking place in the area of interest for an extended period of time, since the early 2000s. The archives of all available satellite sensors were, therefore, considered a good source of data. This would allow for the investigation of settlement dynamics and the quantification of settlement rates over time and space. To gain access to the data archives, a proposal was submitted to the European Space Agency (ESA) under their Cat-1 initiative. The proposal was accepted and this provided access to archived ERS-1 and ERS-2, and ALOS PALSAR data (Section 3.1.1.1 and Section 3.1.1.2). Furthermore, access was not only provided to the archived data but to the new acquisitions of TerraSAR-X data as well (Section 3.1.1.3). Finally, ESA's Copernicus Programme provided open access Sentinel-1A data. Sections 3.1.1.1 to 3.1.1.5, respectively, provide a description of each of the data sets and the dates of data acquisitions.

### 3.1.1.1 ERS-1/2

The European Remote Sensing satellite (ERS-1) was ESA's first Earth Observation satellite and was launched in July 1991. The first results demonstrating its interferometric capability were published in September of 1992 (Ferretti et al. 2007). ERS-2, an identical satellite to ERS-1, was launched in 1995. Both SAR sensors have a 25 m spatial resolution and a 35-day revisit time. The sensors captured data at C-band and in single polarisation VV mode. ERS-1 captured data until 2000 and ERS-2 ceased operations in 2011. A search of the archives revealed that a large number of scenes were available for the area under investigation All images were captured in VV polarisation. The dates of image acquisition as well as if they were acquired in the wet and dry seasons for the study area are summarised in Table 3.1.Table 3.1

Table 3.1 Acquisition dates and polarisation for ERS-1 and ERS-2 data

| **Dates** | **Wet(W)/Dry(D) season** | **Polarisation** | **Date** | **Wet(W)/Dry(D) season** | **Polarisation** |
|---|---|---|---|---|---|
| 1995/12/02 (ERS-2) | W | VV | 2008/08/11 (ERS-2) | D | VV |
| 1996/01/05 (ERS-1) | W | VV | 2008/11/24 (ERS-2) | W | VV |
| 1996/03/15 (ERS-2) | W | VV | 2008/12/29 (ERS-2) | W | VV |
| 1996/05/25 (ERS-1) | D | VV | 2009/05/18 (ERS-2) | D | VV |
| 2002/09/21 (ERS-2) | D | VV | 2010/02/06 (ERS-2) | W | VV |
| 2008/04/12 (ERS-2) | D | VV | 2010/03/29 (ERS-2) | W | VV |
| 2008/06/02 (ERS-2) | D | VV | 2010/05/03 (ERS-2) | D | VV |

### 3.1.1.2 ALOS PALSAR data

The ALOS satellite is a Japanese Earth-Observation satellite developed by JAXA and launched on 24 January 2006. The Phased Array type L-band Synthetic Aperture Radar (PALSAR) is an active microwave sensor that can capture data in single polarisation (HH or VV), dual polarisation (HH/HV or VV/VH), or quad polarisation (HH, HV, VH and VV) mode. The spatial resolution is 10 m for Fine Beam Single polarisation (FBS) and Fine Beam Dual (FBD) polarisation scenes while quad polarisation productions have 30 m resolution scenes. The repeat cycle (temporal resolution or temporal baseline) for ALOS PALSAR data is 46 days. The ALOS PALSAR data was acquired at different polarisation modes and Table 3.2 summaries the dates of

data acquisition and polarisation modes and whether this image was captured in the wet or dry season for the area of interest.

Table 3.2 Dates and polarisation for ALOS PALSAR data

| Date | Wet(W)/Dry(D) season | Polarisation | Date | Wet(W)/Dry(D) season | Polarisation |
|---|---|---|---|---|---|
| 2007/01/27 | W | HH | 2008/12/17 | W | HH |
| 2007/07/30 | D | HH/HV | 2009/02/01 | W | HH |
| 2008/01/30 | W | HH/HV | 2009/08/04 | D | HH/HV |
| 2008/05/01 | D | HH/HV | 2009/12/20 | W | HH/HV |
| 2008/06/16 | D | HH/HV | 2010/04/08 | D | HH |
| 2008/08/01 | D | HH | 2010/05/24 | D | HH/HV |
| 2008/09/16 | D | HH/HV | | | |

#### 3.1.1.3 TerraSAR-X

TerraSAR-X was launched in June 2007 and is a German satellite that was developed in collaboration between German Aerospace Centre (DLR) and EAS Astrium (De Grandi et al. 2013). TerraSAR-X is an X-band sensor (wavelength ~ 3.41 cm) and consists of dual and quad polarimetric imaging capabilities. Fifteen new TerraSAR-X images were captured with a 22-day temporal baseline from 2016/05/17 and to minimise decorrelation effects, an 11-day temporal baseline was captured in the peak of the growing season. Archive data captured over a period of one year from 2008/11/16 to 2009/12/28 were also used. All the TerraSAR-X data was in Single Look Complex (SLC) format and captured in StripMap mode. The spatial resolution is approximately 3 m and all the imagery is dual-polarisation in HH and HV (Table 3.3).

Table 3.3 TerraSAR-X image acquisition dates and polarisation

| Date | Wet(W)/Dry(D) | Polarisation | Date | Wet(W)/Dry(D) | Polarisation |
|---|---|---|---|---|---|
| 2008/11/16 | W | HH/HV | 2016/05/17 | D | HH/HV |
| 2008/12/19 | W | HH/HV | 2016/06/08 | D | HH/HV |
| 2009/01/10 | W | HH/HV | 2016/06/30 | D | HH/HV |
| 2009/02/01 | W | HH/HV | 2016/07/22 | D | HH/HV |
| 2009/02/23 | W | HH/HV | 2016/08/13 | D | HH/HV |
| 2009/03/17 | W | HH/HV | 2016/09/04 | D | HH/HV |
| 2009/04/08 | D | HH/HV | 2016/09/26 | D | HH/HV |
| 2009/04/30 | D | HH/HV | 2016/10/18 | D | HH/HV |
| 2009/05/22 | D | HH/HV | 2016/11/09 | W | HH/HV |
| 2009/06/24 | D | HH/HV | 2016/11/20 | W | HH/HV |
| 2009/07/16 | D | HH/HV | 2016/12/01 | W | HH/HV |
| 2009/09/20 | D | HH/HV | 2016/12/12 | W | HH/HV |
| 2009/10/23 | D | HH/HV | 2016/12/23 | W | HH/HV |
| 2009/11/25 | W | HH/HV | 2017/01/03 | W | HH/HV |
| 2009/12/28 | W | HH/HV | 2017/01/14 | W | HH/HV |

#### 3.1.1.4 Sentinel-1A data

Due to the success of the ERS-1/2 and Envisat campaign and to ensure data continuity, ESA developed and launched the Sentinel-1A and Sentinel-1B SAR satellite constellation in 2014 and 2016, respectively. The Sentinel-1 mission consists of a constellation of two polar-orbiting satellites, capturing C-band synthetic aperture radar data. The satellites orbit at around 693 km and have a 12-day repeat cycle. SAR scenes can be captured at a variety of data acquisition modes, although for interferometric processing, the Interferometric Wide Swath mode with a spatial resolution of 20 m is used. Sentinel-1 provides dual polarisation (VV/VH) scenes. The dates of image acquisition for the area of interest are summarised in Table 3.4.

Table 3.4 Sentinel-1A image acquisitions and polarisation

| **Date** | **Wet(W)/Dry(D) season** | **Polarisation** | **Date** | **Wet(W)/Dry(D) season** | **Polarisation** |
|---|---|---|---|---|---|
| 2015/04/06 | D | VV/VH | 2015/11/20 | W | VV/VH |
| 2015/04/30 | D | VV/VH | 2015/12/02 | W | VV/VH |
| 2015/05/12 | D | VV/VH | 2015/12/14 | W | VV/VH |
| 2015/05/24 | D | VV/VH | 2015/12/26 | W | VV/VH |
| 2015/06/17 | D | VV/VH | 2016/01/07 | W | VV/VH |
| 2015/06/29 | D | VV/VH | 2016/01/19 | W | VV/VH |
| 2015/07/11 | D | VV/VH | 2016/01/31 | W | VV/VH |
| 2015/08/04 | D | VV/VH | 2016/02/12 | W | VV/VH |
| 2015/08/16 | D | VV/VH | 2016/02/24 | W | VV/VH |
| 2015/08/28 | D | VV/VH | 2016/03/07 | W | VV/VH |
| 2015/09/21 | D | VV/VH | 2016/03/19 | W | VV/VH |
| 2015/10/03 | D | VV/VH | 2016/03/31 | W | VV/VH |
| 2015/10/27 | D | VV/VH | 2016/04/12 | D | VV/VH |
| 2015/11/08 | W | VV/VH | | | |

#### 3.1.1.5 RADARSAT-2

The RADARSAT-2 satellite, launched by the Canadian Space Agency, is the follow-on to RADARSAT-1 whose mission terminated in April 2013. RADARSAT-2 is a C-band SAR satellite with multiple polarisation modes, including a quad polarimetric mode in which data from all four polarisations (HH, HV, VV and VH) are acquired (Table 3.5). The satellite consists of a sun-synchronous orbit with a 6 p.m. ascending mode and a 6 a.m. descending mode. It has a temporal resolution of 24-days, a spatial resolution of 10m in Stripmap mode and, more recently (all the images acquired from 2016/01/07), a 5 m resolution in the Extra Fine Mode.

Table 3.5 Image acquisitions dates and polarisation of RADARSAT-2 images (Stripmap Mode)

| **Date** | **Wet(W)/Dry(D) season** | **Polarisation** | **Date** | **Wet(W)/Dry(D) season** | **Polarisation** |
|---|---|---|---|---|---|
| 2014/08/21 | D | HH/HV | 2015/07/23 | D | HH/HV |
| 2014/09/14 | D | HH/HV | 2015/08/16 | D | HH/HV |
| 2014/10/08 | D | HH/HV | 2015/09/09 | D | HH/VH |
| 2014/11/01 | W | HH/HV | 2015/10/03 | D | HH/HV |
| 2014/11/25 | W | HH/HV | 2015/10/27 | D | HH/HV |
| 2014/12/19 | W | HH/HV | 2015/11/20 | W | HH/HV |
| 2015/01/12 | W | HH/HV | 2015/12/14 | W | HH/HV |
| 2015/02/05 | W | HH/HV | 2016/01/07 | W | HH/HV |
| 2015/03/01 | W | HH/HV | 2016/01/31 | W | HH/HV |
| 2015/03/25 | W | HH/HV | 2016/02/24 | W | HH/HV |
| 2015/04/18 | D | HH/HV | 2016/03/19 | W | HH/HV |
| 2015/05/12 | D | HH/HV | | | |

## 3.2 Differential SAR Interferometry data processing

To quantify backfill dynamics on the rehabilitated mine, all the SAR images described in Section 3.1.1 were processed using the conventional differential SAR interferometric processing. Interferometric SAR processing refers to the generation of an interferogram starting from a pair of images in SLC format. The general workflow, presented graphically in Figure 3.1, describes the standard differential interferometry processing sequence.

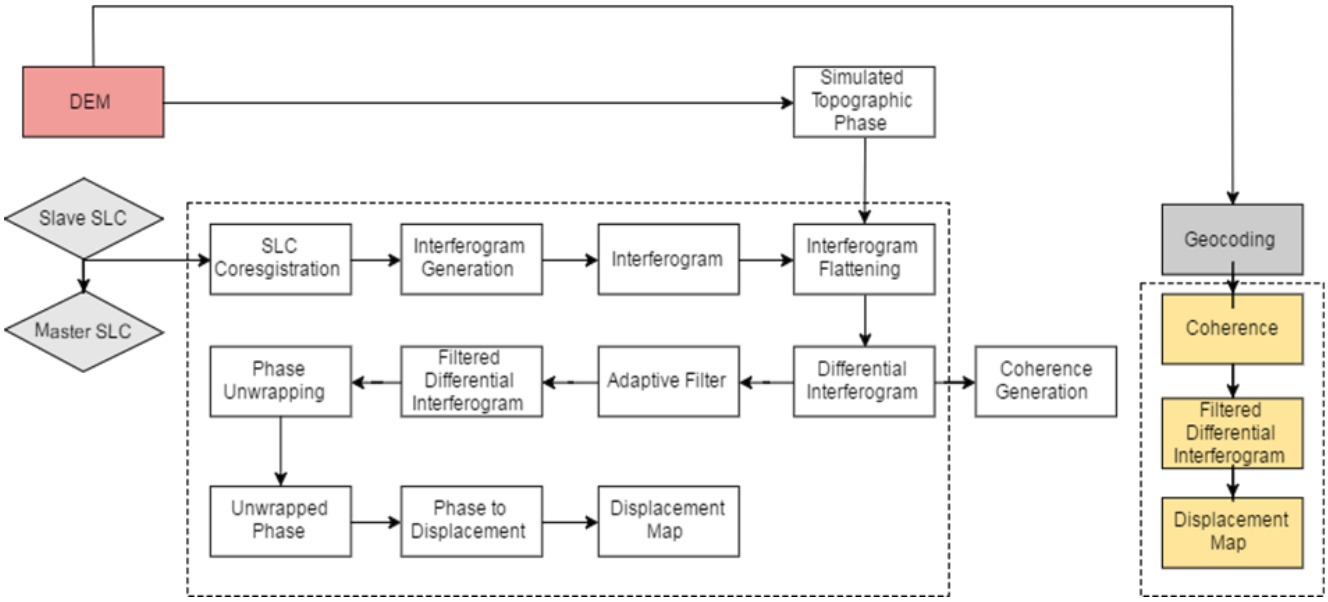


Figure 3.1 Differential Interferometric Processing workflow

The processing was performed using Gamma Remote Sensing software (Gamma Remote Sensing 2011). During the importing of the master and slave scenes the orbital state vectors for the SAR scenes, with the exception of the TerraSAR-X imagery, were updated. The orbital state vectors include the precise position and velocity of the satellite in an Earth centred Cartesian coordinate system. Updated precise orbital information is required to mitigate any further processing errors induced by orbital inaccuracies of the scenes. For TerraSAR-X data, the orbital state vectors imbedded in the SLC data are of high precision and, consequently, do not require additional updates.

Following importation, the resulting master and slave SLC images are coregistered to sub-pixel accuracy, which ensures that the corresponding pixels of the master and slave images match perfectly. Registration accuracies of 0.2 pixels or better are required to ensure that interferometric correlation is not reduced by more than 5% (Gamma Remote Sensing 2011). Following co-registration, a process of complex conjugation of the coregistered SLC scenes calculates an interferogram.

The resulting interferogram contains information about the change in phase between the master and slave scenes. These phase contributions include:

- a phase contribution due to the relative orbital separation of the two satellite positions at the time of data acquisition;
- the flat-earth phase due to the curvature of the earth's surface; and
- topographic variations within the scene.

Further phase contributions could be present due to surface displacements, atmospheric delays and phase noise (Ferretti et al. 2007; Massonnet & Feigl 1998). The Flat earth phase and the topographic phase were removed from the interferogram in a process known as interferogram flattening. The interferogram flattening phase involves the calculation of the synthetic topographic and flat-earth phase using information provided by an external digital elevation model. In this case, the external elevation source used the Shuttle Radar Topography Mission (SRTM) 1- arc second DEM at 30 m resolution. The synthetic phase essentially contains the low-frequency phase contribution due to topography as well as a constant phase contribution due to orbital variations between master/slave scenes. The synthetic phase is subtracted from the interferogram, resulting in a flattened, differential interferogram. The differential interferogram represents only phase information relating to surface displacement and possibly noise and atmospheric artefacts.

Adaptive filtering of the differential interferogram was performed to reduce the inherent phase noise that originates from either low signal-to-noise ratio or temporal decorrelation (Scheiber & Bothale 2002). The Goldstein adaptive filter was used with the minimum and maximum window sizes between three and nine respectively. The filtered differential interferogram contains phase values between 0 and $2\pi$ which is known as the wrapped phase. Each cycle between 0 and $2\pi$ is known as an interferometric fringe. Since the phase is a wrapped modulo $2\pi$, an integer number of $2\pi$ has to be added to each successive fringe cycle to recover the absolute phase difference across the scene (Gamma Remote Sensing 2011). This process is known as phase unwrapping. The Minimum Cost Flow (MCF) technique was used since it is considered to be robust (Gamma Remote Sensing 20). The unwrapped phase is considered the absolute phase variation between master and slave scenes.

Displacement maps can be generated from unwrapped differential interferograms and represents deformation in the Line of Sight (LOS) direction of the satellite. In this investigation, backfill settlement was assumed to be only in the vertical direction. For that reason, the LOS deformation was converted to vertical deformation using simple trigonometric transformation.

As an additional step in the processing sequence, a parameter known as interferometric coherence was calculated. Interferometric coherence is the cross-correlation between the phases of the master and slave scenes and is used to provide an indicator of the phase noise contained in the interferogram. The coherence product presents values between 0 and 1 with 0 indicating total decorrelation and 1 indicating complete correlation. Although the interferometric coherence is not needed explicitly in the interferometric processing, the data provides valuable ancillary information.

The differential interferograms, interferometric coherence and displacement maps were geocoded using the SRTM DEM to transform the imagery from SAR reference geometry to ground geometry for further processing and analysis. Each filtered differential interferogram and the corresponding displacement was then visually analysed for the presence of deformation features.

## 3.3 **Vegetation Monitoring**

The monitoring of vegetation dynamics using remote sensing technologies has reached a level of maturity where operational systems are built using the derived products. This creates an opportunity to study the vegetation dynamics on revegetated mining areas and compare them to the dynamics of the undisturbed vegetation in the surrounding areas. This will allow for the identification of anomalous changes in the health and productivity of revegetated areas compared to natural vegetation, and may be an indicator that additional intervention is required to ensure sustainability. Although multispectral techniques are generally employed and well established, recent contributions is the field of SAR and SAR polarimetry also indicate an ability to derive vegetation metrics from these datasets (Section 2.3.3). Since a large number of SAR scenes were obtained for the backfill settlement dynamics investigation, an opportunity existed to evaluate the contribution of SAR derived metrics to vegetation dynamics investigation.

This section provides details about the processing of both SAR and multispectral data for the monitoring of vegetation health and productivity. This forms the second component of the research design methods described in Section 1.3. This section is divided into two parts. Section

3.3.1 describes the data acquisition. Section 3.3.2 describes the processing sequences for deriving vegetation variables from both multispectral data (Section 3.3.3) and SAR data (Section 3.3.4).

### 3.3.1 **Data collection**

Both multispectral and SAR products were used to assess the contribution of remote sensing derived products for the monitoring of rehabilitated vegetation. Sentinel-1A data in VV/VH polarisation was used for a one-year period between 2015/08/16 and 2016/08/16 to investigate the ability of SAR data and its products to derive vegetation information ( Table 3.6.

Table 3.6). Previous investigations have shown that C-band data is expected to maximise the interaction with the vegetation structure (Section 2.3.3). Section 3.3.2 describes the SAR data processing and analysis approaches used to derive the vegetation metrics.

Landsat-8 OLI scenes were acquired from the U.S Geology Survey Landsat Earth Explorer for the time period corresponding, as closely as possible, to the dates that Sentinel-1A scenes was captured. The Landsat-8 imagery has a 30 m spatial resolution. Although Sentinel-1A data were collected for a one-year period, some Landsat-8 scenes were affected by cloud cover and could, therefore, not be used. Therefore, the investigation focused only on the cloud-free scenes available. The dates of Landsat-8 data acquisition corresponding to Sentinel-1A dates are provided in Table 3.6.

Table 3.6 Image acquisition dates for Sentinel-1A and Landsat 8 data

| ***Date of acquisition*** | | |
|---|---|---|
| **Sentinel-1A** | **Wet(W)/Dry(D)** | **Landsat 8 (OLI)** |
| 2015/08/16 | D | 2015/08/15 |
| 2015/08/28 | D | 2015/08/31 |
| 2015/10/15 | D | 2015/10/11 |
| 2015/12/02 | W | 2015/12/05 |
| 2015/12/26 | W | 2015/12/30 |
| 2016/01/07 | W | 2016/01/06 |
| 2016/01/31 | W | 2016/01/31 |
| 2016/03/07 | W | 2016/03/03 |
| 2016/03/31 | W | 2016/03/26 |
| 2016/04/12 | D | 2016/04/12 |
| 2016/05/30 | D | 2016/05/29 |
| 2016/06/11 | D | 2016/06/07 |

### 3.3.2 **SAR data processing**

Several products can be derived from SAR scenes that have been used to describe vegetation dynamics (Section 2.3.3). The metrics that can be derived from the dual-polarisation Sentinel-1A data include:

- SAR backscatter coefficient ($\sigma^0$) in both VV and VH polarisation;
- interferometric coherence for both the VV and VH polarisation; and
- polarimetric descriptors that can be derived from dual-polarisation data.

Since most polarimetric decomposition algorithms to derive volume scattering contributions require quad-polarisation data, the study was confined to the application of the dual-polarisation Cloude-Pottier (H-A-alpha) decomposition. The H-A-alpha decomposition provided the entropy (H) and alpha (α) parameters, both of which respond to vegetation structure. Where interferometric coherence is concerned, interferometric pairs were confined to pairs providing 12-day temporal baselines in order to minimise the potential negative effect of long temporal baselines and associated low coherence.

To derive the radar backscattering coefficient, the SLC scenes were radiometrically calibrated and normalised to derive backscatter coefficient ($\sigma^0$) for both the VV and VH polarisations (hereafter denoted as $\sigma^0_{vv}$, $\sigma^0_{vh)}$. All datasets, including $\sigma^0_{vv}$, $\sigma^0_{vh}$, coherence in VV and HH as well as H and α parameters were terrain corrected and projected to a common ground projection (UTM Zone 35 S) with a corresponding ground resolution of 14 m. The images were not over-sampled, however the images were multilooked with factors of one in azimuth and four in range. This was undertaken in order to derive square pixels.

### 3.3.3 **Landsat 8 optical data processing and derived products**

In this study, EVI derived from Landsat 8 optical data was used as a proxy for vegetation productivity. It should be acknowledged that although vegetation indices such as EVI have often been employed as proxies for individual and often land-cover-dependent vegetation parameters, models that use remote sensing data to estimate there parameters are subject to error and uncertainty (Glenn et al. 2008). The Landsat-8 data was acquired in Level 1 format, implying

that data were represented in digital numbers. Radiometric and geometric distortions inherent in Level 1 scenes were corrected through a process of atmospheric correction and orthorectification to allow for spatial and spectral comparisons (Muller 2016). The scenes underwent atmospheric correction with the use of the ATCOR 2 algorithm, which converts raw digital number data into the top of canopy reflectance using a Modtran-5 radiative transfer code (Richter 2009). Mid-latitude rural summer and winter atmospheric models were used depending on the date of the acquisition. The visibility was calculated based on the atmospheric model that was chosen and the elevation was kept constant at 1600 m above sea level.

Following the geometric and radiometric correction of the scenes, the Enhanced Vegetation Index (EVI) was calculated for all scenes. In this study, only the 2-band EVI was used and was formulated as follows (Jiang et al. 2008):

$$\text{EVI} = G \times \frac{NIR - RED}{NIR + RED + 1} \qquad \text{Equation 3.1}$$

Where $G$ is the gain or scaling factor = 2.5, and *NIR* is the near-infrared band and *RED* is the red band of the Landsat 8 data.

The resulting EVI datasets were assumed to be representative of the vegetation productivity for each pixel in the datasets and could be used to investigate vegetation dynamics in the area and time-period under observation.

### 3.3.4 **Modelling EVI from SAR observables**

The EVI values derived from Landsat-8 data are assumed to be representative of the vegetation productivity in each of the scenes. Although the maturity of multispectral vegetation indices is well advanced, the major limitation of these datasets for operational use is the presence of cloud cover. This makes the long term monitoring of vegetation dynamics challenging, especially in areas of persistent cloud cover. An opportunity consequently exists to assess the potential contribution of SAR derived variables for the monitoring of vegetative conditions.

To relate the SAR variables, including $\sigma^0_{vv}$, $\sigma^0_{vh}$, coherence in VV and HH as well as H and $\alpha$ parameters, to vegetation conditions, the variables were used as input into a RF algorithm in an attempt to model EVI values from the SAR variables. To achieve this, sample data of each SAR parameter as well as the EVI data were collected and used as training and testing datasets. The National Land Cover Map (2013/2014) was used to digitise training and test areas for both

undisturbed vegetation classes (grassland), and the rehabilitated vegetation on the mine. A total of 100 field boundaries were sampled for the undisturbed vegetation. Figure 3.2 shows the undisturbed vegetation field boundaries and the rehabilitated vegetation fields boundaries found in the mine area.

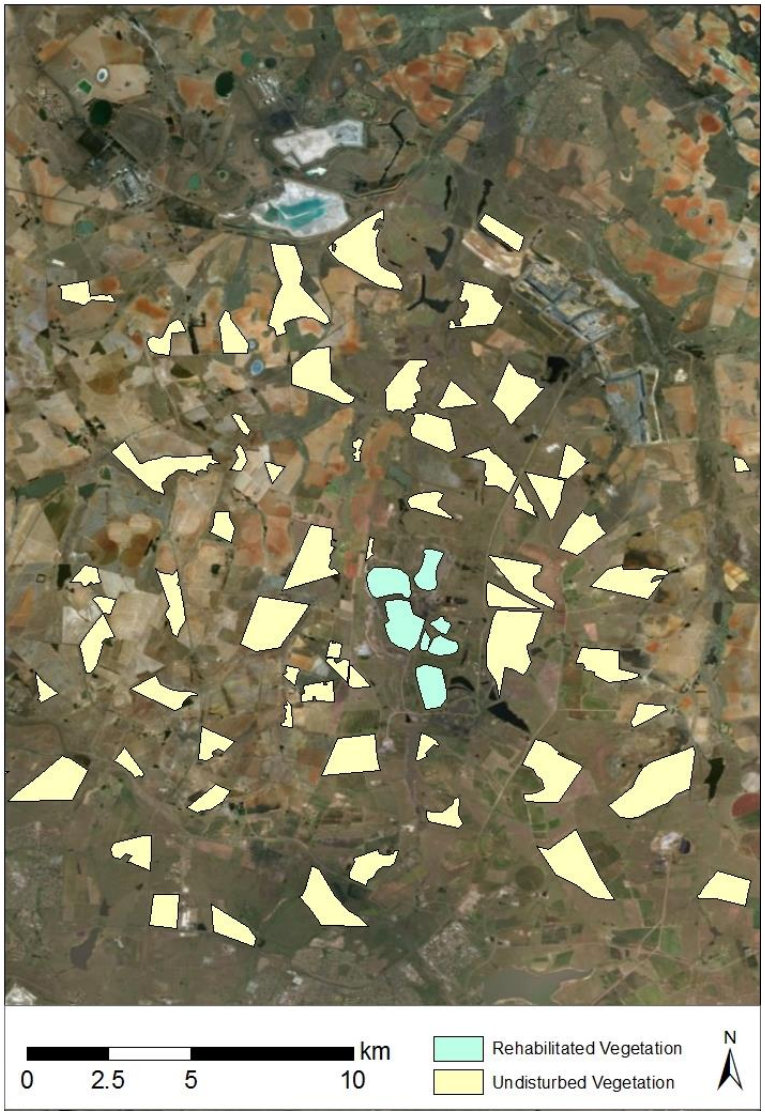


Figure 3.2 Fields boundaries for the undisturbed vegetation and the rehabilitated vegetation used for the vegetation modelling.

For each of the undisturbed vegetation and rehabilitated vegetation field boundaries the average EVI, backscatter for all polarisations, interferometric coherence, alpha and entropy polarimetric decompositions were extracted for each image acquisition date using zonal statistics. Since interferometric coherence is representative of decorrelation during the period between master and slave image acquisition, the coherence data could be used to model EVI either at master or slave image acquisition date. Both cases were investigated. This resulted in a total of eight SAR parameters that could be used as input. The average of the various SAR parameters for each field

boundary was used as input into the nonparametric RF algorithm to predict EVI for both the undisturbed natural and rehabilitated vegetation. The RF algorithm evaluated, the relative importance of each observable and determined its predictive capability. The algorithm was implemented using two main user-defined inputs: the number of decision trees (*ntree)* and the number of variables to be selected and tested for the best split when growing the trees (*mtry)*. The number of trees was set to 500 and the number of possible splitting variables at each node to the square root of the number of input variables, which is 2. RF was applied in the machine learning module of DELL Statistica, with 70% of the data being used for training and 30% of it being used for testing or validation.

The RF algorithm provides an indicator of relative importance for each SAR observable in predicting EVI depicted by computing an importance plot. The first implementation of the RF algorithm used all eight SAR observables as independent variables and EVI as the dependent variable for the undisturbed vegetation field boundaries only. Thereafter 346 different combinations of SAR parameters were used to assess the predictive capability. This was calculated as the maximum number of possible combinations of the SAR observables. To assess the predictive performance of the RF model, the adjusted coefficient of determination (adjusted $R^2$) was calculated for both the training and test data for each combination of predictors. The adjusted $R^2$ is a modified version of the $R^2$ that is adjusted based on the number of predictors in the model. The adjusted $R^2$ would only exhibit an increase if the new term improves the model more than would be expected by chance, whereas the $R^2$ would always increase if a new parameter was added and could never decrease (Obermayer 2009). The top ten different combinations that provided the highest adjusted $R^2$ were assessed. Of these, only the predictors that provided the highest adjusted $R^2$ were used to model EVI using SAR for the rehabilitated vegetation.

Table 3.7 Dates of the training datasets and the test datasets

| Training dates (Landsat 8) | Wet(W)/Dry(D) | Test dates (Sentinel-1A) | Wet(W)/Dry(D) |
|---|---|---|---|
| 2015/10/15 | D | 2015/08/15 | D |
| 2016/01/31 | W | 2015/08/28 | D |
| 2016/03/07 | W | 2015/12/02 | W |
| 2015/03/31 | W | 2015/12/26 | W |
| 2016/05/30 | D | 2016/01/07 | W |
| 2016/06/11 | W | 2016/07/05 | D |

Finally, to test the scenario where there is no or limited optical imagery available to model SAR EVI, representative images of optical imagery acquired in wet and dry seasons were chosen to train an RF model. Table 3.7 indicates which optical images were used to train the model and which SAR images were used for testing. The model was then tested on a combination of images found in the wet and dry seasons for both the undisturbed and rehabilitated vegetation. The results of the analysis are presented in Section 4.2.

# 4 RESULTS

The basic levels of rehabilitation require post-mining landforms to be stable, safe and sustainable. To overcome the limitations of field-based methods for monitoring post-mining rehabilitation, remote sensing techniques were used to monitor both the backfill settlement and revegetation. Differential SAR interferometry techniques have successfully detected and measured deformation in mining landscapes (Section 2.2). To quantify backfill settlement rates, dInSAR techniques were tested on multi-frequency SAR data. Deformation measurements were extracted for X-, C- and L-band SAR imagery and the results are presented in Section 4.1. Furthermore, revegetation practices need to be monitored until the land is deemed sustainable (Section 2.3). Both multispectral and SAR techniques were used to assess the proxies of vegetation productivity of revegetated areas. Section 4.2 describes the results of using these two remote sensing sources to monitor revegetation practices in the area of interest. EVI values for the revegetated areas on the mine were evaluated over a period of time and compared to the undisturbed vegetation surrounding the area (Section 4.2.1). Thereafter, SAR variables extracted over a period of time were used to predict EVI values for both the undisturbed and rehabilitated vegetation (Section 4.2.2). Finally, a comparison was made between the modelled EVI and optically derived EVI for both undisturbed vegetation and revegetated areas (Section 4.2.3).

## 4.1 **Backfill settlement observations**

The results of the dInSAR processing sequence, discussed in Section 3.2, include the differential interferogram, the displacement map and the coherence images. To better understand the backfill settlement dynamics experienced in the area over time and space, 25 random sample points were collected over the rehabilitated mine. The sampling of the 25 points used was a random sampling scheme that was digitised for the area of interest. Historical aerial imagery was used to assess which areas of the mine were revegetated and which areas were not. Figure 4.1 provides the distribution of the points in relation to the mine in question. The measured deformation for each point on each data set was extracted and the cumulative deformation over time was calculated. Note, however, that high confidence interferometric measurements are not possible for coherence values smaller than 0.3. For that reason, measurements exhibiting coherence values less than 0.3 were excluded from the analysis. Sections 4.1.1 to 4.1.3 respectively, present the results of the data processing for X-band, C-band and L-band data.

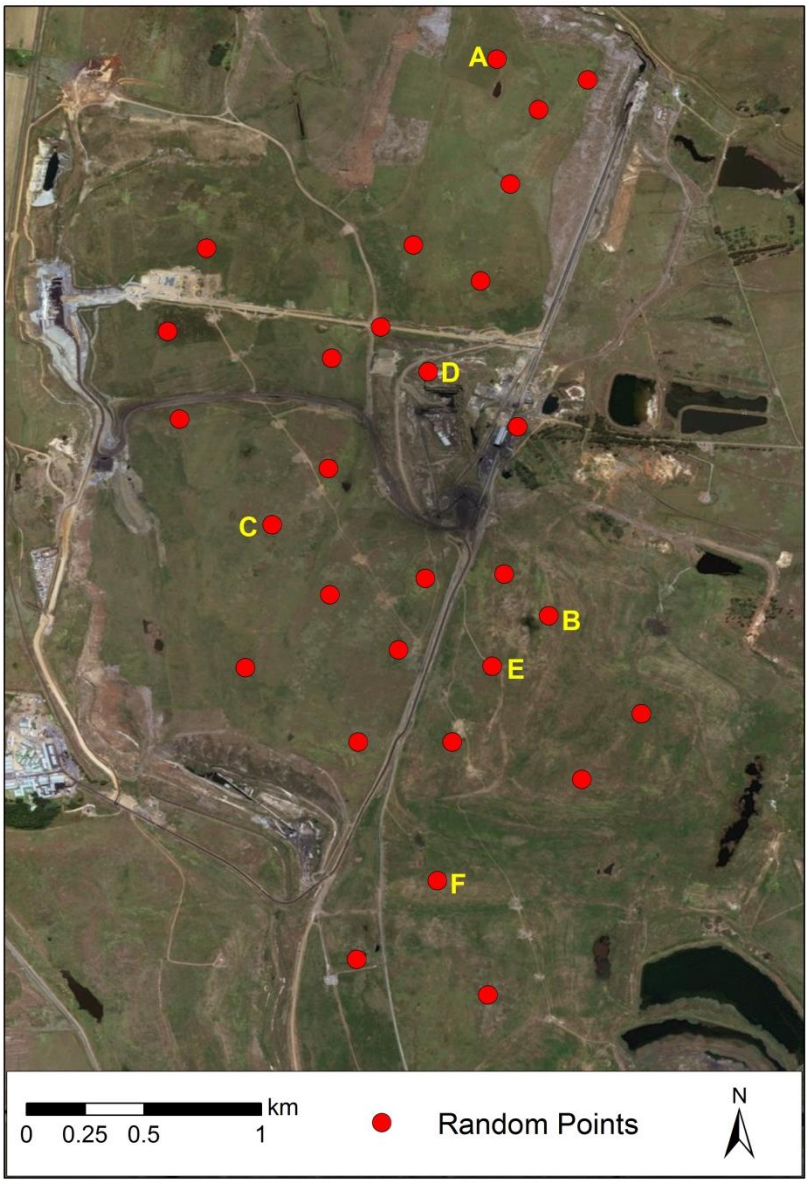


Figure 4.1 Random points selected to extract deformation measurements over the mine area

### 4.1.1 **X-band**

To detect and measure backfill settlement for X-band SAR data, 13 differential interferograms were produced from TerraSAR-X SAR scenes for the period 2008/11/16 to 2009/12/28 and 14 differential interferograms for 2016/05/17 to 2017/01/14. Once all the outputs were visually inspected, the displacement was extracted for the 25 random points (Figure 4.1). Figure 4.2 presents the time series of the TerraSAR-X differential interferograms. These images show the interferograms for the period between 2008/11/16 and 2009/11/25. The differential interferograms between 2016/05/17 and 2017/01/03 presented in Figure 4.3. For all the differential interferograms, the height of ambiguity, which is inversely proportional to the sensitivity to topography, is also shown.

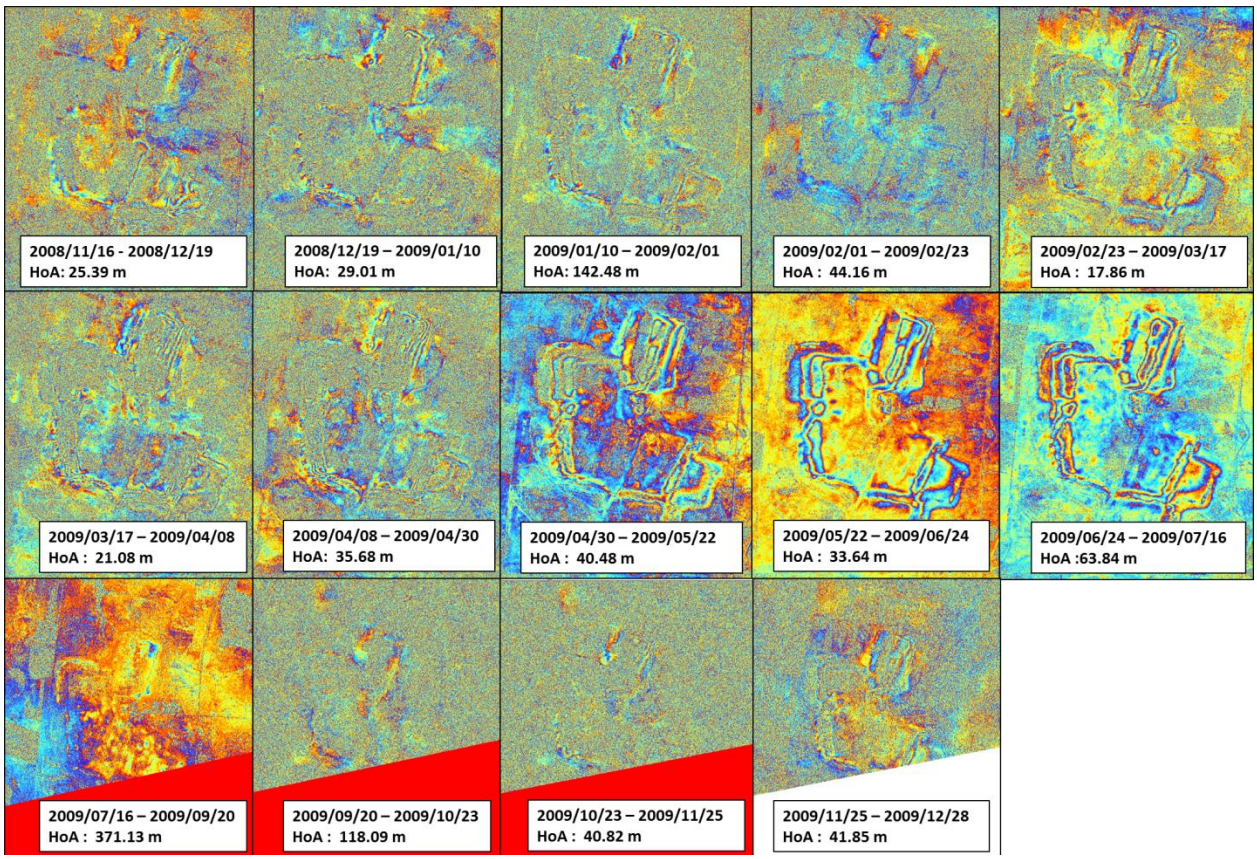


Figure 4.2 Time series of all differential interferograms for TerraSAR-X showing the height of ambiguity (HoA)

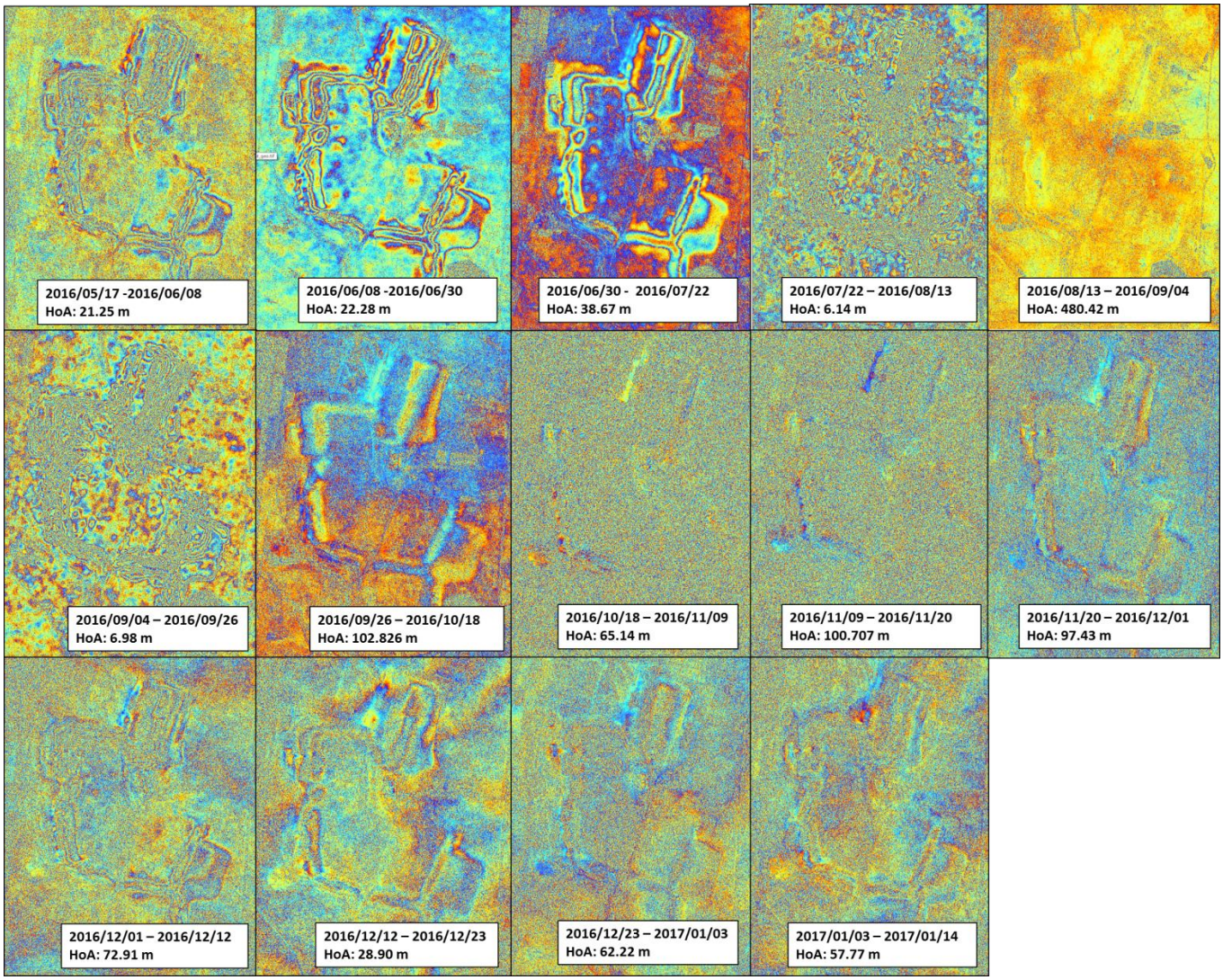


Figure 4.3 Time series of differential interferograms for TerraSAR-X for the period between 2016/05/17 and 2017/01/03

The visual inspection of all the X-band interferograms showed that residual topographic phase may be present in the differential interferograms. For each interferogram, the height of ambiguity is shown on the time series. Figure 4.2 and Figure 4.3 shows the amount of height change that leads to a $2\pi$ change in interferometric phase. If the height of ambiguity is large, there is a lower sensitivity to topography in the area. Therefore, if uncompensated topographic phase is present, then an increased height of ambiguity shows less topographic fringes than a smaller height of ambiguity. This is exhibited in the differential pair for the period 2016/09/04 to 2016/09/26 Figure 4.3 where the higher number of fringes is associated with a lower height of ambiguity (6.98 m). In contrast, there are very few fringes in the differential interferogram pair for the period of 2016/08/13 to 2016/09/04 because the height of ambiguity is large (480.42 m). The correlation between the height of ambiguity and the associated increase or decrease in

interferometric fringes provides evidence that uncompensated topographic phase is present. This would compromise our ability to derive accurate deformation measurements.

In addition to the uncompensated topographic phase, a speckle effect is present for several differential interferograms. The speckle noise is characteristic of a decrease in the phase coherence between interferometric pairs and is particularly evident in the presence of vegetation where land cover changes between image acquisitions occur. The noise introduced during the peak of the growing season is particularly evident for the differential interferograms produced between 2016/10/18 and 2017/01/15 (Figure 4.3). This will further compromise our ability to extract high confidence deformation measurements. These effects are explained further in Section 5.1.

Despite the uncertainties introduced by residual topography and speckle noise effects, the deformation measurements were extracted for each pair and the cumulative deformation was plotted over time for a subset of points exhibiting coherence values larger than 0.3. The cumulative deformation was extracted for points in revegetated areas (points A to C in Figure 4.4) and in areas that were not revegetated (points D to F in Figure 4.5). The maximum total deformation measured in revegetated areas was 0.84 cm (Figure 4.4) while areas that did not undergo revegetation exhibited a total of 0.39 cm deformation (Figure 4.5). For deformation points that were extracted from revegetated areas the cumulative deformation decreases in the winter season (May to August) and then increases during the start of the spring. Similarly, for the areas that were not revegetated the deformation rate decreases in winter then increases during the start of the growing season (Figure 4.5).

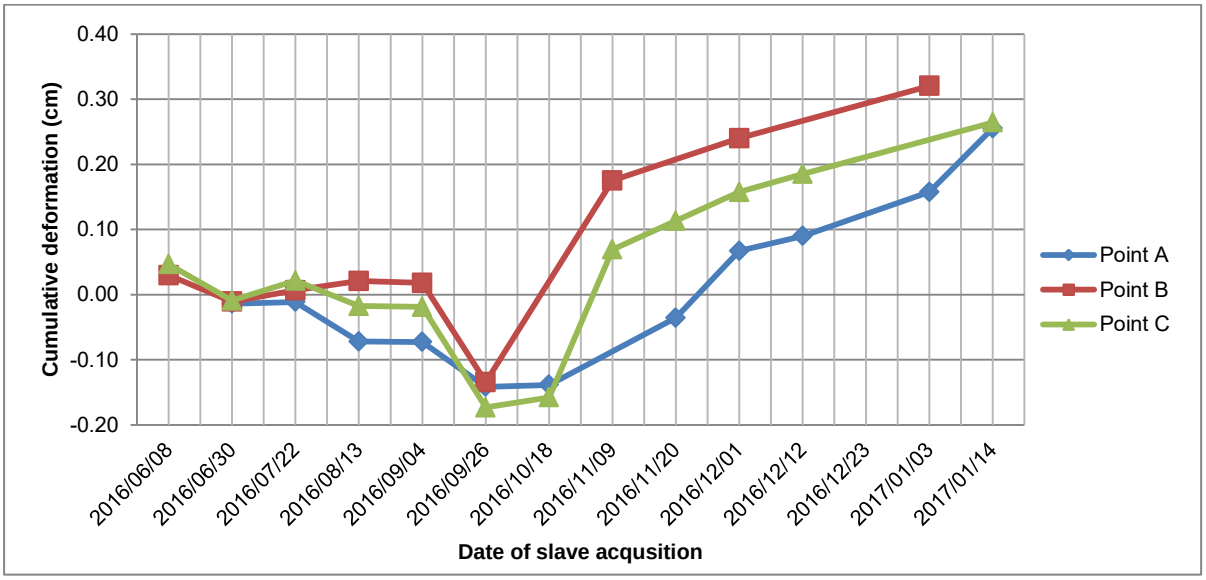


Figure 4.4 Example of cumulative deformation for three points extracted in revegetated areas

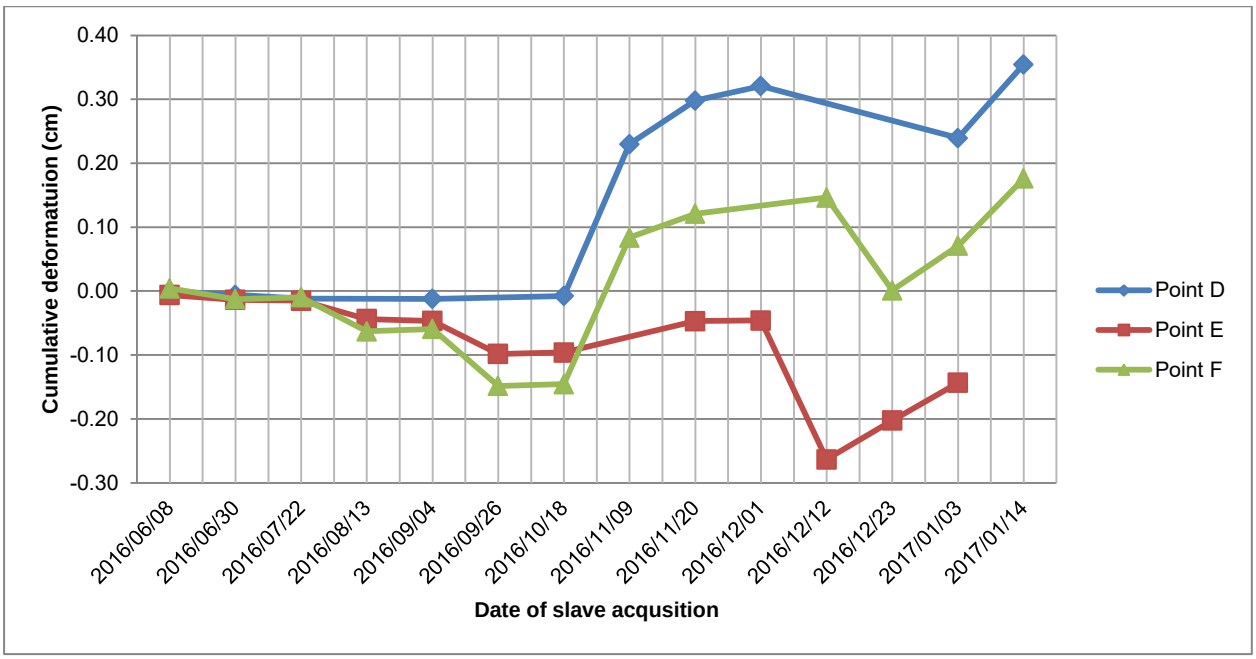


Figure 4.5 Cumulative deformation measured for points in the mine area that had not undergone revegetation

It should be noted that there are heave (also referred to as uplift) features recorded for some of the dates. This is shown by an increase in deformation. The heave features are recorded for the dates 2016/11/09, 2016/12/01, 2016/01/03 and 2016/01/14 for the revegetated area and for the period 2016/11/09 to 2017/01/14 for the un-vegetated areas. The total heave recorded for revegetated areas ranges between 0.06 cm and 0.32 cm while non-vegetated areas are associated with between 0.08 cm and 0.35 cm of heave. Although the results suggest that more heave is associated with non-vegetated areas, the cumulative deformation is higher. The observed heave is unexpected for backfill settlement observations and warrants further investigation. Potential causes for heave observation are explored further in Section 5.1.

### 4.1.2 **C-band**

C-band SAR data available for the study consisted of ERS-1/2, RADARSAT-2 and Sentinel-1A. The RADARSAT-2 scenes were captured in the period between 2014/08/21 and 2016/03/29, while Sentinel-1A scenes were processed from 2015/04/06 to 2016/04/12. ERS-1/2 data were captured between 1995/12/02 and 2010/05/03. However, it was observed that a large number of the images pairs were not interferometrically compatible due to the Doppler Centroid difference values that exceeded their critical centroid difference. For this reason, an assessment of the cumulative deformation for the period of ERS-1/2 could not be extracted.

The RADARSAT-2 data yielded 25 differential interferograms, while Sentinel-1A data yielded 17 differential interferograms. Figure 4.6 and Figure 4.7 respectively, displays the RADARSAT-2 and Senitnel-1A differential interferograms. The figures indicate the master and slave acquisition date for each differential interferogram and the height of ambiguity.

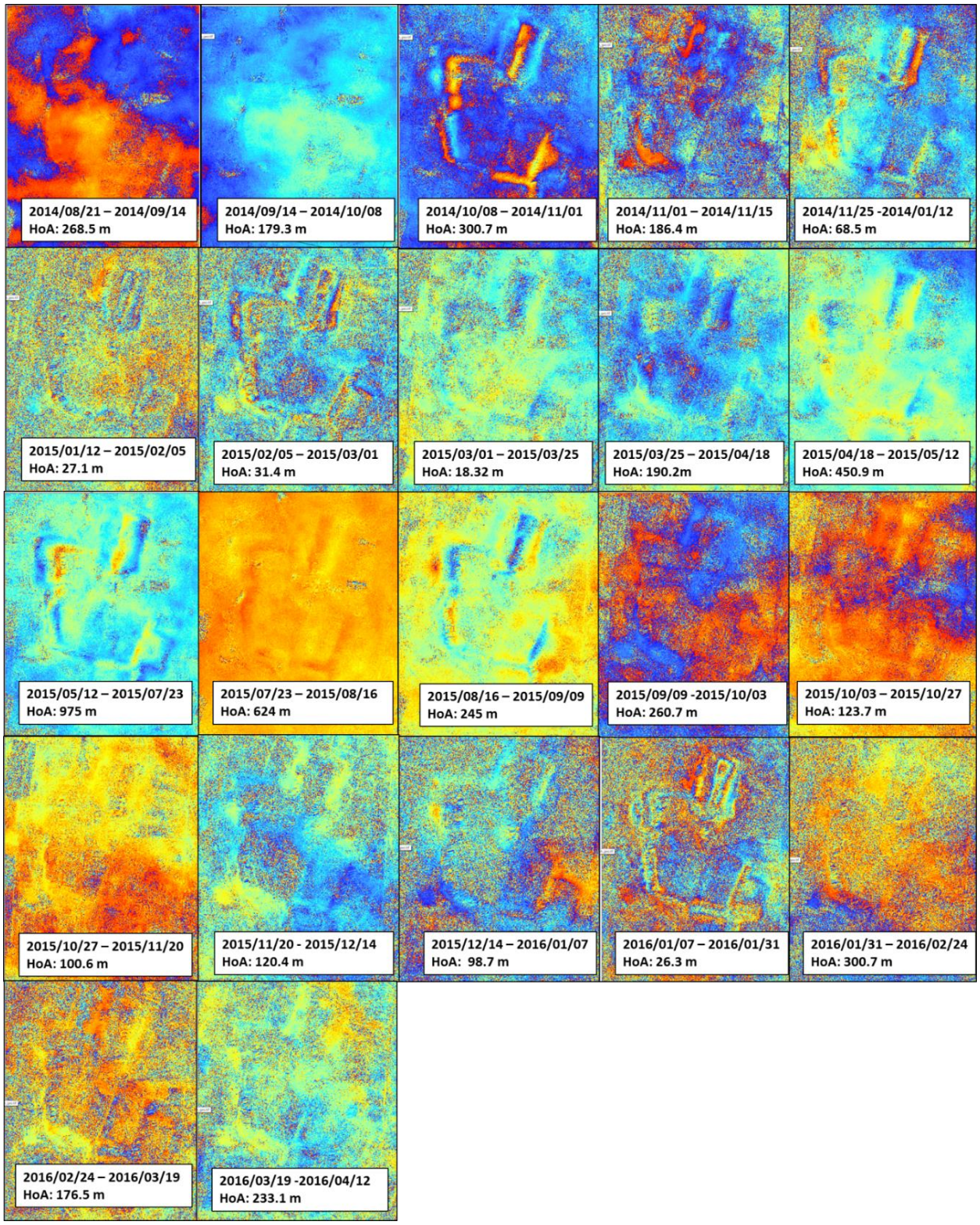


Figure 4.6 Time series of RADARSAT-2 interferograms

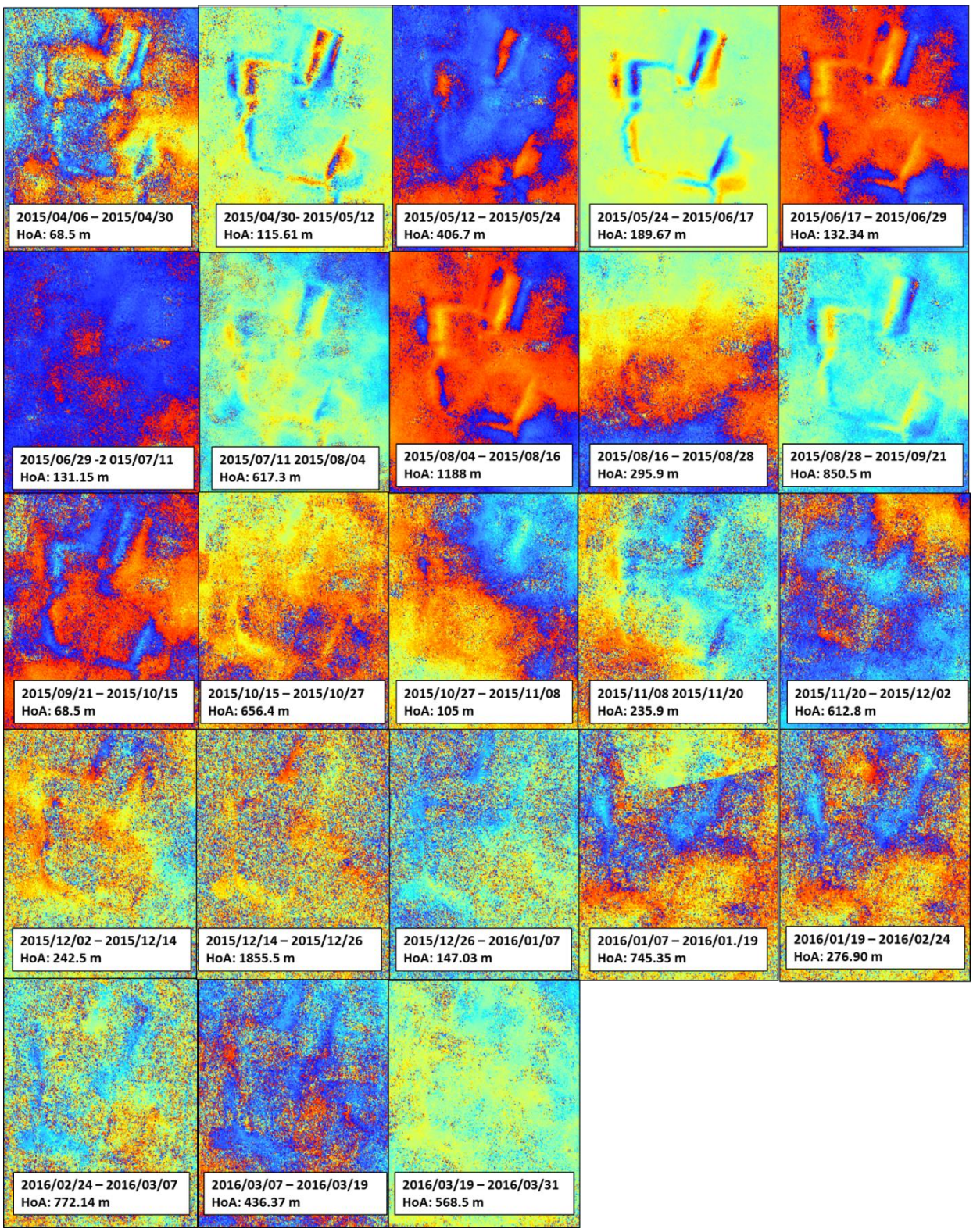


Figure 4.7 Differential interferograms for Sentinel-1A data

In assessing the time series of the RADARSAT-2 differential interferograms (Figure 4.6), residual topography is present for differential interferograms for date pairs, namely, 2015/01/12-2015/02/05, 2015/02/05-2015/03/01 and 2015/01/07-2016/01/31. This is associated with a smaller height of ambiguity ranging from 26.3 m to 31.4 m and an increased sensitivity to the topography of the area of interest. The differential interferogram for the date pair 2015/07/23-

2015/08/16 has a lower sensitivity to the topography, which is attributed to the large height of ambiguity (625 m). There is speckle in the differential interferograms for the date periods 2014/11/01 to 2014/03/25 and 2015/09/09 to 2016/03/19. This suggests that the presence of vegetation and vegetation growth may affect our ability to extract deformation measurements accurately. The temporal baseline for all the available RADARSAT-2 acquisitions is 24 days. The tie periods associated with the high speckle noise coincides with the peak of the growing season for vegetation in the area.

Figure 4.7 shows the Sentinel-1A differential interferograms. Sentinel-1A data were processed for approximately one year. Residual topographic phase contributions are evident particularly on pairs exhibiting low height of ambiguity values. The speckle noise is prominent in many differential interferograms, particularly for those generated over dates that fall in the peak of the growing season. The speckle noise effects are particularly evident for all Sentinel-1A interferograms generated between 2015/11/08 and 2016/03/31.

To assess the backfill settlement patterns for the C-band SAR data, the cumulative deformation was extracted for both sets of C-band data. The cumulative deformation for the random points for the RADARSAT-2 data for areas that had been revegetated and not revegetated are illustrated Figure 4.8 and Figure 4.9 respectively. Similarly, the cumulative deformation was extracted for Sentinel-1A (Figure 4.10 and Figure 4.11).

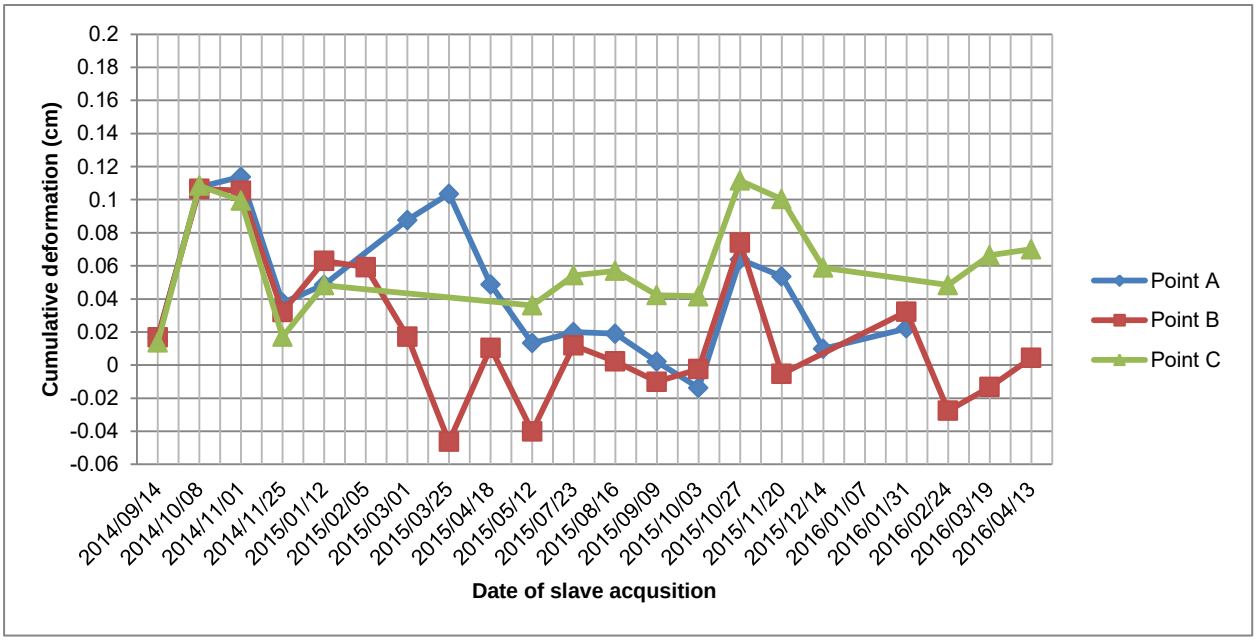


Figure 4.8 Cumulative deformation of points in revegetated areas for RADARSAT-2 data

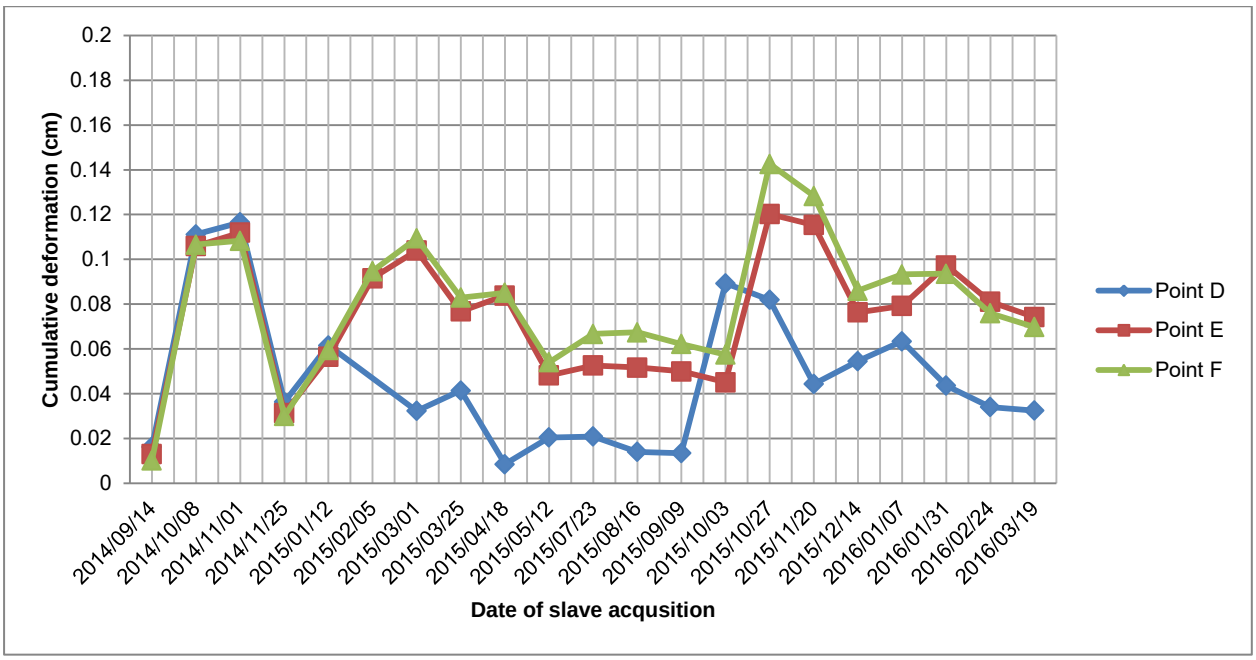


Figure 4.9 Cumulative deformation in areas that were not revegetated for RADARSAT-2 data

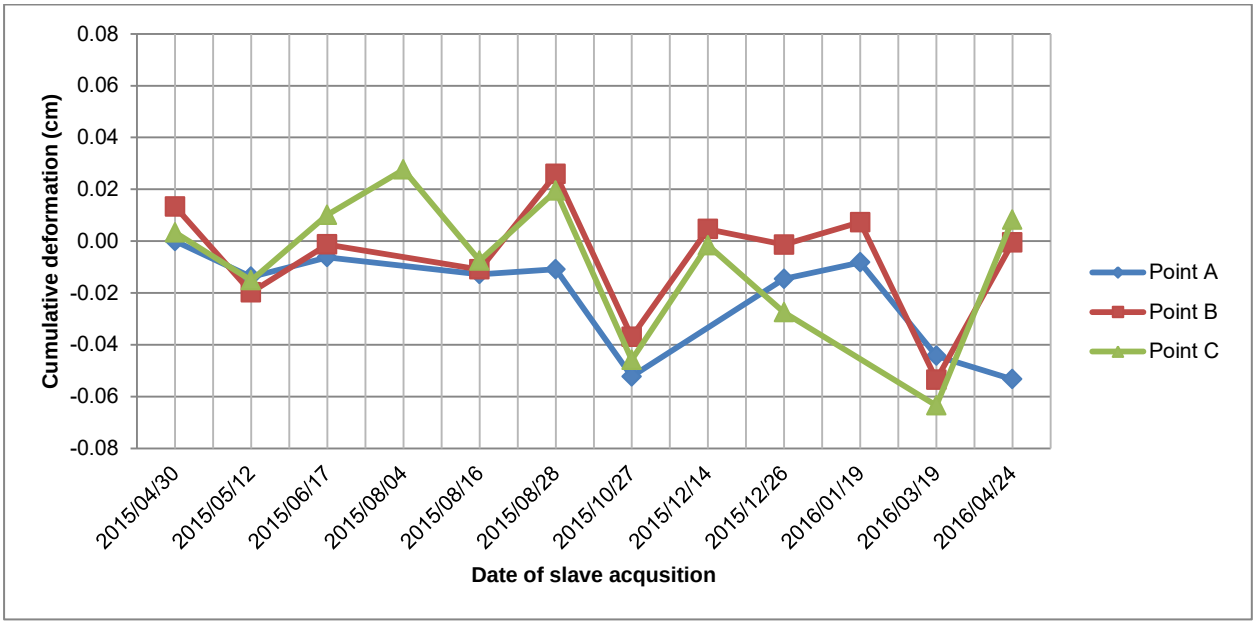


Figure 4.10 Cumulative deformation for points in revegetated areas for Sentinel-1A

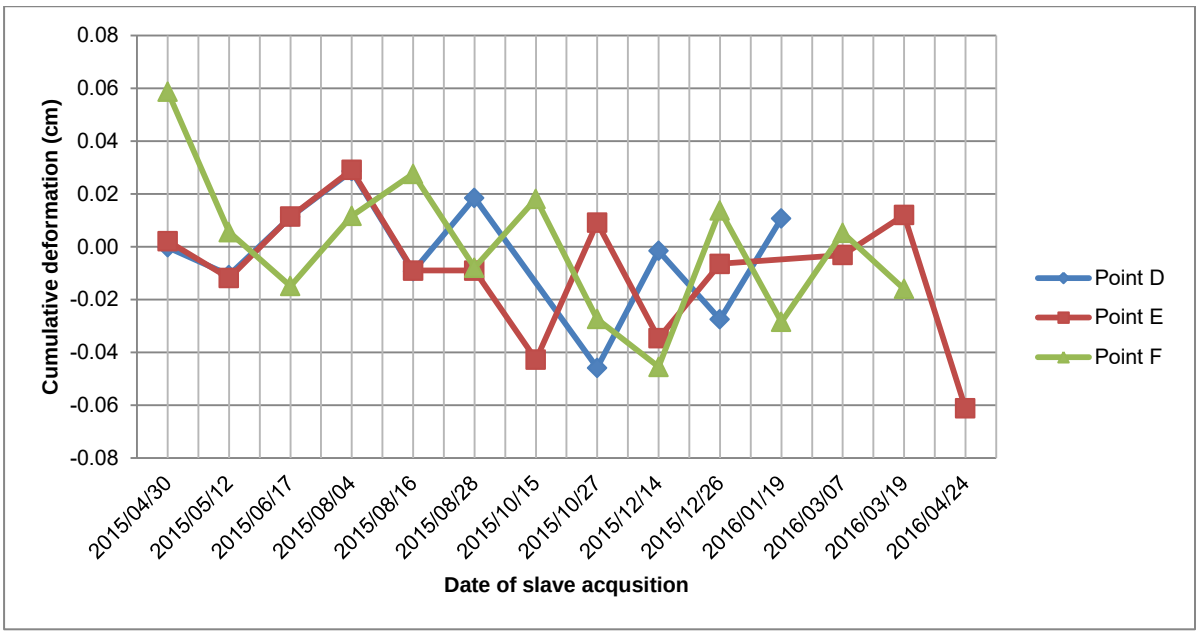


Figure 4.11 Cumulative deformation for points that were not revegetated for Sentine-1A

The surface deformation for the RADARSAT-2 data (Figure 4.8 and Figure 4.9) ranged between -0.05 cm and 0.14 cm with a total observed cumulative deformation of 0.27 cm. Similar to the TerraSAR-X results, several heave features were observed (which is indicated by an increase in cumulative deformation), most notably for the dates between 2014/10/08-2014/11/01, 2015/10/03-2015/10/27, 2015/10/27-2015/11/20 and 2016/01/31 to 2016/03/19. The measured surface deformation extracted for the Sentinel-1A scenes (Figure 4.10 and Figure 4.10) ranged between -0.06 cm and 0.06 cm with a total observed cumulative deformation of -0.12 cm. Similarly, to the RADARSAT-2 and TerraSAR-X results, several heave features were observed, most notably for the dates between 2015/08/04-2015/08/16, 2015/08/28-2015/10/03, and 2015/12/14-2016/12/26. The total cumulative deformation was compared for the points extracted from the vegetated areas and non-vegetated areas for both the RADARSAT-2 and the Sentinel-1A data. Surface deformation ranging between 0.01 cm and 0.11 cm was observed for points extracted from RADARSAT-2 data that were not vegetated, with a total cumulative deformation of 0.07 cm over the period. The heave features observed warrant further investigation since backfilled areas are expected to be associated with settlement and not heave. The heave features and potential causal links will be explored further in Section 5.1.

### 4.1.3 **L-band**

L-band ALOS PALSAR data were processed and comprised 13 scenes from dates ranging from 2007/08/16 to 2010/04/08. The differential interferograms depicted in Figure 4.12, show all the available data for the area under investigation. Due to the limited amount of L-band data

available for the study area, the temporal baselines of the ALOS PALSAR data are considerably larger than the data available for X-band and C-band. The largest temporal baseline is 322 days and the smallest is 46 days. Similar to the observations for X- and C-band data, the residual topographic phase contributions are evident in the differential interferograms that have a smaller height of ambiguity. The differential interferograms for the periods 2008/02/16-2008/08/18 and 2009/02/18-2010/01/06 show this. Although longer wavelength data is expected to have a decreased sensitivity to the presence of vegetation, speckle effects are present, most notably for the differential interferograms for dates 2007/08/16-2008/12/16, 2008/02/16-2008/08/18 and 2010/04/08-2010/04/30. The speckle noise may be due to the longer temporal baseline of these acquisitions.

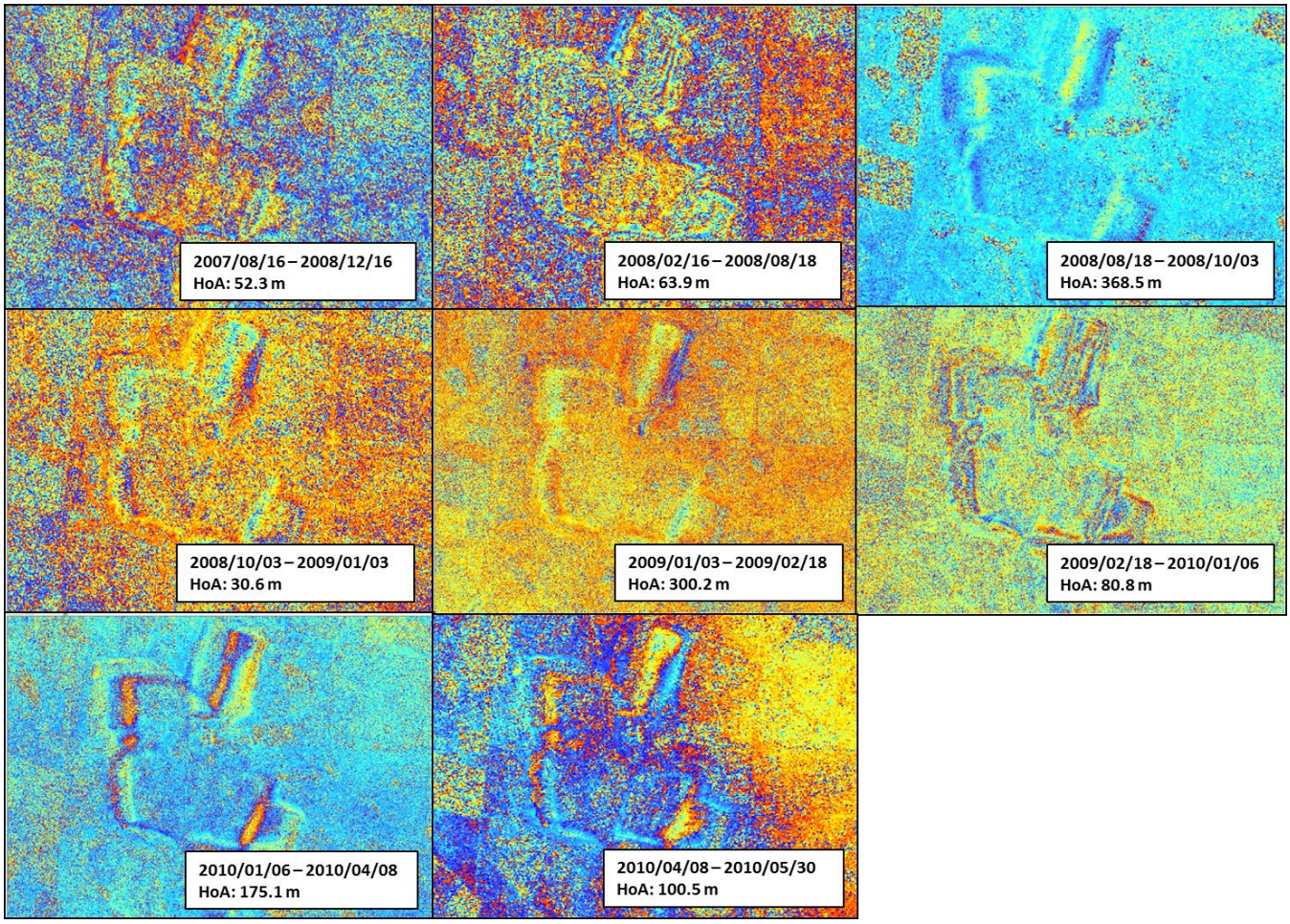


Figure 4.12 ALOS PALSAR time series of interferograms

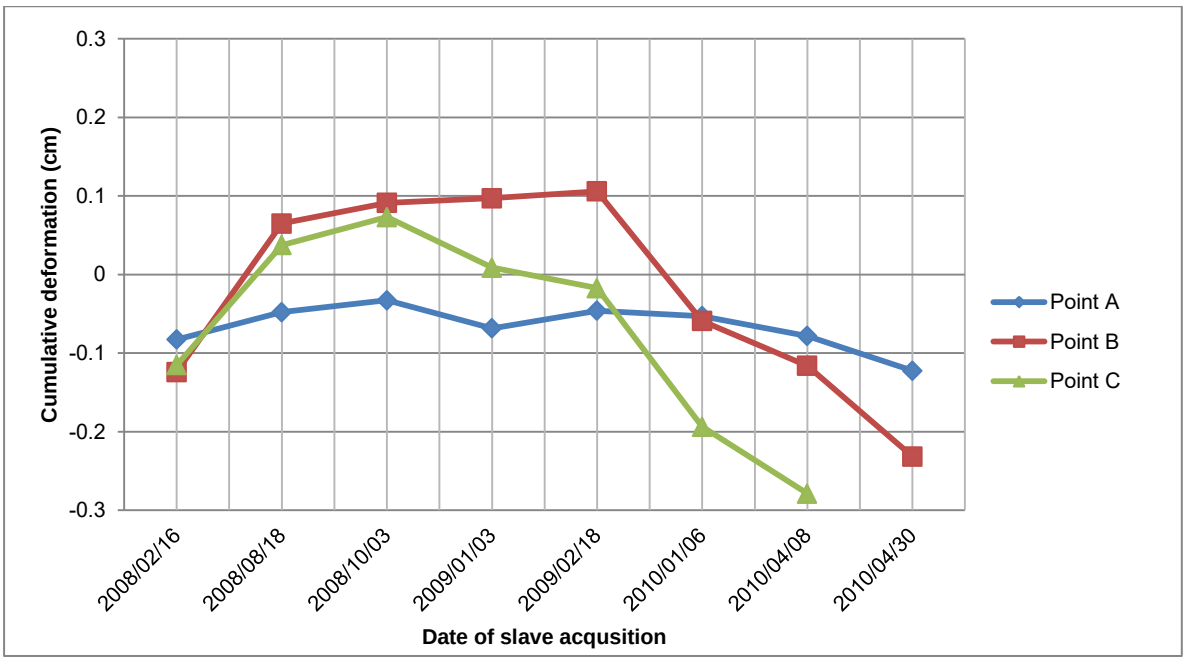


Figure 4.13 Cumulative deformation for ALOS PALSAR points that were found in revegetated areas

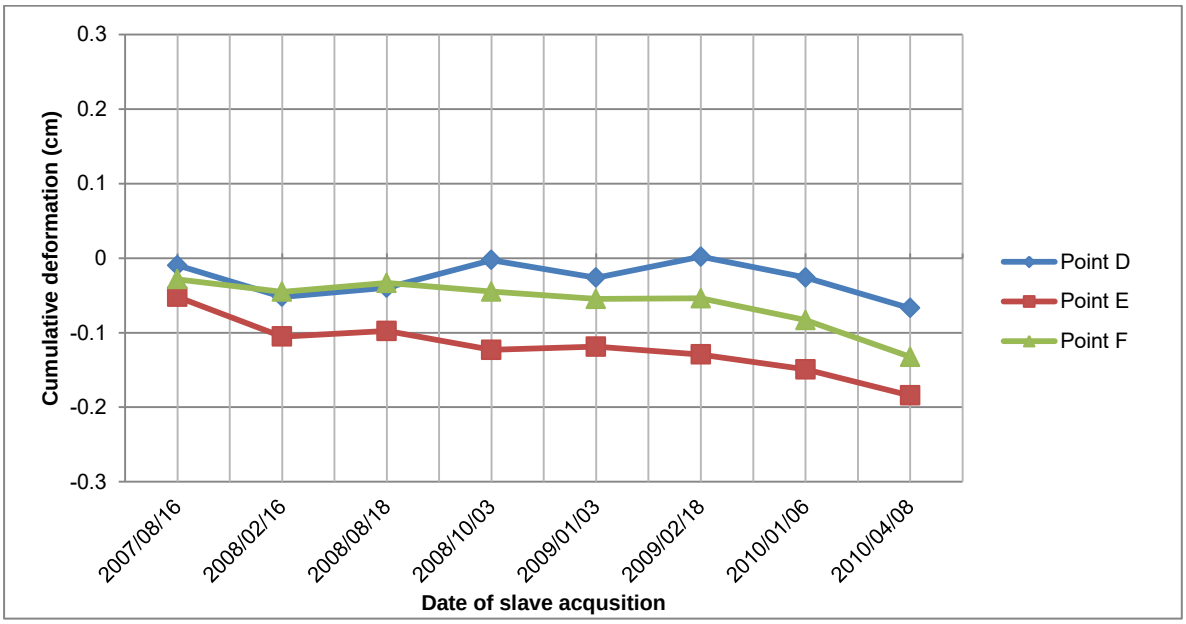


Figure 4.14 Cumulative deformation of ALOS PALSAR points that were found in areas that were not revegetated

Figure 4.13 and Figure 4.14 depicts the evolution of the cumulative deformation for the points on revegetated areas and areas that were not revegetated. Surface deformation measurements range from -0.11 cm to 0.105 cm and the total cumulative deformation was -0.73 cm. The cumulative deformation for the points that had been revegetated was -0.35 cm, and -0.38 cm for the points that were not. Some heave features were found for the dates 2008/02/16-2008/08/18, 2008/10/03-2009/01/03 and 2009/01/03-2009/02/18. The possible cause for these heave features is explored further in Section 5.1.

## 4.2 Component 2: Vegetation monitoring results

As part of the post-mining rehabilitation process, backfilled areas are revegetated in attempt to re-establish the disturbed ecosystem (Section 2.3). Restoration of the natural vegetation is critical, as is monitoring the success of rehabilitation efforts over time (Section 2.3.1). The vegetation productivity associated with the rehabilitated open-pit mine were assessed using remote sensing techniques (Section 3.3). Firstly, EVI derived from Landsat 8 imagery assessed the condition of the undisturbed and rehabilitated vegetation over time (Section 4.2.1). Thereafter, SAR parameters were used to model EVI (known as simEVI) extracted from dual-polarised Sentinel-1A for both the undisturbed and rehabilitated vegetation (Section 4.2.2). Finally, a comparison was made between the optical derived EVI and the simEVI for both the undisturbed and rehabilitated vegetation (Section 4.2.3).

### 4.2.1 Enhanced Vegetation Index (EVI)

Spectral radiances in the red and near-infrared region can be directly related to the fraction of photosynthetic active radiation by incorporating these into spectral vegetation indices (Section 2.3.2). The vegetation index used in this study was EVI, which was calculated from Landsat 8 imagery (Section 3.3.3). The graph in Figure 4.15 shows the average EVI over time across 13 dates for both the natural vegetation surrounding the mined area as well as the rehabilitated vegetation. The highest average EVI value for the study area is approximately 0.4 and the lowest is less than 0.10. EVI results for natural vegetation areas show that the highest EVI values are experienced between January and March, which coincides with the peak of the natural vegetation growing season (Section 1.4). In contrast, lower EVI values are observed for June to August. In the area of interest, this period coincides with the dry winter season, which is generally associated with low EVI values (Section 1.4). Low EVI from the start date in August (2015/08/16) gradually increases to the peak of the growing season in January (2016/01/31) and then decreases again to the end date which is 2016/07/05.

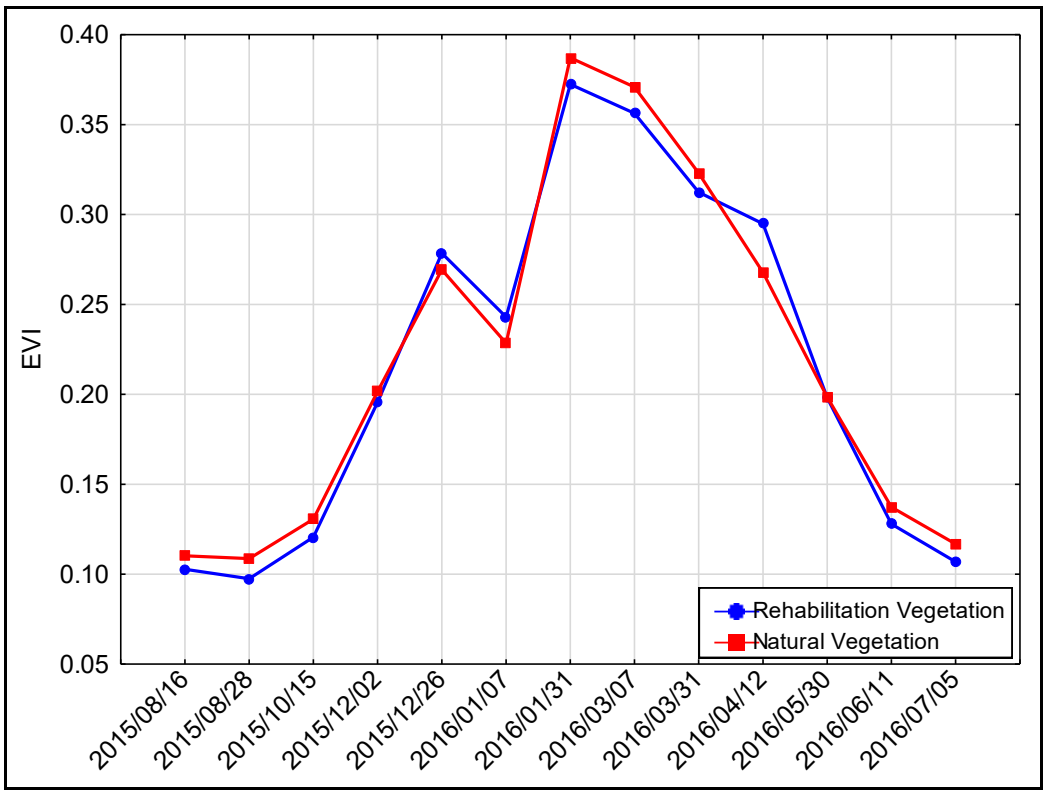


Figure 4.15 Comparison of EVI for natural vegetation and rehabilitated vegetation

The mean EVI was also extracted for the rehabilitated vegetation on the mine area. Figure 4.15 shows the EVI values for the rehabilitated vegetation for all 13 dates. Similar to the mean EVI for the natural vegetation, low EVI values are observed on 2015/08/16 (coinciding with the dry period) and gradually increases until the peak of the growing season is reached on 2016/01/31. Thereafter, EVI values gradually decrease during the drier winter months. When the EVI values for natural vegetation are compared to the rehabilitated vegetation, similar seasonal fluctuations are observed for both vegetation scenarios. Marginally higher EVI values are observed for natural vegetation during the peak of the growing season and during the dry periods. However, these effects are considered negligible and the revegetated area is considered to approach the conditions experiences by natural vegetation areas. This could suggest that the rehabilitated vegetation has reached conditions that are similar to an undisturbed state.

### 4.2.2 **Modelled EVI from SAR parameters**

Although EVI extracted from multispectral approaches are well suited to monitor the productivity of vegetation (Section 2.3.1), long-term monitoring depends on the availability of cloud free data. This may be problematic in areas affected by persistent cloud cover. Therefore, the potential contribution of SAR data to monitor vegetation dynamics was considered. The approach adopted (Section 3.3.4) derived SAR calibrated backscatter in VV and VH polarisation

($\sigma^0_{vv}$, $\sigma^0_{vh}$), alpha-angle ($\alpha$), entropy (H), and interferometric coherence at VV and VH polarisation ($CC_{vv}$ and $CC_{vh}$). Furthermore, since coherence could be used to model EVI either at the date of master image acquisition ($CC_{vv\_master}$ and $CC_{vh\_master}$) or at the date of slave image acquisition ($CC_{vv\_slave}$ and $CC_{vh\_slave}$), both scenarios were included.

The implementation of the RF algorithm to model EVI from the SAR observables provided an indication of the relative importance of each parameter for deriving EVI. The variable importance plot, illustrated in Figure 4.16, suggests that when considering all of the parameters as predictors for the model, $\sigma^0_{vh}$ is the most important predictor of EVI for the natural vegetation field boundaries. This was followed by interferometric coherence in VV polarisation for the slave acquisition and VV polarisation coherence for the master acquisition. The least important variables were entropy, interferometric coherence in VH polarisation for the slave acquisition and VH coherence for the master acquisition.

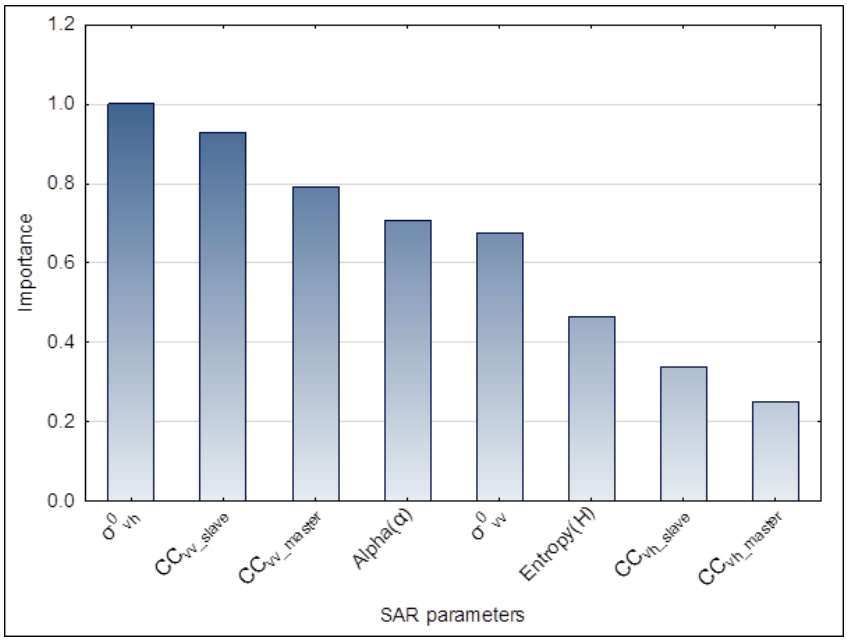


Figure 4.16 Importance plot of all the SAR parameters in decreasing order of importance

To model EVI, over 300 possible combinations of the SAR parameters were tested as possible predictors of EVI for the natural vegetation class samples. Table 4.1 presents the top ten combinations of SAR observables that had the highest predictive capacity. The results suggest that the combination of all eight SAR parameters yielded the highest predictive capacity with an adjusted $R^2$ =0.715 (Mean square error (MSE) =0.002) for the test data. The combination of the backscattering coefficient in both polarisations attained the lowest adjusted $R^2$ for both the training data set and for the test data set.

Table 4.1 Predictive capacity of the top ten combinations of predictors

| | Predictors (in order of importance) | Adjusted $R^2$ |
|---|---|---|
| **1** | $\sigma^0_{vh}$, $CC_{VV}$(slave), $CC_{VV}$(master), alpha, $\sigma^0_{vv}$, entropy, $CC_{vh}$(slave), $CC_{vh}$(master) | Test = 0.715<br>MSE= 0.0002 |
| **2** | $\sigma^0_{vh}$, $CC_{VV}$(master), $CC_{VV}$(slave), alpha, $\sigma^0_{vv}$, entropy | Test = 0.706<br>MSE=0.0002 |
| **3** | $\sigma^0_{vh}$, $CC_{VV}$(master), $CC_{VV}$(slave), | Test = 0.6987<br>MSE= 0.00012 |
| **4** | $\sigma^0_{vh}$, $\sigma^0_{vv}$,, $CC_{VV}$(slave), | Test = 0.6977<br>MSE=0.00012 |
| **5** | $\sigma^0_{vh}$, $CC_{VV}$(slave), $CC_{vh}$(slave), alpha | Test = 0.688<br>MSE=0.00010 |
| **6** | $\sigma^0_{vh}$, $\sigma^0_{vv}$,, $CC_{VV}$(slave),alpha | Test = 0.669<br>MSE=0.00009 |
| **7** | $\sigma^0_{vh}$, $CC_{VV}$(slave) | Test = 0.662<br>MSE=0.0009 |
| **8** | $\sigma^0_{vh}$, $\sigma^0_{vv}$, $CC_{VV}$(slave), $CC_{vh}$(master), alpha, entropy | Test = 0.6585<br>MSE=0.0009 |
| **9** | $\sigma^0_{vh}$, $CC_{VV}$(master), $CC_{VV}$(master), $\sigma^0_{vv}$ | Test = 0.641<br>MSE=0.0009 |
| **10** | $CC_{VV}$(slave), $\sigma^0_{vh}$, , $CC_{VV}$(master), alpha, $\sigma^0_{vv}$, entropy | Test = 0.6385<br>MSE=0.0009 |

### 4.2.3 **Comparison between optical derived EVI and predicted SAR EVI**

To compare the results obtained from conventional Landsat 8 derived EVI with the results of the modelled SAR EVI (simEVI), the EVI and simEVI values were compared for the natural vegetation classes (Figure 4.17). The results, presented in Figure 4.17 indicate slight variations between the EVI values obtained. Most notably, for periods where low EVI is observed (June to August), the simEVI results exhibit higher values compared to conventional EVI. Conversely, for the periods where EVI values are high (January to April), the simEVI exhibits lower values compared to conventional EVI. The results suggest that during the peak of the growing season SAR derived EVI values may underestimate the vegetation productivity while vegetation status may be overestimated in the dry season.

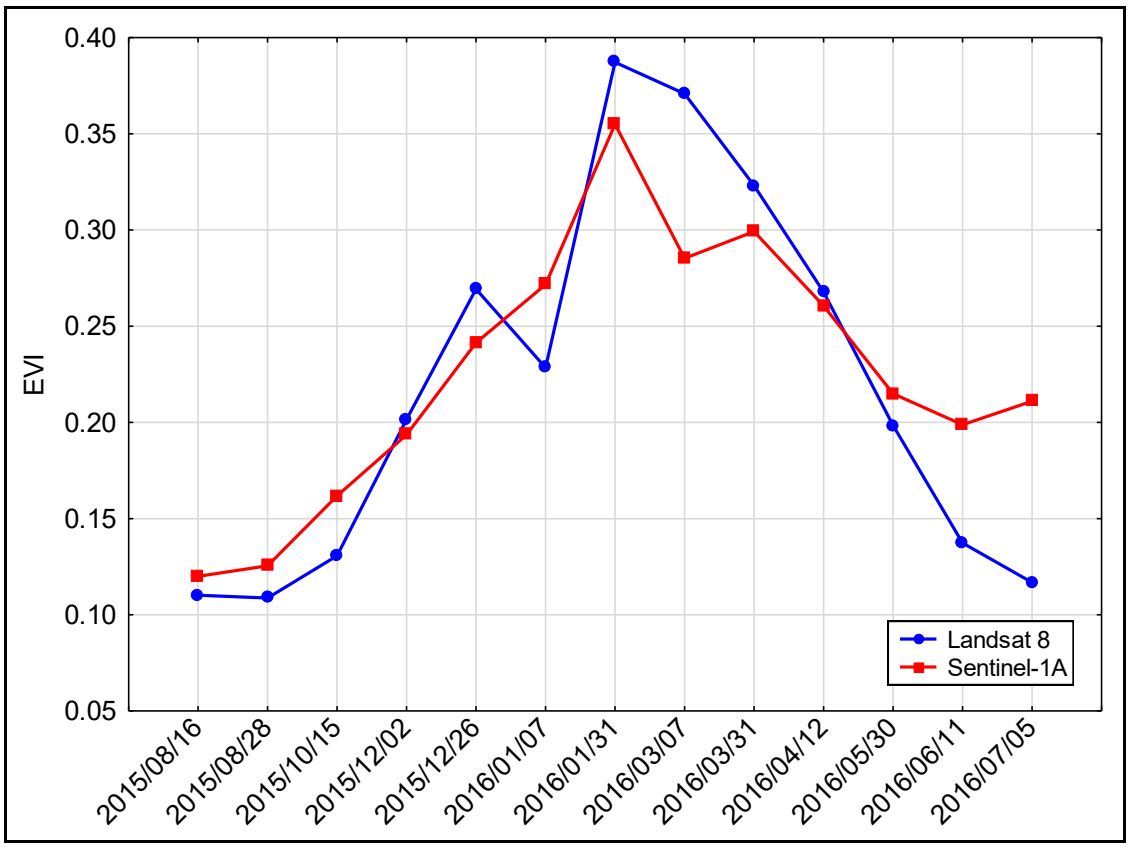


Figure 4.17 Comparison of simEVI and EVI for natural vegetation classes

A similar effect is observed when the EVI and simEVI values for the rehabilitated mine are considered (Figure 4.18). The results suggest that both the underestimation of vegetation status during the peak of the growing season and the overestimation during the low EVI periods are observed for modelled SAR derived EVI. The effect is also more pronounced for rehabilitated vegetation when compared to natural vegetation

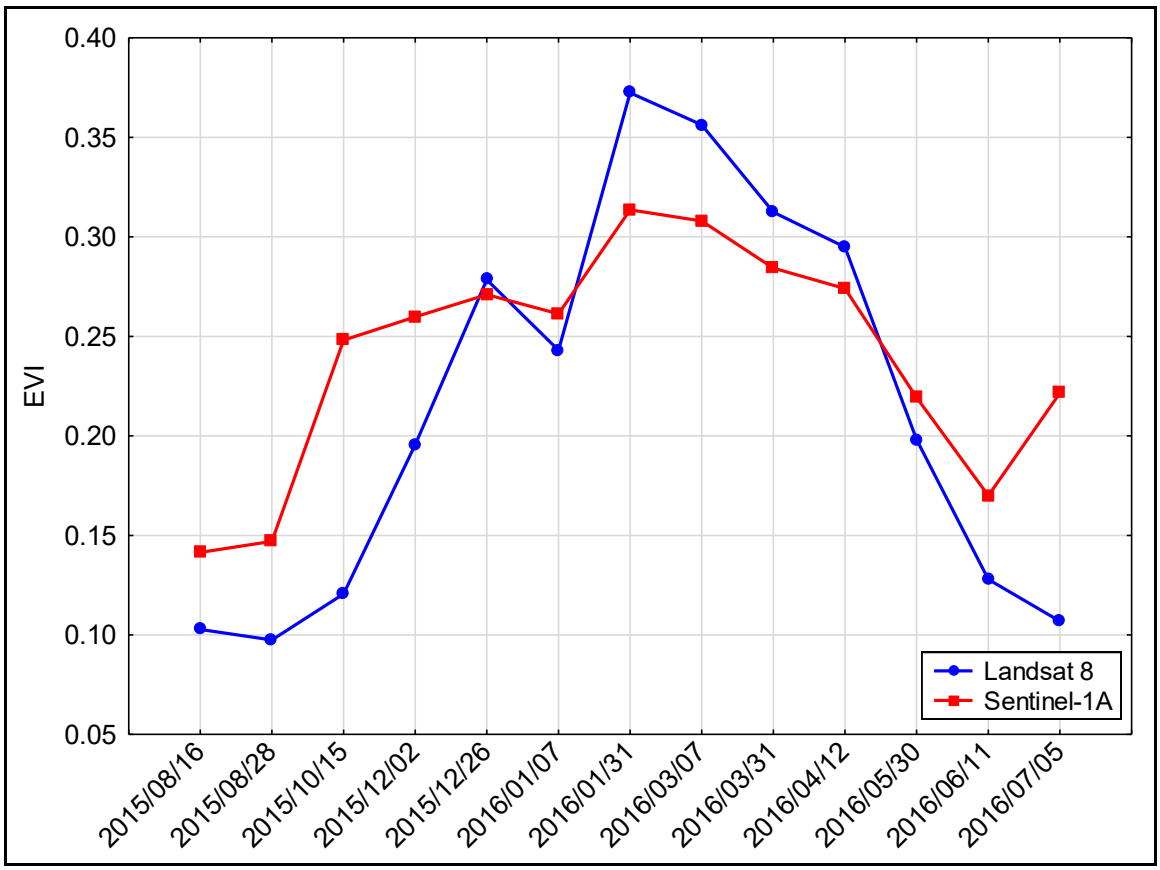


Figure 4.18 Comparison of simEVI and EVI for rehabilitated classes

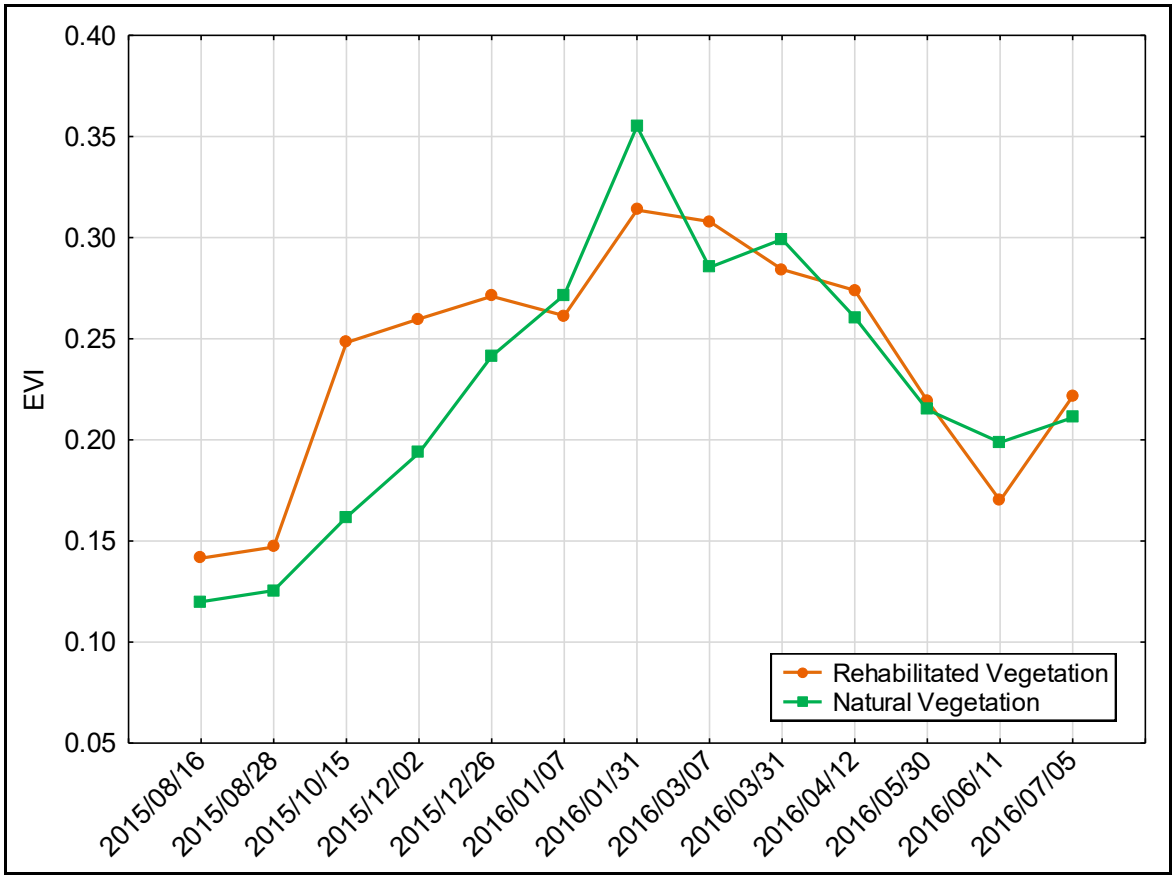


Figure 4.19 SimEVI for both rehabilitated vegetation and natural vegetation

Figure 4.19 presents the results obtained for the SAR-derived EVI for both natural and rehabilitated vegetation. It shows that the simEVI values for the natural vegetation were lower than the simEVI values for rehabilitated vegetation for the period between 2015/08/16 and 2015/12/26. The highest simEVI for both vegetation types was observed on 2016/01/31, and this coincides with the observations of EVI values derived from the Landsat 8 imagery. The overestimation of simEVI in low vegetation conditions may be problematic since any underperforming vegetation types may appear to perform better than in reality

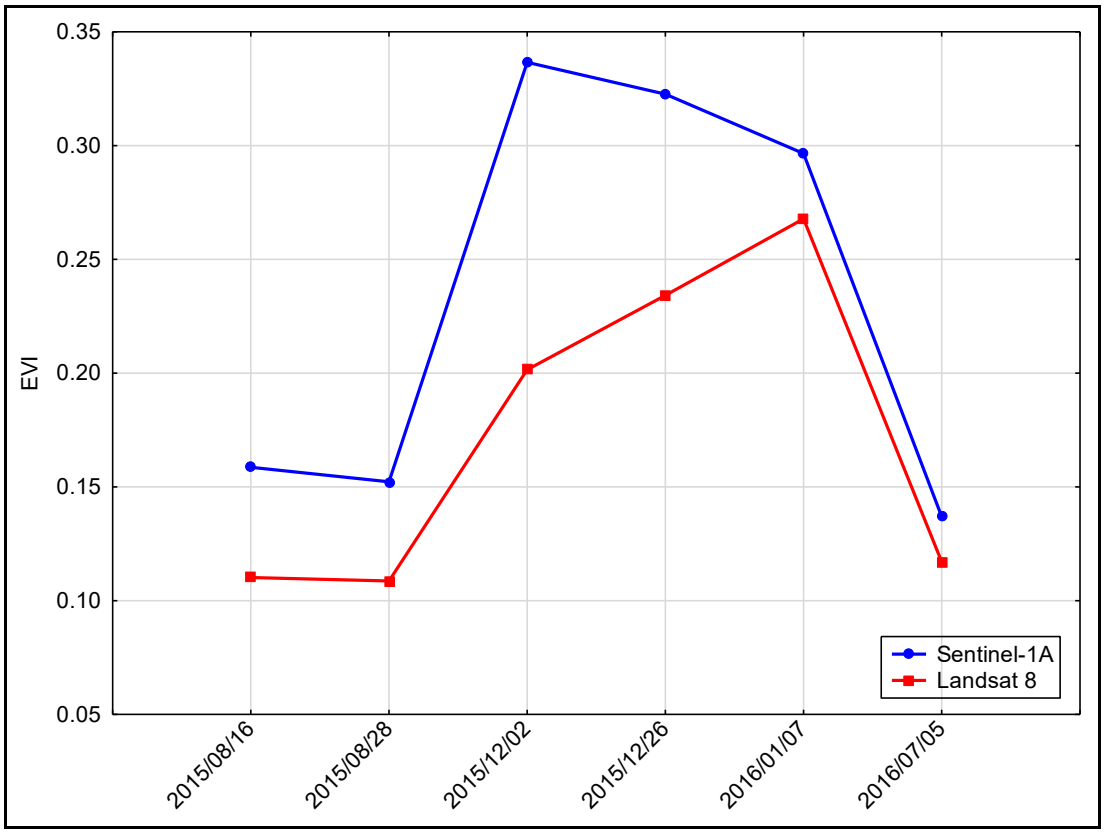


Figure 4.20 Modelled EVI and Landsat 8 EVI for undisturbed vegetation.

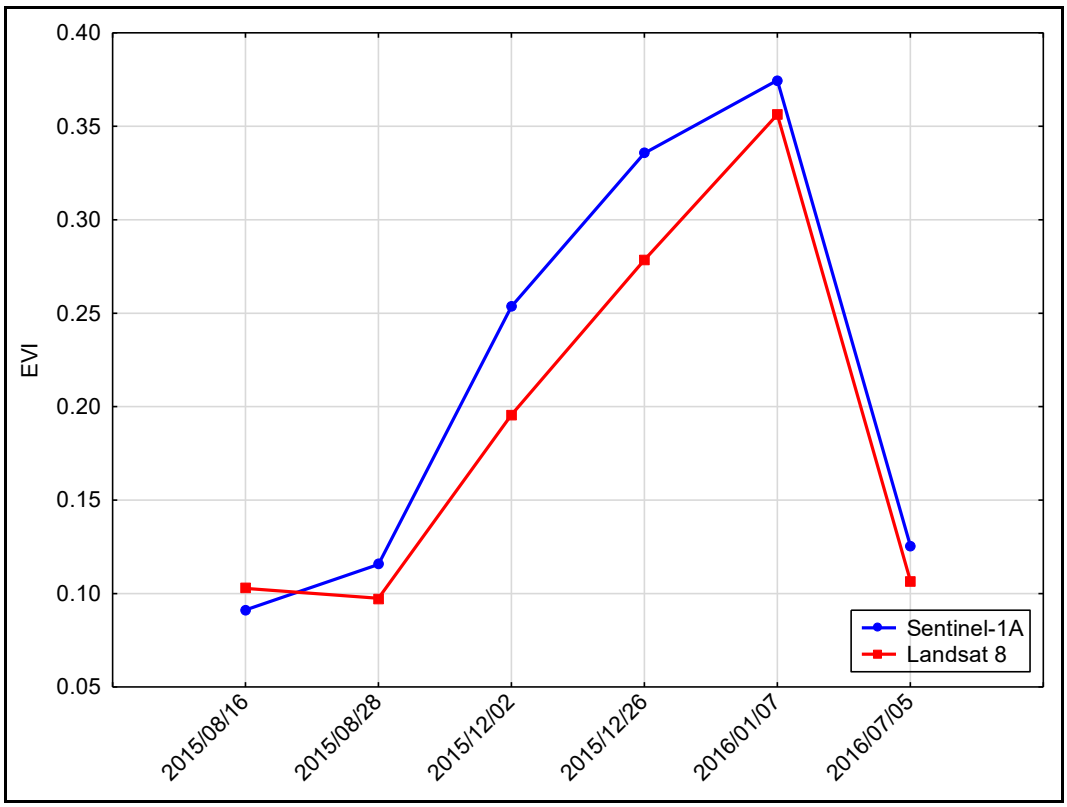


Figure 4.21 Modelled EVI and Landsat 8 EVI for rehabilitated vegetation.

To test the scenario where there is limited or no optical imagery available, the RF model was trained using a combination of representative summer and winter optical imagery. The model was then tested on summer and winter dates and EVI was modelled using the combination of all the SAR observables. Figure 4.20 indicates the comparison of the modelled SAR EVI and the Landsat 8 derived EVI for the undisturbed vegetation. The results indicate that the modelled SAR EVI is overestimated for the summer and winter dates when there is a limited representative of optical imagery available. Similarly, Figure 4.21 illustrates that modelled EVI show an overestimation of EVI when representative images of optical data is used as training for the model. Section 5.2 explores possible reasons for the overestimation of the optical derived EVI when there is limited optical imagery available.

# 5 DISCUSSION

Monitoring both the deformation measurements and the revegetation are important for post-mining rehabilitation. Deformation measurements were extracted from X-, C- and L-band SAR to observe the backfill settlement patterns of the open-pit mine area. Section 5.1 presents a discussion of these results. Furthermore, the results of monitoring of the productivity of the vegetation to assess the success of revegetation practices are in Section 5.2.

## 5.1 Backfill settlement observations

To assess the potential of using dInSAR to quantify backfill settlement rates the deformation measurements were extracted from multi-sensor SAR data and the results were presented in Section 4.1. There are two main limitations that inform the discussion of these results, namely 1) the sensor parameters and 2) the characteristics of the deformation feature including size and deformation rate. Despite the general deformation patterns observed, some anomalous patterns were present when assessing the cumulative deformation over time. For specific points, heave as opposed to subsidence was observed. These anomalies were observed for various date ranges and for all the respective SAR wavelengths. Heave has been known to occur in backfilled areas. It is associated with the removal of the overburden and in some cases with the saturation of the upper few metres of backfill due to the natural recharge of the groundwater (Hills 1994). Monthly rainfall for the study area was compared to the cumulative deformation for each of the SAR datasets (Figure 5.1A to Figure 5.1D).

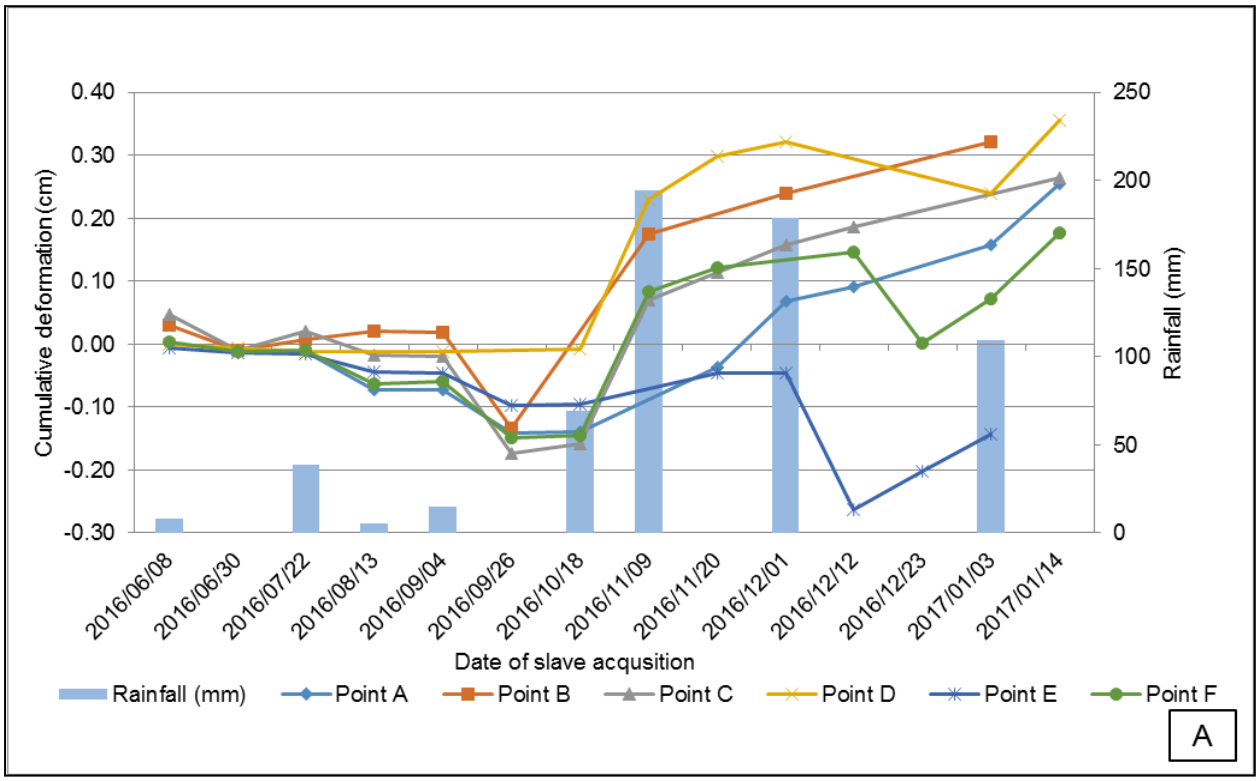


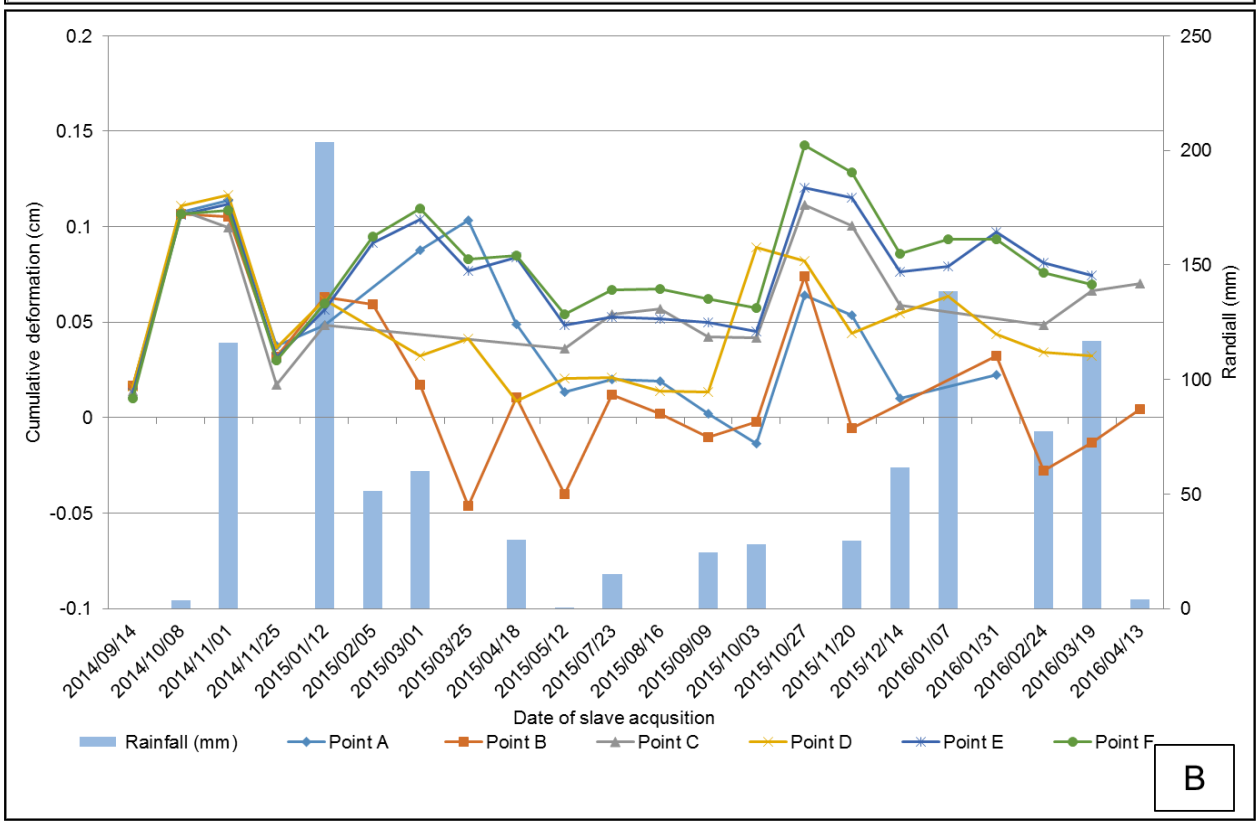

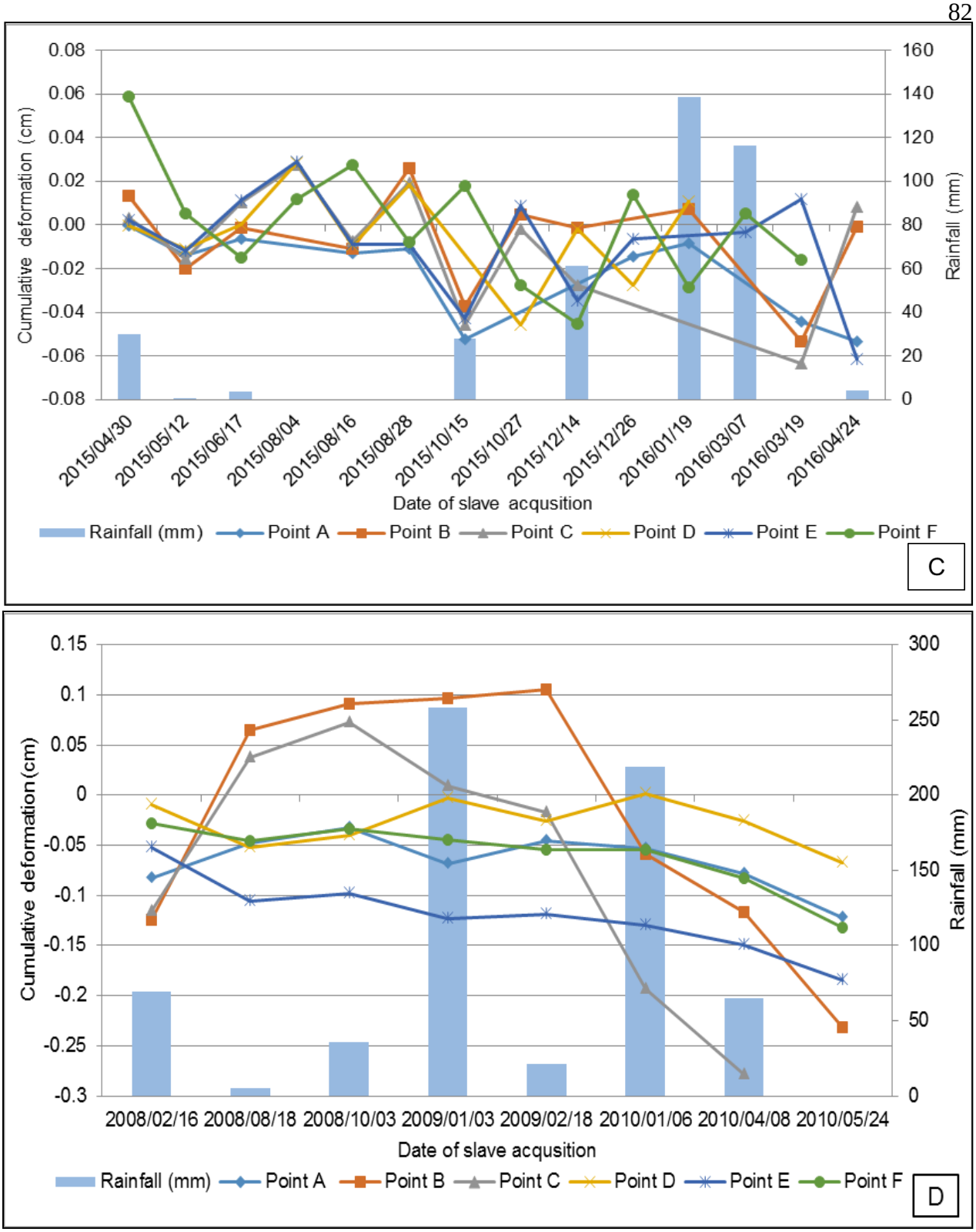


Figure 5.1 Cumulative deformation and the monthly rainfall for A) TerraSAR-X B) RADARSAT-2 C) Sentinel-1A and D) ALOS PALSAR

The assessment of the local rainfall patterns for the study area have, indicated that the rainfall events preceded heave events for TerraSAR-X (Figure 5.1A). Heave features for the dates 2016/10/18-2016/11/09 and 2016/11/20-2016/12/01 coincided with large rainfall events that occurred during the month. As the rain saturates the ground surface, this could cause an upwelling of the water and could present itself as heave or uplift. Furthermore, when there were

no large rainfall events the cumulative deformation decreased as exhibited for the dates 2016/09/04-2016/09/29 and 2016/12/01-2016/12/12. This, however, was not observed for C-band and L-band data where there was no strong correlation between the rainfall events and heave features (Figure 5.1B to Figure 5.1D). It should be noted that the rainy season for the area under investigation corresponds with the peak of the growing season and therefore the effect of the presence of vegetation also needs to be investigated.

The effect of the presence of vegetation, was observed for X-band (Section 4.1.1), C-band (Section 4.1.2) and L-band (Section 4.1.3) data, when there was an increase in speckle effects for interferograms covering the peak of the growing season. To assess the effect of signal noise on deformation measurements, the cumulative deformation was compared to Landsat EVI measurements at the time of data acquisition (Figure 5.2A to Figure 5.2D)

Figure 5.2A depicts EVI and cumulative deformation for various points of TerraSAR-X data. The cumulative deformation increases as EVI values increase. Furthermore, heave features coincide with the start and peak of the growing season (2016/11/09 to 2017/01/14). Short wavelength SAR signals, including X- and C-band, are known to interact with smaller scattering elements, including leaves and twigs of vegetation (Section 2.3.3). The heave features observed during the peak of the growing season for X-band results may therefore be indicative of the signal interaction with vegetation elements higher up in the vegetation canopy and not on the ground surface. Therefore, a vegetation induced “topographic effect” may be responsible for the observed heave features especially on the short wavelength X-band results.

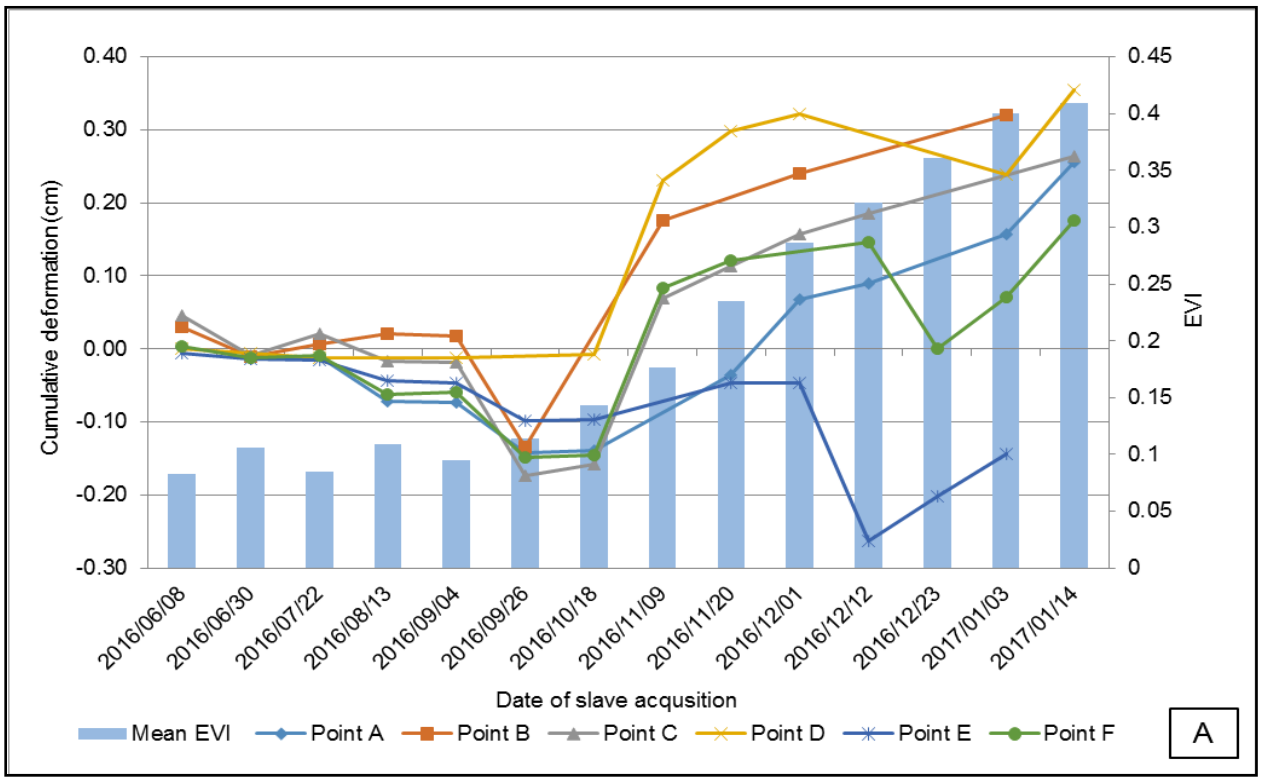


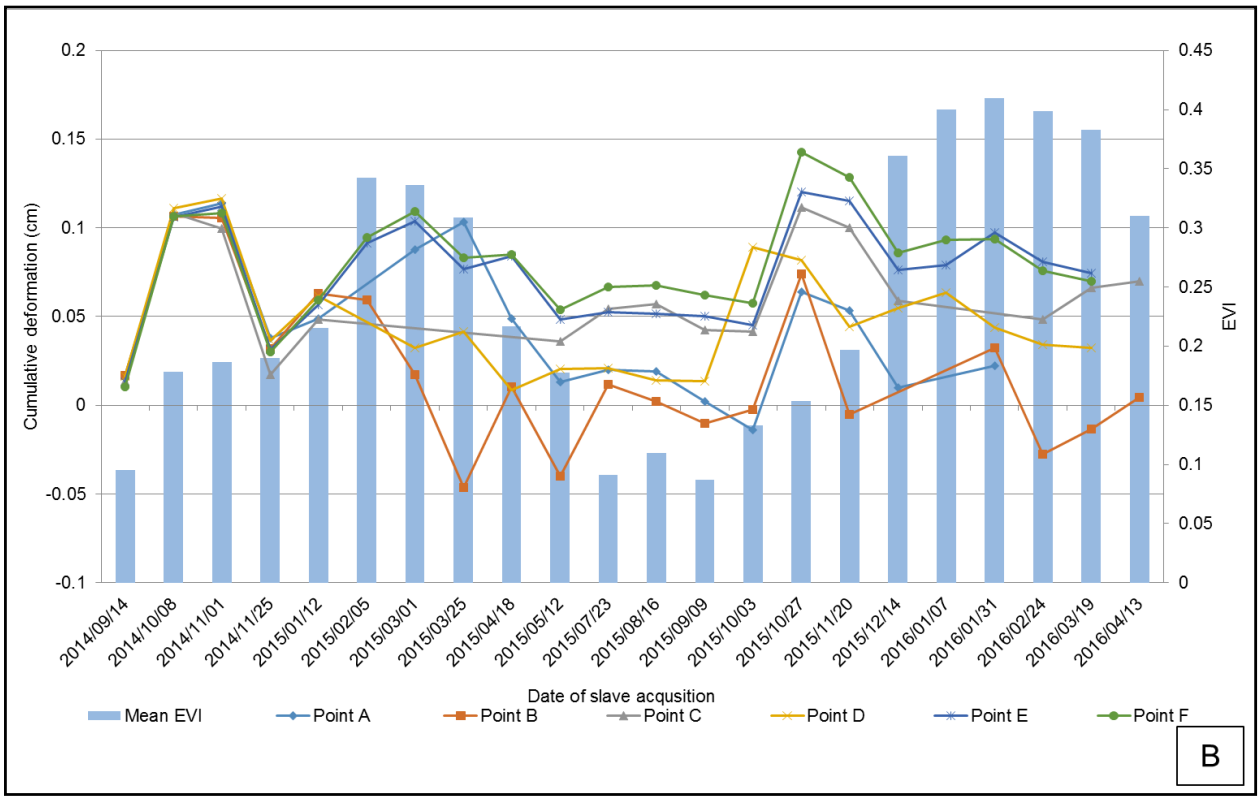

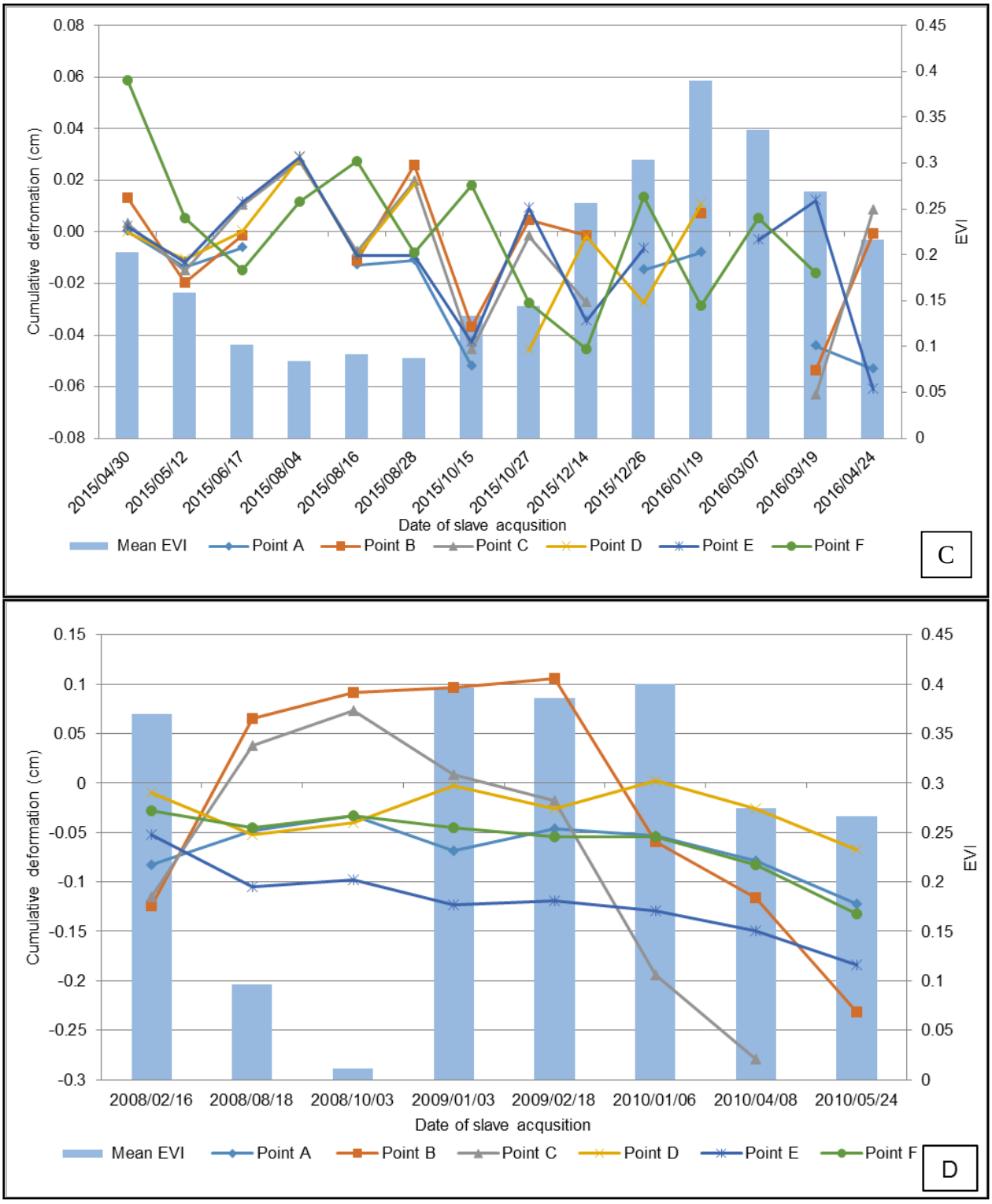


Figure 5.2 Mean EVI and the cumulative deformation to assess the effect of the presence of vegetation for A) TerraSAR-X B) RADARSAT-2 C) Sentinel-1A and D) ALOS PALSAR

The effects of the presence of vegetation were also assessed for C-band RADARSAT-2 and Sentinel-1A data (Figure 5.2B and Figure 5.2C, respectively).

A number of heave features extracted from the RADARSAT-2 data, were found in high EVI scenarios as indicated for the dates 2015/01/12-2015/02/05, 2015/02/05-2015/03/01 and 2015/03/01-2015/03/25 (Figure 5.2B). This result is not unexpected because C-band SAR data is

known to be sensitive to vegetation (Section 2.3.3). However, this was not observed for Sentinel-1A data, where heave features did not coincide with high EVI scenarios (Figure 5.2C). In fact, the heave features that were extracted correspond to the dry season in the area of interest. This was exhibited in the period between 2015/06/17 and 2015/08/15 where heave features coincide with low EVI scenarios. This suggests that heave has a stronger association with the residual topography still present in the deformation maps than it does with the presence of vegetation. The link between vegetation and the deformation features were also assessed for ALOS PALSAR data (Figure 5.2D).

The results indicate that when EVI values are high, as for the dates 2008/10/03-2009/01/03 and 2009/01/03-2009/02/018, there are heave features. It is a known fact that when using L-band data for vegetated areas there will be less interaction is with the canopy of the vegetation and more interaction with the ground surface (Sang et al. 2014). As can be seen in Figure 5.2D heave features that in EVI scenarios may be an effect of the long temporal baseline of the acquisitions. The effect of vegetation dynamics was also observed in previous investigations (Engelbrecht 2013). The relationship between an increase in vegetation density (as approximated by EVI) and the decrease in coherence was observed for X- and C-band data but only to a limited extent for L-band data (Engelbrecht 2013). It was concluded that the presence of vegetation in SAR scenes could limit the successful measurement of surface deformation. It was recommended that shorter temporal baselines are preferable to mitigate the vegetation decorrelation effects.

To further investigate the potential causes of the anomalies, the various phase contributions to the interferograms should be considered. A significant contribution to interferometric phase is the phase contribution due to topographic variations in the area under observation. Although the process of interferogram flattening (Section 3.2), in theory, removes the topographic phase contributions, external DEM errors may lead to residual topographic phase being present.

In fact, residual topographic phase was present in numerous differential interferograms in this study. However, the degree of this was dependent on the height of ambiguity, as was observed for X-band (Section 4.1.1), C-band (Section 4.1.2) as well as L-band data (Section 4.1.3). The 1 – arc second SRTM DEM was used to simulate the topographic phase in the study (Section 3.2). In scenarios of deformation measurement estimation, if topographic phase residuals are not accurately estimated and removed, residual topographic phase contributions can be mistaken as a deformation signal (Du et al. 2016).

In the case of the SRTM DEM the absolute vertical accuracy is estimated at 15 m and may introduce a source of residual topographic phase. In addition to the vertical inaccuracies posed

by the SRTM data set, it should be noted that the SRTM DEM was produced in 2003. Using a DEM that is more than ten years older than the interferometric SAR datasets under investigation can introduce some errors when trying to compensate topography, especially in areas of dynamic land-use activity such as mining. Mining activities, including the removal of material and backfilling, would introduce significant changes in the local topography, even over a short period of time. If these changes took place after the DEM generation, the DEM would not be an accurate model of local topography. Therefore, changes in local topography subsequent to DEM model generation would manifest in the differential interferogram as uncompensated topography.

An assessment of the phase contribution due to topography was performed by calculating the HoA for each scene. Visual assessment of the differential interferograms confirmed that small HoAs were associated with an increase in residual topographic fringes for the mine residue areas under investigation (Sections 4.1.1, 4.1.2 and 4.1.3). On the other hand, scene pairs associated with high HoA values exhibited a decrease in topographic phase. The TerraSAR-X differential interferograms for the dates 2016/05/17-2016/06/08 and 2016/08/13-2016/09/04 where the HoA is 21.25 m and 480.42 m respectively, exhibit this (Figure 5.3).

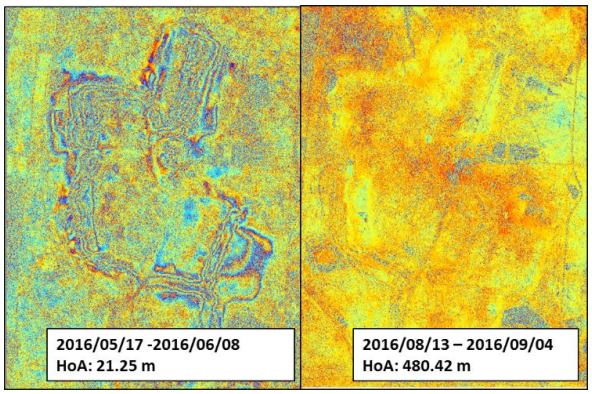


Figure 5.3 TerraSAR-X differential interferograms showing the height of ambiguity (HoA).

To assess if anomalous heave features may be related to uncompensated topography, the perpendicular baseline for each of the interferometric pairs was compared to the deformation measurements extracted. Figure 5.4A to Figure 5.4D indicate the cumulative deformation for the revegetated and un-vegetated points extracted from X-, C- and L-band versus the perpendicular baseline.

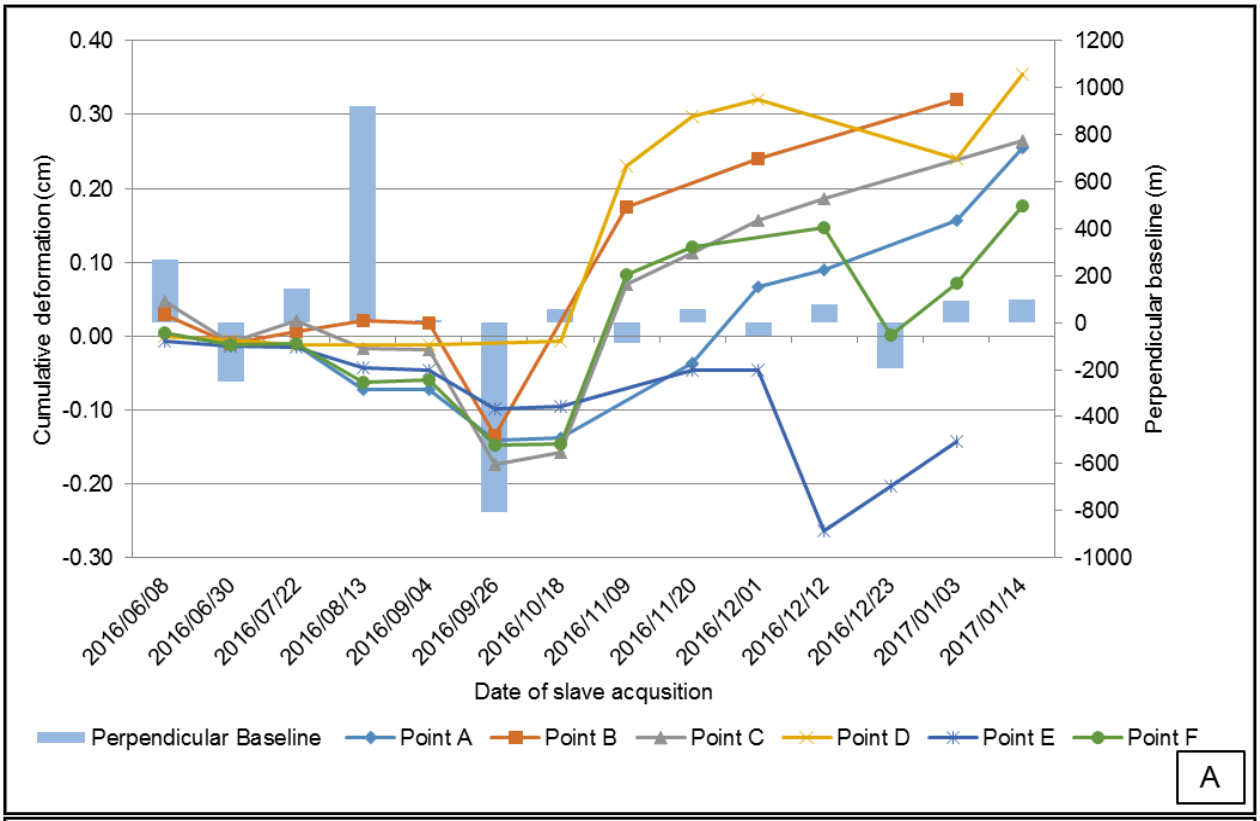


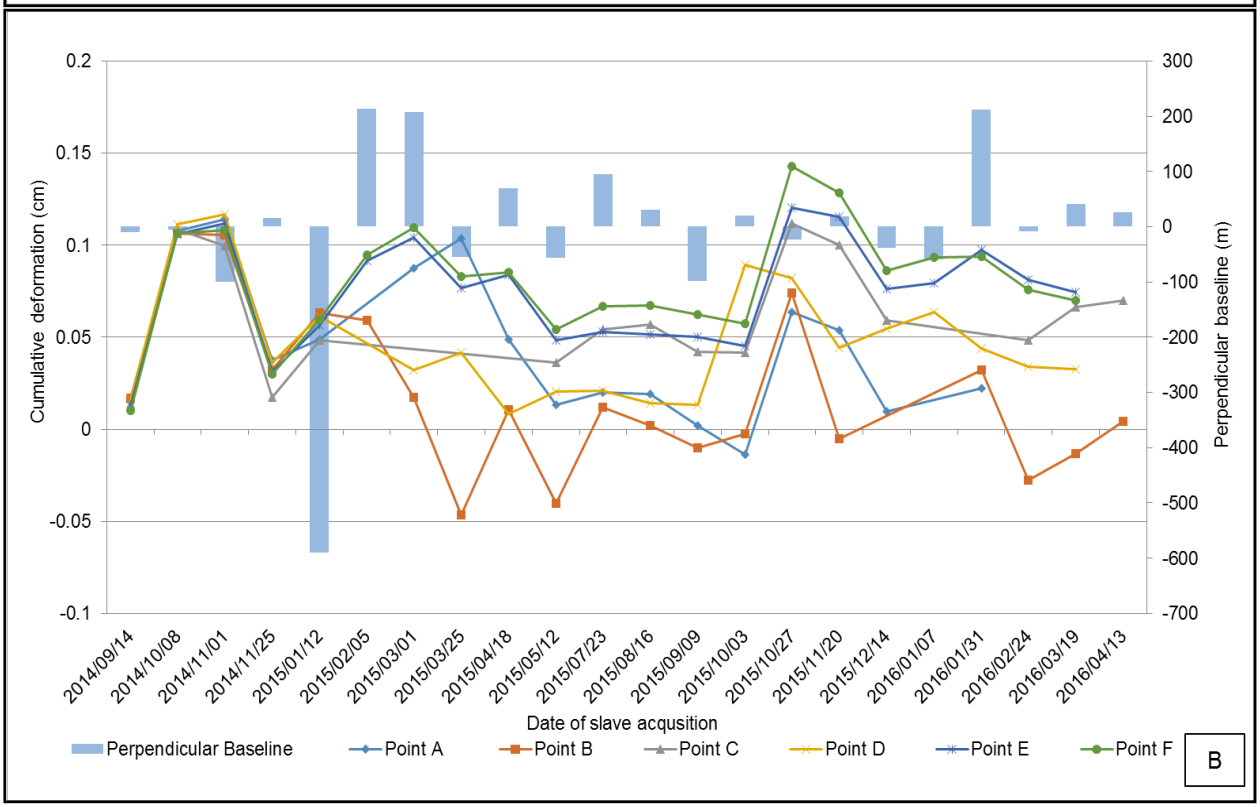

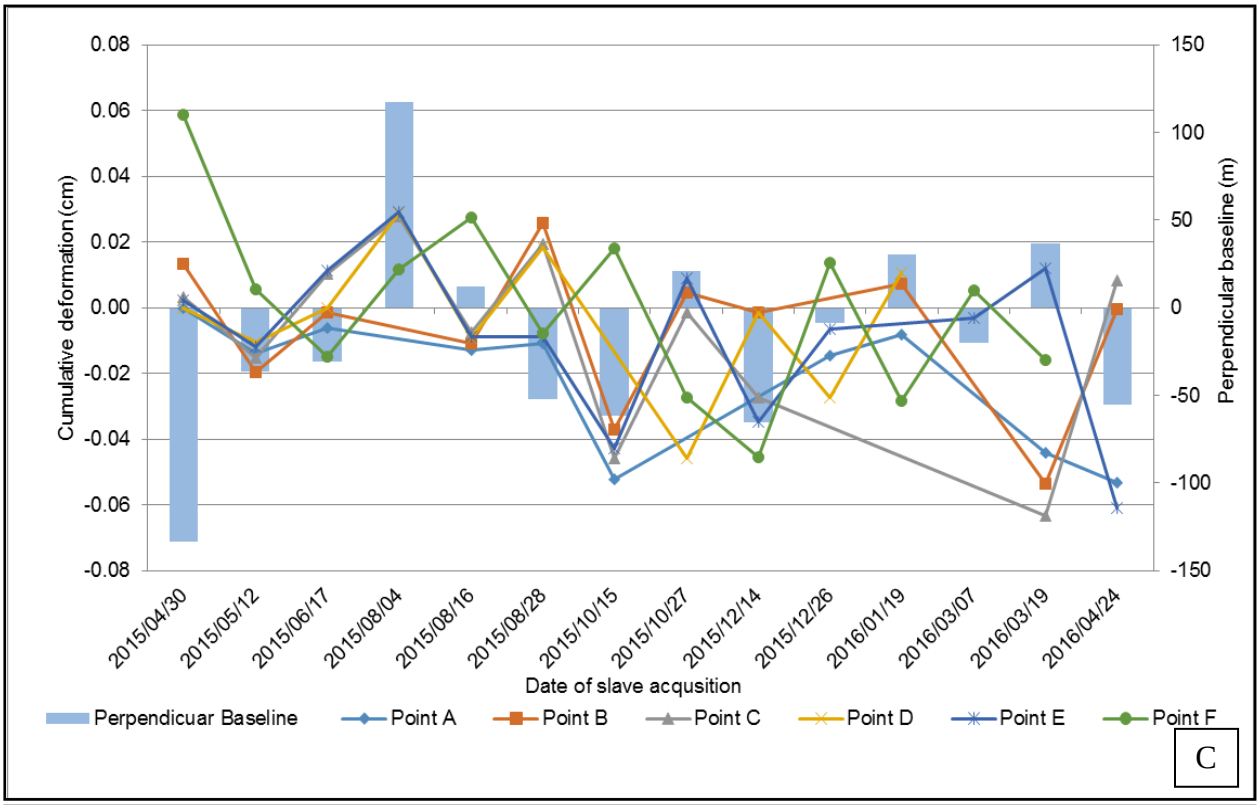


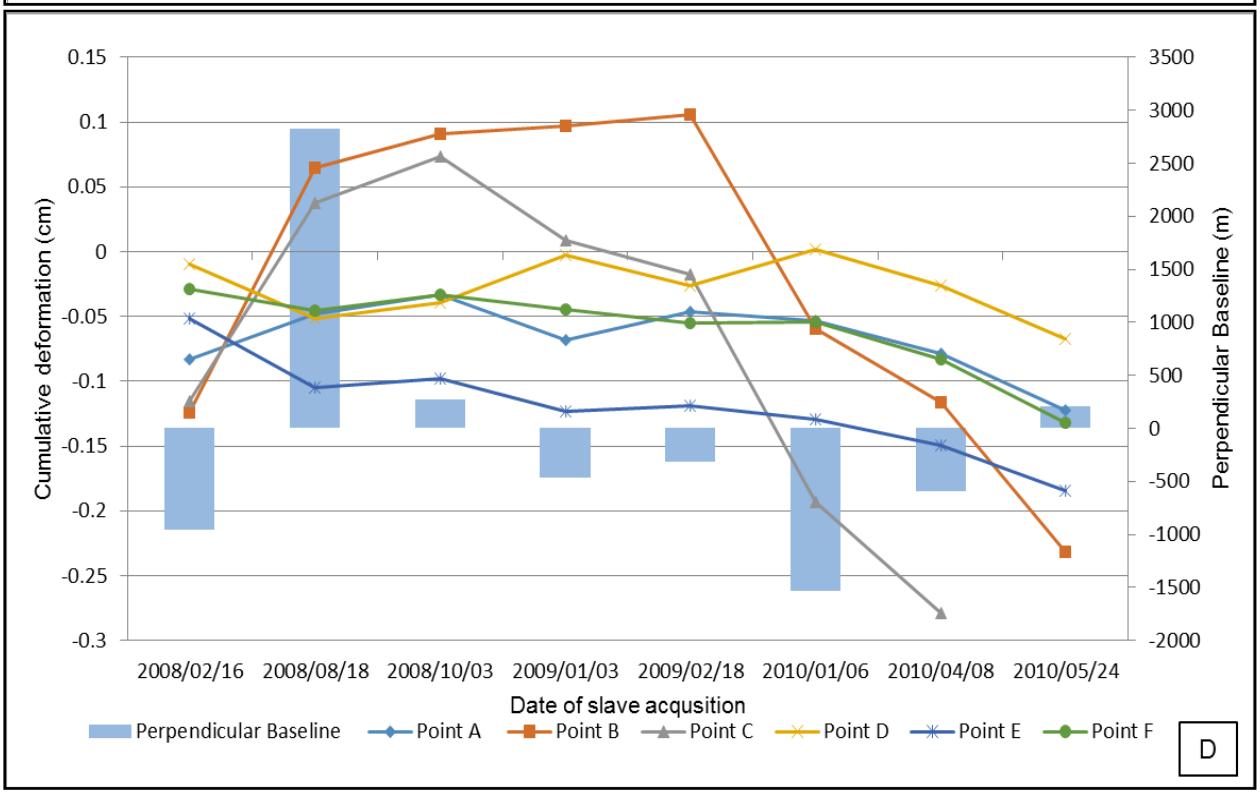


Figure 5.4 Cumulative deformation for A) TerraSAR-X data B) RADARSAT-2 C) Sentinel-1A, D) ALOS PALSAR and the perpendicular baseline

For TerraSAR-X data (Figure 5.4A) there are positive and negative perpendicular baselines that could be associated with positive and negative deformation over the timeline. This is true for the dates 2016/05/17-2016/06/08, 2016/06/08-2016/06/30 and 2016/09/04-2016/09/26 where the positive and negative cumulative deformation is associated with negative and positive

perpendicular baselines. There were heave features present in the growing season, from November to March, which are considered anomalous (Section 4.1.1). When assessing the perpendicular baseline that corresponds to the heave features (from the date 2016/10/18-2016/11/09 to 2017/01/03-2017/01/14), there do not appear to be any large positive or negative perpendicular baselines that could explain the large heave features. Therefore, the temporal decorrelation due to the presence of vegetation could possibly explain the heave features. The relationship between cumulative deformation and the perpendicular baseline for RADARSAT-2 and Sentinel-1A data was evaluated (Figure 5.4B and Figure 5.4C).

For the RADARSAT-2 data, there is no strong association between positive and negative cumulative deformation and positive and negative perpendicular baselines (Figure 5.4B). However, the dates 2015/01/12-2015/02/05, 2015/02/05-2015/03/01 and 2015/04/18-2015/05/12 show positive and negative deformation features which could be attributed to the positive and negative perpendicular baseline. On the other hand, when assessing the perpendicular baseline and the cumulative deformation for the Sentinel-1A data, there is a strong association between the deformation features and the perpendicular baseline (Figure 5.4C). The dates pairs 2015/04/30-2015/05/12, 2015/05/12-2015/06/17, 2015/07/16-2015/08/04, 2015/10/03-2015/10/15, 2015/10/15-2015/10/27 and 2015/12/02-2015/12/24 indicate this. For these dates, positive deformation features or heave can be attributed to positive perpendicular values and negative deformation can be associated with negative perpendicular baselines. This also applies to the ALOS PALSAR data (Figure 5.4D) where positive deformation features can be explained by positive perpendicular baselines. An example of this is shown for the dates 2008/02/16-2008/08/18 and 2008/08/18-2008/10/03. The association between heave features extracted from X-, C- and L-band data and the corresponding perpendicular baseline leads to the conclusion that, despite interferogram flattening, residual topographic phase contributions are affecting the ability to accurately quantify backfill dynamics. This compromises our ability to draw accurate conclusions on the nature of backfill settlement in the area.

When considering the backfill settlement rates (Section 2.1), the settlement associated with the area under investigation was expected to take place at an accelerated pace shortly after backfilling was completed. This is followed by a progressive decrease in settlement rates with occasional collapse settlement events (Section 2.1). However, the results of the deformation measurement for the study area suggest that extracted deformation rates are highly variable over space and time with occasional unexplained heave events. The results suggest that uncompensated topography and signal noise, introduced due to the presence of vegetation and other possible external influences may be affecting the results. Therefore, the conventional

dInSAR approach adopted in this investigation may be unsuitable for the quantification of backfill dynamics in rehabilitated open-pit mines.

## 5.2 **Vegetation Monitoring**

To monitor the vegetation dynamics on rehabilitated open-pit mines, a time series of conventional EVI datasets derived from Landsat-8 and EVI data modelled from SAR observables were extracted. The results for the undisturbed vegetation and revegetated areas were compared to determine the success of the rehabilitation efforts. EVI for the natural vegetation and rehabilitation vegetation was evaluated (Section 4.2.1). The results show that the EVI trends for natural and revegetated areas are similar on the Landsat 8 derived EVI measurements. This suggests that the phenological response of revegetated areas is similar to the natural vegetation for the period under observation and rehabilitation efforts have been successful in bringing revegetated areas to a similar state as surrounding undisturbed vegetation.

Although, the monitoring of the vegetation condition and productivity using multispectral vegetation indices is well established, their use is limited in areas with persistent cloud cover. Therefore, to compliment observations by multispectral sensors, the use of SAR derived observables to model EVI was investigated. When the relative importance of SAR observables in predicting EVI was considered, RF indicated, that the most important predictor was the backscattering coefficient in the HV polarisation ($\sigma^0_{vh}$) (Section 4.2.2). This is in agreement with previous observations that indicate statistically significant correlation between HV backscatter and vegetation (Jiao et al. 2010; McNairn & Brisco 2004). Cross-polarized backscatter is primarily associated with volume scattering from within the target which occurs within vegetation canopies (McNairn & Brisco 2004). Therefore, the high variable importance backscatter coefficient in HV polarisation is not unexpected.

In addition to SAR backscatter, interferometric coherence, used for predicting EVI either at master or slave acquisition date was shown to be the second most important predictor of EVI. This confirms the findings in previous investigations that interferometric coherence has a strong inverse relationship with EVI (Section 2.3.3) (Engelbrecht 2013). While, interferometric coherence for the VV polarisation data was shown to be an important predictor for EVI, the VH polarisation coherence was shown to be the least important predictor of EVI. The result was unexpected since, as demonstrated using VH backscatter, the VH polarisation data is sensitive to the presence of vegetation. However, for vertically orientated vegetation, as with the grasslands associated with the area under investigation, VV polarisation have been shown to interact with

the vegetation structure (Engelbrecht 2013). Therefore, the relatively high importance of VV coherence is expected.

Although, a change in vegetation growth will lead to a decrease in coherence, coherence is also sensitive to other surface changes including for example changes in soil moisture, surface roughness variations and surface deformation (Section 2.3.3). Furthermore, sensor related parameters such as perpendicular baseline, temporal baseline and wavelength, could also cause changes in coherence (Section 2.2.1). The low importance of VH coherence as predictor of EVI may therefore indicate that the VH coherence is more sensitive to surface changes.

Polarimetric decompositions provide the ability to retrieve information on the scattering mechanisms (including vegetation scattering contributions) present in a resolution cell (Section 2.3.3). The dual-polarisation Cloude-Pottier (H-A-α) decomposition was, therefore, applied to extract the entropy (H) and alpha (α) parameters. The importance measures revealed that, contrary to expectations, these parameters were not the most important predictors of EVI. There is a possible explanation for this lower importance. The Cloude-Pottier (H-A-α) decomposition on fully polarimetric data has been successful in discriminating between surface and vegetation scattering mechanisms (Cloude & Pottier 1996), however, the modified dual-polarisation approach has been found to be ineffective for discriminating between vegetation and surface scattering mechanisms where one cross-polarised channel is present (Ji & Wu 2015). Therefore, since Sentinel-1A imagery consists of one co-polarised (VV) channel and one cross-polarised channel (VH), the use of the dual-polarisation H-A-α decomposition for extracting vegetation descriptors may not be ideal. However, including these parameters leads to better predictive performance ($adjR^2 = 0.72$) when simulating EVI compared to $adjR^2 = 0.63$ when H and α was omitted.

The modelled EVI results were compared to Landsat EVI. The results showed that in the dry season or periods of low EVI scenarios, the predicted Sentinel-1A EVI was higher than Landsat EVI for both the natural vegetation and the revegetated areas (Section 4.2.3). This suggests that, in conditions of low vegetation productivity, SAR derived EVI would overestimate the performance compared to real conditions. This may give a false impression that the vegetation conditions are favourable on rehabilitated mines. Any overestimation of vegetation status will be problematic, as it will delay interventions.

In contrast to the overestimation of vegetation performance in low EVI conditions, during the peak of the growing season, model EVI values were underestimating vegetation status compared

to Landsat 8 EVI results. Similar patterns of over and underestimation in low and high biomass conditions, respectively, have also been observed in an investigation on the relationship between C-band backscatter and savannah woody cover and volume (Main et al. 2016). There was an overestimation in high-density areas and underestimation in low-density areas (Main et al. 2016).

The polarisation of the Sentinel-1A data used for the derivation of simEVI can explain the overestimation of modelled EVI in the low range of EVI values. Even though, the grasslands are less dense in the dry seasons, its vertical structure may have a stronger interaction with the VV/VH polarised signal of Sentinel-1A.

As the growing season starts, biomass of the grass increases rapidly and reaches its maximum in the summer months (December to March). Although there is a strong relationship between SAR backscatter and vegetation density (Baghdadi et al. 2009; Ferrazzoli et al. 1997; McNairn et al. 2014) there is a known saturation of SAR backscatter intensity at high vegetation densities for C-band data (Betbeder et al. 2016; Lopez-Sanchez & Ballester-Berman 2009), (Section 2.3.3). The saturation of C-band data was also observed for C-band HH polarisation data for crop heights greater than 1 m (McNairn et al 2000). Furthermore, the saturation effect was considered to be a hindrance for biomass estimation for a variety of crop types (Ferrazzoli et al. 1997).

In addition to backscatter saturation, a saturating dependency between the change in EVI and interferometric coherence has been shown in previous investigations (Engelbrecht 2013). This observation showed that the inverse relationship between coherence and EVI is less significant during periods when rapid changes in EVI are experienced between master and slave acquisition dates, as exhibited during the peak of the growing season. Therefore, the saturating relationships between EVI and both coherence and backscatter may explain the underestimation of the modelled SAR EVI at EVI values > 0.30. To overcome this limitation, the acquisition of SAR data at longer wavelengths may be considered to compensate for saturation effects.

The saturation of SAR backscatter and wavelength limitations may, respectively, be responsible for the patterns of overestimation and underestimation in low EVI and high EVI conditions. However, the statistical phenomenon, known as regression dilution bias, likely has an effect on the results. The regression dilution is known to affect statistical models where training samples are normally distributed, which leads to similar over- and under- estimations of variables. Potential corrective measures should be considered in future research. This includes the selection of an equal number of training samples across the entire EVI range. Alternatively, under certain

assumptions, known ratios between the observed and predicted values can be used to correct the predicted gradient slope of the model (Hutcheon, Chiolero & Hanley 2010).

Finally, the scenario where there is limited or no optical data available was tested in order to assess the predictive capability of the SAR observables. Representative summer and winter imagery was used to train the RF model and the results indicated that the modelled EVI from the SAR observables were overestimated for both the winter and summer dates for the undisturbed vegetation (Figure 4.20 and Figure 4.21 in Section 4.2.2). These results suggests that if there is limited or no optical imagery available then using SAR observables to model EVI is not the preferred method because it may give the false impression that the vegetation productivity is increasing when in fact it may not be. However, this can only be validated with the use of ground truth data.

# 6 CONCLUSION AND RECOMMENDATIONS

Following the discussion of how remote sensing can be used to monitor post-mining rehabilitation, this chapter presents a summary of the findings for the two objectives of the study. It also includes the success, limitations and recommendations for future research.

The study aimed to use remote sensing techniques to monitor post-mining rehabilitation. The objectives of the study included the use of SAR data to detect and measure deformation to quantify backfill settlement rates and to use a combination of SAR and optical data to monitor revegetation of an open-pit mine. As opposed to subsidence monitoring, there has been limited research using satellite-based techniques to quantify backfill settlement dynamics in rehabilitated open-pit mines. DInSAR observations could provide an alternate and robust method to monitor backfill settlement rates, and this could be valuable for mine closure practices. In the mining industry, satellite dInSAR technologies are becoming more relevant for several reasons. This includes the fact that satellite observations provide a synoptic view of the deformation field affecting the area of interest with a dense a time series. This allows for the monitoring of the spatio-temporal evolution of deformation events over time. Additionally, dInSAR techniques allow mining engineers to detect deformation at low cost without having to install in situ instruments, which can often be costly. Remote sensing techniques used to monitor vegetation productivity also provide an opportunity to evaluate the success of rehabilitation initiatives. Information gathered from the findings of this research will aid the operational monitoring of post-mining rehabilitation. Furthermore, information could be used to assist various stakeholders in improving post-mining rehabilitation strategies.

## 6.1 **Backfill settlement monitoring using dInSAR**

The first objective of the study was to evaluate the use of multi-sensor SAR data to quantify backfill settlement rates in an open-pit mine by using conventional dInSAR techniques. The results indicated that deformation measurements could be extracted using X-, C- and L-band SAR data over the period 2007 to 2017 (Section 4.1). In addition to the general deformation patterns observed, some anomalous patterns were present when assessing the cumulative deformation over time. In particular, heave features were observed which is unexpected for areas undergoing long-term backfill settlement. Potential reasons for anomalous deformation features were investigated in Section 5.1.

Phase contributions were assessed and the results showed that there were residual topographic phase contributions for several differential interferograms across all the respective SAR wavelengths. This was a limitation of the study because if the topography is not accurately estimated and removed, then residual topographic contributions can be mistaken for a deformation signal. The source of the residual topographic phase may be due to the use of the 1-arc SRTM DEM for differential interferometry processing sequence. The SRTM DEM is more than ten years old compared to the interferometric SAR datasets used in the investigation. This could introduce potential errors when trying to compensate topography, especially in the area under investigation, which has a dynamic mining land-use activity. Due to the notable presence of residual topography, a recommendation would be to use an updated high-resolution DEM for the study area such as one derived from LiDAR.

In addition to the uncertainties introduced by the residual topographic phase, the results of the study showed that there was an increase in speckle effects for differential interferograms in the peak of the growing season (November to March). Although the presence of vegetation can lead to an increase in speckle noise and a decrease in coherence, the presence of vegetation also has an effect on the SAR signal and how it interacts with the scattering elements in the resolution cell. Shorter wavelength data, like X- and C- band for example, will interact with smaller vegetation elements while long wavelength L-band data will interact with larger vegetation components (i.e. trucks of trees, large branches), but also increase the interaction with the ground surface. The impact of the presence of vegetation on the deformation measurements were observed and described in Section 5.1. In general, the results indicated during the peak of the growing season, there were increased speckle effects, which could affect the accurate retrieval of deformation. Furthermore, the X-band data results indicated that during the growing season, the interaction of the X-band sensor with the vegetation canopy introduced a “topographic” phase contribution that manifested as heave in deformation measurements. Although the correlation was less significant, the same observation could be made for C-band data. In contrast, L-band data did not exhibit the same phenomenon. A suggested recommendation is that, to use a longer wavelength to minimise the impact of vegetation on the extraction of backfill settlement measurements. The use of X- and C-band data is not recommended in the presence of vegetation especially during the peak of the growing season, since the interaction of the signal with vegetation leads to unreliable deformation measurements. However, the use of L-band data could have a decreased sensitivity to small-scale deformation and it also does not have the temporal frequency, therefore, a trade-off should be considered.

Future studies should consider the use of advanced interferometry approaches for the extraction of backfill settlement rates as outlines in Section 2.2.2. Advanced approaches, like persistent scatterers interferometry and Small Baseline Subset (SBAS) techniques, allow for the extraction of very small deformation rates while compensating for the effects of residual topography and atmospheric effects. These approaches also focus on coherent targets, which could mean that temporal decorrelation, and vegetation effects can be minimised. Therefore, the main limitations of conventional dInSAR, as highlighted in this investigation, could be addressed by using these advanced techniques.

Overall, the results suggest that uncompensated topography and signal noise introduced by the presence of vegetation and possibly other external influences may be affecting the results and the conventional dInSAR approach adopted in this investigation. Therefore, conventional dInSAR is considered unsuitable for the quantification of backfill dynamics in rehabilitated open-pit mines and more advanced dInSAR techniques should be considered.

## 6.2 **Vegetation monitoring**

The second objective of this study was to assess the health and productivity of the revegetated areas using SAR and optical data and to compare it to the undisturbed vegetation of the area (Section 1.2). The Enhanced Vegetation Index (EVI) was extracted from Landsat 8 imagery and was assessed over time for undisturbed vegetation surrounding the mine area and the revegetation on the mine. However, a limitation of using optical data is the susceptibility to cloud–cover; therefore, Sentinel-1A data SAR parameters were used to model simEVI (simEVI) using RF regression analysis. The results indicated that when a combination of all eight of the SAR parameters were used, the highest adjusted $R^2$ was obtained (adjusted $R^2$ = 0.72, MSE= 0.0002). The most important parameters were the backscatter in HV polarisation and the coherence of the slave acquisition in the VV polarisation. A comparison was made between the optical derived EVI and the modelled EVI using SAR data for natural and rehabilitated vegetation. The results indicated that there was an overestimation of the simEVI in the dry season and an underestimation in the peak of the growing season.

The main limitation of this investigation was the use of C-band Sentinel-1A data to model EVI. C-band SAR signals are known to interact with smaller scattering elements and consequently, they are affected by the presence of vegetation. Most notably, there is a known saturation of SAR backscatter intensity at high vegetation densities. A recommendation to mitigate this effect would be to use longer wavelength SAR data in the peak of the growing season to address the

limitation of C-band saturation effects. Although short wavelength signal saturation may be responsible for the underestimation of EVI during the peak of the growing season, it is likely that the statistical phenomenon, known as regression dilution, may be responsible for the effects observed. It is therefore recommended that additional machine-learning approaches for the simulation of EVI from SAR observables be considered for investigation in future research. Alternatively, if RF is said to be used for deriving simEVI, the careful selection of equal number of training samples across the entire EVI range should be performed in future investigations.

The results indicated a fair agreement between the multispectral EVI and the simEVI when using a combination of all eight SAR parameters. However, the overestimation and underestimation in the low and high EVI scenarios suggests that SAR observables might not be as suitable as multispectral data to monitor revegetation over time. In particular, overestimation of simEVI in low biomass conditions may lead to the delay in implementation of corrective measures due to an overestimation of the productivity of vegetation.

The scenario was also tested where there is limited optical imagery available to model the EVI from the SAR observables. The results indicated that the modelled EVI overestimated the EVI derived from Landsat 8. This results suggests that in the absence of optical data (which was the preferred data used as a proxy for vegetation productivity for this study), modelled SAR EVI may not be suitable to monitor the vegetation for this investigation. Finally, a limitation of this investigation is the lack of ground truth data. All remote sensing data such as vegetation indices provide a representation of the landscape and therefore cannot be seen as the “true” or actual value on the ground. For future studies, biophysical parameters collected from ground truth methods could be used to train the RF models and should provide a more accurate representation of the vegetation productivity for post-mining rehabilitation.

## 6.3 **Concluding Remarks**

Mining has severe social and environmental consequences, and to comply with mine closure legislation, monitoring post-mining rehabilitation practices is mandatory. In the mining industry, satellite technologies are becoming more relevant. This is due to the ability to provide a synoptic view of an area and with a dense time series of data, monitoring the spatio-temporal evolution of rehabilitation initiatives over time. The study aimed to use remote sensing techniques to monitor post-mining rehabilitation. The objectives of the study included the use of SAR data to detect and measure deformation to quantify backfill settlement rates and to use a combination of SAR and optical data to monitor revegetation of an open-pit mine.

The results of the first objective indicated that although dInSAR approaches are ideal for monitoring deformation over large areas, external factors influencing conventional dInSAR measurements suggest that the technique is not suitable for long-term monitoring. However, advanced approaches could be used in future to address this limitation. Furthermore, the use of EVI derived from conventional multispectral data provides a reliable and mature approach to monitoring the vegetation productivity and should be included in long-term monitoring programmes. Although, simEVI derived from SAR observables can complement observations in areas of persistent cloud cover, it should be noted that low biomass conditions may be underestimated and this may lead to delayed interventions. Future research into the use of remote sensing to monitor post-mining rehabilitation is recommended and this could provide valuable information to assist various stakeholders in improving post-mining rehabilitation strategies. Furthermore, even though the findings of this investigation suggests that conventional dInSAR techniques are not suitable to quantify backfill settlement rates, more advanced dInSAR techniques should be considered as the findings could contribute toward the operational monitoring of post-mining rehabilitation.

# REFERENCES


Ardejani FD, Singh R, Baafi E, Shafaei SZ & Aryafar A 2007. *Prediction of post-mining groundwater reocovery pattern in an unconfined aquifer to predict opencast mine backfill settlement*. IMWA Symposium 2007, 27th -31st May 2007, Cagliari, Italy.

Atzberger C 2013. Advances in remote sensing of agriculture: Context description, existing operational monitoring systems and major information needs. *Remote Sensing* 5: 949–981.

Audet P, Gravina A, Glenn V, McKenna P, Vickers H, Gillespie M & Mulligan D 2013. Structural development of vegetation on rehabilitated North Stradbroke Island: Above/belowground feedback may facilitate alternative ecological outcomes. *Ecological Processes* 2, 1: 20.

Baghdadi N, Boyer N, Todoroff P, El Hajj M & Bégué A 2009. Potential of SAR sensors TerraSAR-X, ASAR/ENVISAT and PALSAR/ALOS for monitoring sugarcane crops on Reunion Island. *Remote Sensing of Environment* 113, 8: 1724–1738.

Bamler R & Hartl P 1998. Synthetic aperture radar interferometry. *Inverse Problems* 14, 4: 1–54.

Barla G, Giannico C, Tamburini A & Del Conte S 2016. InSAR monitoring of tunnel induced ground movements. *Geomechanics and Tunnelling* 9, 1: 15–22.

Bell FG, Stacey TR & Genske DD 2000. Mining subsidence and its effect in the environment: Some differing examples. *Environmental Geology* 40, 1–2: 135–152.

Betbeder J, Fieuzal R, Philippets Y, Ferro-Famil L & Baup F 2016. Contribution of multitemporal polarimetric synthetic aperture radar data for monitoring winter wheat and rapeseed crops. *Journal of Applied Remote Sensing* 10, 2: 26020

Blaes X & Defourny P 2003. Retrieving crop parameters based on tandem ERS 1/2 interferometric coherence images. *Remote Sensing of Environment* 88, 4: 374–385.

Breiman L 2001. Random forests. *Machine Learning* 45, 1: 5–32.

Brom J, Nedbal V, Procházka J & Pecharová E 2012. Changes in vegetation cover, moisture properties and surface temperature of a brown coal dump from 1984 to 2009 using satellite data analysis. *Ecological Engineering* 43: 45–52.

Carbutt C, Tau M, Stephens A & Escott B 2011. The conservation status of temperate grasslands in southern Africa. *Grassroots* 11,1: 17–23.

Carvalho A, Nabais C, Roiloa SR & Rodríguez-Echeverría S 2013. Revegetation of abandoned copper mines: The role of seed banks and soil amendments. *Web Ecology* 13: 69–77.

Chandarana UP, Momayez M & Taylor KW 2016. Monitoring and predicting slope instability: A review of current practices from a mining perspective. *International Journal of Research in Engineering and Technology* 5, 11: 139–151.

Chen G, Wang M, Liu Z & Chi W 2017. The biogeophysical effects of revegetation around mining areas: A case study of Dongsheng mining areas in Inner Mongolia. *Sustainability* 9, 628: 9-4.

Cloude SR & Pottier E 1996. A review of target decomposition theorems in radar polarimetry. *IEEE Transactions on Geoscience and Remote Sensing* 34, 2: 498–518.

Colesanti C & Wasowski J 2006. Investigating landslides with space-borne Synthetic Aperture Radar (SAR) interferometry. *Engineering Geology* 88: 173–199.

De Grandi E, Lucas R, Clewley D, Bunting P & Mitchard E 2013. Analysis of TanDEM-X InSAR data aimed ate the characterisation of vegetation vertical structure: A case study in Injune (Queensland, Australia). Proceedings of IEEE International Geoscience and Remote Sensing Symposium held 21-26 July, Melbourne, Australia: 180–183.

Dong S, Samsonov S, Yin H, Yao S & Xu C 2015. Spatio-temporal analysis of ground subsidence due to underground coal mining in Huainan coalfield, China. *Environmental Earth Sciences* 73, 9: 5523–5534.

Du Y, Zhang L, Feng G, Lu Z & Sun Q 2016. On the accuracy of topographic residuals retrieved by MTInSAR. *IEEE Transactions on Geoscience and Remote Sensing* 55, 2: 1053–1065.

Engelbrecht J, Inggs MR & Makusha G 2011. Detection and monitoring of surface subsidence associated with mining activities in the Witbank Coalfields, South Africa, using differential radar interferometry. *South African Journal of Geology* 114, 1: 77–94.

Engelbrecht J & Inggs MR 2011. *Detection and monitoring of surface subsidence associated with miniing activities in the Witbank coalfields, South Africa, using differential radar interferometry*. 24-29 July, Vancouver, Canada: 1596–1599

Engelbrecht J 2013. Parameters affecting interferometric coherence and implications for long-term operational monitoring of mining-induced surface deformation. Univeristy of Cape Town.

Engelbrecht J & Inggs M 2013. Differential interferometry techniques on L-Band data employed for the monitoring of surface subsidence due to mining. *South African Journal of Geomatics* 2, 2: 82–93.

Engelbrecht J, Kemp J & Inggs M 2013. The phenology of an agricultural region as expressed by polarimetric decomposition and vegetation indices. Proceedings of IEEE International Geoscience and Remote Sensing Symposium held 21-26 July, Melbourne, Australia: 3339–3342.

Engelbrecht J, Musekiwa C, Kemp J & Inggs MR 2014. Parameters affecting interferometric coherence-The case of a dynamic agricultural region. *IEEE Transactions on Geoscience and Remote Sensing* 52, 3: 1572–1582.

Engelbrecht J & Inggs MR 2016. Coherence optimization and its limitations for deformation monitoring in dynamic agricultural environments. *IEEE Journal of Selected Topics in Applied Earth Observations and Remote Sensing*: 9,12: 5647-5654.

Erener A 2011. Remote sensing of vegetation health for reclaimed areas of Seyitömer open cast coal mine. *International Journal of Coal Geology* 86, 1: 20–26.

Felinks B, Pilarski M & Wiegleb G 1998. Vegetation survey in the former brown coal mining area of eastern Germany by integrating remote sensing and ground-based methods. *Applied Vegetation Science* 1: 233–240.

Fenn D, du Kanda A & Dukhan D 2015. Determining settlement rates and surface stability using in situ density of backfill as a proxy for displacement. *The Journal of Southern African Institute of Mining and Metallurgy*. 115: 1035-1043.

Ferrazzoli P, Paloscia S, Pampaloni P, Schiavon G, Sigismondi S & Solimini D 1997. The potential of multifrequency polarimetric SAR in assessing agricultural and arboreous biomass. *IEEE Transactions on Geoscience and Remote Sensing* 35, 1: 5–17.

Ferretti A, Monti-guarnieri A, Prati C, Rocca F & Massonnet D 2007. InSAR Principles: Guidelines for SAR interferometry processing and interpretation. ESA Publications. [online]. Available from: http://www.esa.int/About_Us/ESA_Publications [Accessed 14 March 2016].

Formaggio A R, Epiphanio JCN & Simóes MS 2001. Radarsat backscattering from an agricultural scene. *Pesquisa Agropecuaria Brasileira* 36, 5: 823–830.

Gamma Remote Sensing 2011. GAMMA V1.8 . Interferometric SAR, Differential Interferometry and Geocoding Software User's guide [confidential]

GDACE 2008. *Mining and Environmental Impact Guide*. Johannesburg: Gauteng Department of Agriculture, Conservation and Environment.

Ge L, Chang H & Rizos C 2007. Mine subsidence monitoring using multi-source satellite SAR images. *Photogrammetric engineering and remote sensing* 73, 3:1-8

Glenn EP, Huete AR, Nagler PL & Nelson SG 2008. Relationship between remotely-sensed vegetation indices, canopy attributes and plant physiological processes: What vegetation indices can and cannot tell us about the landscape. *Sensors* 8: 2136-2160.

Goodwin AK, O'Neill MA & Anderson WF 2003. The use of X-ray computer tomography to investigate particulate interactions within opencast coal mine backfills. *Engineering Geology* 70: 331–341.

Gould SF 2012. Comparison of post-mining rehabilitation with reference ecosystems in monsoonal eucalypt woodlands, Northern Australia. *Restoration Ecology* 20, 2: 250–259.

Gourc JP, Arif N & Olivier F 2007. Long term settlement of domestic waste in landfill: Ispm Method. Proceedings of 18th French Congress of Mechanics held 27-31 August, Grenoble, France: 1-6

Hanssen RF 2001. *Radar Interferometry - data interpretation and error analysis*. Berlin: Springer Science & Business Media.

Hanssen RF 2005. Satellite radar interferometry for deformation monitoring: A priori assessment of feasibility and accuracy. *International Journal of Applied Earth Observation and Geoinformation* 6: 253–260.

Hassani FP, Mortazavi A & Shabani M 2008. An investigation of mechanisms involved in backfill-rock mass behaviour in narrow vein mining. *The Journal of the Southern African Institute of Mining and Metallurgy* 108, 8: 463–472.

Helinski M 2007. Mechanics of Mine Backfill. The Univeristiy of Western Australia

Hermanus M 2014. Mining sector to benefit from the CSIR's multidisciplinary research, development and innovation approach [online]. Available from https://www.csir.co.za/mining-sector-benefit-csirs-multidisciplinary-research-development-and-innovation-approach [Accessed 27 March 2017]

Herrera G, Tomás R, Lopez-Sanchez JM, Delgado J, Mallorqui JJ, Duque S & Mulas J 2007. Advanced DInSAR analysis on mining areas: La Union case study (Murcia, SE Spain). *Engineering Geology* 90: 148–159.

Herrera G, Tomas R, Vicente F, Lopez-Sanchez JM, Mallorquí JJ & Mulas J 2010. Mapping ground movements in open pit mining areas using differential SAR interferometry. *International Journal of Rock Mechanics and Mining Sciences* 47, 7: 1114–1125.

Horning N 2010. Introduction to decicion trees and random forests. American Museum of Natural History's Center for Biodiversity and Conservation.

Hills C 1994. The examination and prediction of opencast backfill settlement. University of Nottingham.

Hu W, Wu L, 2016. Ground deformation extraction using visible images and LiDAR data in mining area. Proceedings of International Archives of the International Archives of the Photogrammetry, Remote Sensing and Spatial Information Sciences held 12–19 July, Prague, Czech Republic.

Huete A, Didan K, Miura T, Rodriguez EP, Gao X & Ferreira LG 2002. Overview of radiometric and biophysical performance of the MODIS vegetation indices. *Remote Sensing of Environment* 83: 195–213.

Huete AR, Liu HQ, Batchily K & Leeuwen W Van 1995. A comparison of vegetation indices

over a Global Set of TM Images for EOS-MODIS. *Remote Sensing of Environme*nt 59: 440-451.

Hutcheon JA, Chiolero A & Hanley JA 2010. Random measurement error and regression dilution bias. *BMJ* 340: 2289

Ji K & Wu Y 2015. Scattering mechanism extraction by a modified Cloude-Pottier decomposition for dual Polarization SAR. *Remote Sensing* 7, 6: 7447–7470.

Jiang Z, Huete AR, Didan K & Miura T 2008. Development of a two-band enhanced vegetation index without a blue band. *Remote Sensing of Environment* 112, 10: 3833–3845.

Jiao X, McNairn H, Shang J & Liu J 2010. The sensitivity of multi-frequency (X, C and L-band) radar backscatter signatures to bio-physical variables (LAI) over corn and soybean fields. Proceedings of International Archives of the Photogrammetry, Remote Sensing and Spatial Information Sciences held 5-7 July, Vienna, Austria.

Joyce KE, Samsonov SV, Levick SR, Engelbrecht J & Belliss S 2014. Mapping and monitoring geological hazards using optical, LiDAR, and synthetic aperture RADAR image data. *Natural Hazards* 73, 2: 137–163.

Karan SK, Samadder SR & Maiti SK 2016. Assessment of the capability of remote sensing and GIS techniques for monitoring reclamation success in coal mine degraded lands. *Journal of Environmental Management* 182: 272–283.

Karjalainen M, Kaartinen H & Hyyppä J 2008. Agricultural Monitoring Using Envisat Alternating Polarization SAR Images. *Photogrammetric Engineering and Remote Sensing* 74, January: 117–126.

Kemp J & Burns J 2016. *Agricultural monitoring using pursuit monostatic TanDEM-X coherence in the Western Cape, South Africa*. Proceedings of 11th European Conference on Synthetic Aperture Radar held 6-9 June, Hamburg, Germany.

Koruyan K, Deliormanli AH, Karaca Z, Momayez M, Lu H & Yalçin E 2012. Remote sensing in management of mining land and proximate habitat. *Journal of the Southern African Institute of Mining and Metallurgy* 112, 7: 667–672.

Latifovic R, Fytas K, Chen J & Paraszczak J 2005. Assessing land cover change resulting from large surface mining development. *International Journal of Applied Earth Observation and Geoinformation* 7, 1: 29–48.

Li P, Vanapalli S & Li T 2016. Review of collapse triggering mechanism of collapsible soils due to wetting. *Journal of Rock Mechanics and Geotechnical Engineering* 8, 2: 256–274.

Limpitlaw D, Aken M, Lodewijks H & Viljoen J 2005. Post-mining rehabilitation, land use and pollution at collieries in South Africa. Proceedings of Colloquium: Sustainable Development in the Life of Coal Mining, held 13 July, Johannesburg, South Africa

Limpitlaw D 2006. Use of remotely sensed imagery and methods for mapping and planning of mine waste facilities. Proceedings of SAIMM Colloquium: Mine Waste Disposal and Achievement of Mine Closure - What Doest it Take, held 2 November, Johannesburg, South Africa.

Lopez-Sanchez JM & Ballester-Berman JD 2009. Potentials of polarimetric SAR interferometry for agriculture monitoring. *Radio Science* 44: 1–20.

Main R, Mathieu R, Kleynhans W, Wessels K, Naidoo L & Asner GP 2016. Hyper-temporal C-band SAR for baseline woody structural assessments in deciduous savannas. *Remote Sensing* 8: 1–19.

Makineci E, Gungor BS & Kumbasli M 2011. Natural plant revegetation on reclaimed coal mine landscapes in Agacli-Istanbul. *African Journal of Biotechnology* 10, 16: 3248–3259.

Massonnet D & Feigl KL 1998. Radar interferometry and its application to changes in the Earth's surface. *Reviews of Geophysics* 36, 4: 441.

Matsushita B, Yang W, Chen J, Onda Y & Qiu G 2007. Sensitivity of the Enhanced Vegetation Index (EVI) and Normalized Difference Vegetation Index (NDVI) to topographic Effects: A case study in high-density cypress forest. *Sensors* 7, 11: 2636–2651.

Mcclusky S & Tregoning P 2013. Background paper on subsidence monitoring and measurement with a focus on coal seam gas ( CSG ) activities. Canberra: NSW Chief Scientist and Engineer.

McNairn H, Ellis J, Van Der Sanden JJ, Hirose T & Brown RJ 2002. Providing crop information using RADARSAT-1 and satellite optical imagery. *International Journal of Remote Sensing* 23, 5: 851–870.

McNairn H & Brisco B 2004. The application of C-band polarimetric SAR for agriculture: A review. *Canadian Journal of Remote Sensing* 30, 3: 525–542.

McNairn H, Shang J, Jiao X & Champagne C 2009. The contribution of ALOS PALSAR multipolarization and polarimetric data to crop classification. *IEEE Transactions on Geoscience and Remote Sensing* 47, 12: 3981–3992.

McNairn H, Kross A, Lapen D, Caves R & Shang J 2014. Early season monitoring of corn and soybeans with TerraSAR-X and RADARSAT-2. *International Journal of Applied Earth Observation and Geoinformation* 28, 1: 252–259.

Mensah AK 2015. Role of revegetation in restoring fertility of degraded mined soils in Ghana: A review. *International Journal of Biodiversity and Conservation* 7, 2: 57–80.

Mirzaee S, Motagh M, Arefi H & Nooryazdan A 2015. *Phenological tracking og agricultural feilds investigated by using dual polarimetry tanDEM-X images*. Proceedings of International Archives of the Photogrammetry, Remote Sensing and Spatial Information Sciences held 11-15 May, Berlin, Germany.

Moreira A, Prats-iraola P, Younis M, Krieger G, Hajnsek I & Papathanassiou KP 2013. A Tutorial on Synthetic Aperture Radar. *IEEE Geoscience and Remote Sensing Magazine*: 6–43.

Morse-Mcnabb E, Sheffield K & Clark R 2013. Time series analysis of MODIS EVI data for regular land cover mapping in Victoria, Australia. Proceedings of *International Geoscience and Remote Sensing Symposium held 21-26 July, Melbourne Australia*

Mucina L & Rutherford MC 2006. *The Vegetation of South Africa, Lesotho and Swaziland*. *Strelitzia 19*. Pretoria: South African Biodiversity Institute.

Muller SJ 2016. Indirect soil salinty detection in irrigated areas using earth observation methods. Stellenbosch University.

Navarro A, Rolim J, Miguel I, Catalão J, Silva J, Painho M & Vekerdy Z 2016. Crop monitoring based on SPOT-5 Take-5 and Sentinel-1A data for the estimation of crop water requirements. *Remote Sensing* 8, 1-20.

Nazare F 2005. National grassland biodiversity programme. South African National Biodiversity Institue.

Ng AH-M, Ge L, Yan Y, Li X, Chang HC, Zhang K & Rizos C 2010. Mapping accumulated mine subsidence using small stack of SAR differential interferograms in the Southern coalfield of New South Wales, Australia. *Engineering Geology* 115, 1–2: 1–15.

Obermayer J 2009. An analysis of the fundamental price drivers of EU ETS carbon credits KTH, Stockholm, Sweden.

Osmanoğlu B, Sunar F, Wdowinski S & Cabral-Cano E 2015. Time series analysis of InSAR

data: Methods and trends. *ISPRS Journal of Photogrammetry and Remote Sensing*. (Article in Press).

Petja MB 2009. Satellite-derived monitoring of asbestos mine rehabilitation in the post mining environments of Mafefe and Mathabatha. University of Limpopo.

Petropoulos GP, Partsinevelos P & Mitraka Z 2013. Change detection of surface mining activity and reclamation based on a machine learning approach of multi-temporal Landsat TM imagery. *Geocarto International* 28, 4: 323–342.

Przylucka M, Herrera G, Graniczny M, Colombo D & Béjar-Pizarro M 2015. Combination of conventional and advanced DInSAR to monitor very fast mining subsidence with TerraSAR-X data: Bytom City (Poland). *Remote Sensing* 7: 5300–5328.

Randall J 2004. Ecosystem Function Analysis - a tool for monitoring mine-site rehabilitation success. *MESA journal* 35: 24–27.

Raucoules D, Colesanti C & Carnec C 2007. Use of SAR interferometry for detecting and assessing ground subsidence. *Comptes Rendus - Geoscience* 339: 289–302.

Reed S, Hughes D & Singh R 1987. Backfill settlement of restoed strip mine sites-case histories. *International Journal of Mining and Geological Engineering* 5: 161–169.

Reed S & Singh R 1986. Ground water recovery problems associated with opencast mine backfills in the United Kingdom. *International Journl of Mine Water* 5, 3: 47–74.

Richter R 2009. Atmospheric/Topographic correction for satellite imagery (ATCOR-2/3 User Guide 7.0). DLR: Germany.

Rocha AV & Shaver GR 2009. Advantages of a two band EVI calculated from solar and photosynthetically active radiation fluxes. *Agricultural and Forest Meteorology* 149: 1560–1563.

Sang H, Zhang J, Lin H & Zhai L 2014. Multi-polarization ASAR backscattering from herbaceous wetlands in poyang lake region, China. *Remote Sensing* 6, 5: 4621–4646.

Samsonov S, d'Oreye N & Smets B 2013. Ground deformation associated with post-mining activity at the French – German border revealed by novel InSAR time series method. *International Journal of Applied Earth Observations and Geoinformation* 23: 142–154.

Scheiber R & Bothale VM 2002. Interferometric multi-look techniques for SAR data. Proceedings of IEEE International Geoscience and Remote Sensing Symposium held 24-28 June, Toronto, Canada.

Shang J, McNairn H, Champagne C & Jiao X 2009. Application of Multi-Frequency Synthetic Aperture Radar (SAR) in Crop Classification. *Advances in Geoscience and Remote Sensing*. InTech.

Shao Z & Zhang L 2016. Estimating forest aboveground biomass by combining optical and SAR data: A case study in Genhe, Inner Mongolia, China. *Sensors* 16, 834.

Singh KB & Dhar BB 1997. Sinkhole subsidence due to mining. *Geotechnical and Geological Engineering* 15, 4: 327–341.

South Africa 1996. Mine health and safety Act, Act 29 of 1996. *Government Gazette of South Africa* 17242, 15.01.2009.

Swart E 2003. The South African legaslative framework for mine closure. *The Journal of the South African institute of Mining and Metallurgy* 103, 8: 489–492.

Szwedzicki T 2001. Geotechnical precursors to large-scale ground collapse in mines. *International Journal of Rock Mechanics and Mining Sciences* 38, 7: 957–965.

Tahsin S, Medeiros SC, Hooshyar M & Singh A 2017. Optical cloud pixel recovery via machine

learning. *Remote Sensing* 9, 6: 527.

Tamm T, Zalite K, Voormansik K & Talgre L 2016. Relating Sentinel-1 interferometric coherence to mowing events on grasslands. *Remote Sensing* 8, 10: 802.

Tanner P & Möhr-Swart M 2007. *Guidelines for the Rehabilitation of Mined Land*. Johannesburg: Coaltech Research Association and the Chamber of Mines of South Africa.

Tote C, Reusen I, Delalieux S, Goossens M & Kolodyazhnyy O 2010. Report on the limitations and potentials of satellite EO Data: Impactmin.

Tucker CJ & Sellers PJ 1986. Satellite remote sensing of primary production. *International Journal of Remote Sensing* 7, 11: 1395–1416.

Vickers H, Gillespie M & Gravina A 2012. Assessing the development of rehabilitated grasslands on post-mined landforms in north west Queensland, Australia. *Agriculture, Ecosystems and Environment* 163: 72–84.

Wegmüller U, Werner C, Strozzi T & Wiesmann A 2007. Monitoring of mining induced surface deformation. Proceedings of IEEE International Geoscience and Remote Sensing Symposium held 20-24 September, Anchorage, USA.

Weydahl DJ 2001. Analysis of ERS SAR coherence images acquired over vegetated areas and urban features. *International Jornal of Remote Sensingn* 22, 14: 2811–2830.

Woo KS, Eberhardt E, Rabus B, Stead D & Vyazmensky A 2012. Integration of field characterisation, mine production and InSAR monitoring data to constrain and calibrate 3-D numerical modelling of block caving-induced subsidence. *International Journal of Rock Mechanics and Mining Sciences* 53: 166–178.

Zalite K, Antropov O, Praks J, Voormansik K & Noorma M 2016. Monitoring of Agricultural grasslands with time series of X-Band repeat-pass interferometric SAR. *IEEE Journal of Selected Topics in Applied Earth Observations and Remote Sensing* 9, 8: 3687–3697.

Zhao H, Ma F, Zhang Y & Guo J 2014. Monitoring and assessment of mining subsidence in a metal mine in china. *Environmental Engineering and Management Journal* 13, 12: 3015–3024.

Zhou X, Chang N & Li S 2009. Applications of SAR Interferometry in Earth and environmental science research. *Sensors* 9: 1876–1912.